

POLITECNICO DI MILANO
Since 1863

Scuola di Ingegneria Industriale e dell'Informazione
Laurea Magistrale ENERGY ENGINEERING



**1D FLUID DYNAMIC SIMULATION OF TURBOCHARGERS FOR I.C.
ENGINES BOOSTING.**

Supervisor: Prof. Angelo ONORATI
Co-Supervisors: Ing. Tarcisio CERRI
Giorgio Attilio D'ANTONIO

Author:

Sunny Sunny Matr. 835333

Academic Year - 2015/2016

Acknowledgement:

My first thanks go to my family for their love and support over me in joyous moments and as well as in difficult times during all these years. Without them this day would not have come, and I would not be doing in my life, what I am doing today.

A second thank to the Energy Department of Politecnico di Milano, with whom I got this opportunity to study Masters in Science course and shared a very interesting, exciting and sometimes hectic life.

In particular, I am very grateful to Professor. Angelo Onorati, for teaching me I.C. Engines subject and for giving me the opportunity to carry out this thesis. He is one of the three greatest teachers I have met in my life. I really appreciate for the time he has given to me, despite being very busy, and for guiding me in my path of training and personal growth. With his calm, courteous and professional attitude, as well as with great rigor, he further induced a great amount of interest in me for Engines (CFD simulation). Thanks to Ing. Tarcisio Cerri, whose help was critical to quickly learn several aspects of Gasdyn. whose ability to always find positives in the results, when things were going slim, helped me to stay motivated.

Last, but not least, thanks to Giorgio Attilio D'Antonio and Andrea Montorfano, for their invaluable assistance provided to me and for showing me how simple concepts can make big change and contribution in simulation codes, thanks to the commitment and dedication of the Giorgio.

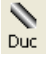

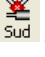





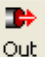

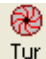

I would also like to express my gratitude to all the people who have been close to me in the last two years. My colleagues, classmates and friends for supporting me in the hard time and great learning experience in abroad.

Sunny Verma

Acknowledgement:

Table of Contents:

ACKNOWLEDGEMENT:	1
TABLE OF CONTENTS:	3
ABSTRACT:	7
(ENGLISH LANGUAGE):	7
(ITALIAN LANGUAGE):	8
INTRODUCTION:	9
1. GOVERNING EQUATIONS	11
1.1. EQUATIONS OF DYNAMIC EQUILIBRIUM INDEFINITE.....	11
1.2. ONE-DIMENSIONAL MODEL.....	13
1.2.1. <i>Mass conservation equation (continuity)</i>	14
1.2.2. <i>Equation of conservation of momentum</i>	15
1.2.3. <i>Energy conservation equation</i>	16
1.2.4. <i>Formulation of the equations in conservative form.</i>	18
2. NUMERICAL METHODS	30
2.1. INTRODUCTION:.....	30
2.1.1. <i>The Method of Characteristics:</i>	31
2.2. SHOCK-CAPTURING METHODS:.....	48
2.2.1. <i>Lax-Wendroff method:</i>	50
2.2.2. <i>MacCormack method:</i>	53
2.3. THE PROBLEM OF SPURIOUS OSCILLATIONS:.....	55
2.4. THE FCT TECHNIQUE:	56
2.5. FLOW RESTRICTORS:.....	58
3. MODELING OF TURBOCHARGER IN GASDYN	62
3.1. MODELING TURBINES:	63
3.1.1. <i>Features of the radial turbine steady stream:</i>	63
3.1.2. <i>Performance of turbines with variable outlet pressure:</i>	65
3.1.3. <i>Work and Efficiency of turbines:</i>	73
3.2. MODELING OF CENTRIFUGAL COMPRESSORS:.....	75
3.2.1. <i>Characteristics of centrifugal compressors steady stream:</i>	75
3.2.2. <i>Performance of centrifugal compressors with variable inlet pressure:</i>	77
3.2.3. <i>Work and Efficiency for centrifugal compressors:</i>	79
3.3. TURBO-MATCHING IN GASDYN:	82
3.3.1. <i>Cyclic Matching:</i>	82
3.3.2. <i>Instant Matching:</i>	83

4. TURBO-MATCHING STEADY STATE	85
4.1. INTRODUCTION:	85
4.2. EXPERIMENTAL RIG:	86
4.2.1. Features of the IHI turbo RHF3:	87
4.3. MODELLING OF STEADY FLOW THROUGH TURBOCHARGER IN GASDYN	88
4.3.1. Duct:  Duc	88
4.3.2. Constant pressure junction:  Jun	88
4.3.3. Sudden diameter variation:  Sud	88
4.3.4. Volume:  Vol	89
4.3.5. Orifice:  Orif	90
4.3.6 Air Injection: 	90
4.3.7. Y junction:  Y ,  Y	90
4.3.8. Outlet:  Out	91
4.3.9. Output pick-up:  Out	91
4.4. TURBINE:  Tur	92
4.4.1. Chart type – Map:	92
4.4.2. Chart type – Efficiency:.....	93
4.5 COMPRESSOR:  Com	94
4.5.1. Chart type – Map:	95
4.5.2. Chart type - Efficiency:	96
4.6. SMOOTHING AND EXTRAPOLATING OF COMPRESSOR AND TURBINE CURVES:.....	97
4.6.1. Extrapolated and smooth Turbine curves:	98
4.6.2 Extrapolated and smooth Compressor curves:	99
4.7. GASDYN MODELLING AND SIMULATION FOR STEADY STATE:.....	100
4.7.1. Input circuit of the turbine:	100
4.7.2. Output circuit of the turbine:	100
4.7.3. Input circuit of the Compressor:.....	101
4.7.4. Output circuit of the Compressor:.....	101
4.7.5. Boundary conditions:	102
4.7.6. Results:	103
4.8. CONCLUSION AND FUTURE WORK:	110

5. CONVERGENCE ALGORITHM FOR TURBOCHARGER:	111
5.1. OLD CONDITION FOR TURBOCHARGER CONVERGENCE (v.10.2.1):	111
5.1.1. Condition 1:	111
5.1.2. Condition 2:	113
5.1.3 Condition 3:	113
5.2. ENGINE 1 "TD-4"	114
5.2.1. Specification:	115
5.2.2. Results:	115
5.3. ENGINE 2 "F1C".	116
5.3.1. Specification:	117
5.3.2. Results:	117
5.4. NEW ALGORITHM FOR TURBOCHARGER CONVERGENCE:	119
5.4.1. Condition 1 (Derivative + Error):	120
5.4.2. Condition 2 (Oscillation, check forced fluctuations in boost pressure and turbocharger power balance):	122
5.4.3 Condition 3 (Steady turbocharger speed and turbocharger power balance):	123
5.5. CONVERGENCE RESULTS ON TD-4:	124
5.5.1. One Constrain:	124
5.5.2. Two Constrain:	126
5.5.3. Three Constrain:	128
5.6. CONVERGENCE RESULTS ON F1C:	131
5.6.1. Two Constrain:	131
5.7. PID CONTROL:	134
LIST OF FIGURES:	136
LIST OF TABLES:	138
BIBLIOGRAPHY	139

Table of Contents:

Abstract:

(English Language):

Nowadays, the numerical modelling of thermo-fluid dynamic processes that occurs in the internal combustion engines is an indispensable tool of analysis in the design and development of engines. In fact, the use of reliable software and correct processes modelling, can predict the engine performance with a sufficient degree of accuracy, in terms of: power, fuel consumption, pollutants and all the variables that characterize its operation.

The software used for the thesis work is Gasdyn, developed at Politecnico di Milano by the I.C. Engine research team. First part of the thesis includes turbo-matching of steady flow through a turbocharger (whose experimental investigation is carried out on the University of Genova (UNIGE) test facility). Where results obtained from experimental rig are compared with results achieved on Gasdyn simulation platform for turbo-matching.

In the second part of the thesis work, a new algorithm is made and executed in Gasdyn code, to achieve convergence of turbocharger simulation accurately and efficiently. Then this new algorithm is validated and checked for two set of engines “TD-4” and”F1C”

Keywords: *Turbocharger, Gasdyn, turbo-matching, numerical modelling, steady flow.*

(Italian Language):

Oggigiorno, la modellazione numerica dei processi termofluidodinamici che si verificano all'interno dei motori a combustione interna rappresenta uno strumento indispensabile per l'analisi del progetto e sviluppo dei motori. Infatti l'uso di software affidabile e di modelli corretti dei processi, può consentire la previsione delle prestazioni del motore con un sufficiente grado di accuratezza, in termini di potenza, consumi, inquinanti emessi e di tutte le variabili che caratterizzano il suo funzionamento.

Il software impiegato per questo lavoro di tesi è stato Gasdyn, sviluppato al Politecnico di Milano dal Gruppo Motori. La prima parte della tesi riguarda il turbo-matching di un flusso stazionario attraverso il turbogruppo (l'analisi sperimentale è stata condotta nei laboratori dell'Università di Genova (UNIGE)). I risultati ottenuti sperimentalmente sono stati confrontati con quelli forniti dalle simulazioni in Gasdyn.

Nella seconda parte del presente lavoro di tesi, è stato implementato un nuovo algoritmo all'interno di Gasdyn, con lo scopo di raggiungere più accuratamente e in modo più efficiente durante la simulazione, la convergenza dei turbogruppi. Questo nuovo algoritmo è stato poi validato e testato su i due modelli motore denominati "TD-4" e "F1C".

Parole chiave: turbocompressore, Gasdyn, turbo-matching, modellazione numerica, flusso stazionario.

Introduction:

The computing speed of today's computers has allowed the development of models that can simulate the operation of internal combustion engines in their entirety. The modeling through calculation codes has become essential in the design and optimization as it greatly reduces time and cost. The realization of an engine of the model allows the limitation of experimental tests to only configurations that have produced satisfactory results in the numerical simulation. It makes possible a further reduction of the measurement campaigns, as it facilitates the identification of the key variables of the phenomenon and estimate the value of quantities which are not easily measured, such as the internal temperature of the cylinders.

The predictive tool used within "Politecnico di Milano" is the Gasdyn software, developed at the Department of Energy from Motors group. It is a thermo-1D computational fluid dynamics model that offers the possibility to calculate the properties of air and flue gas at every point of the engine, in a short time compared to multi-dimensional predictive codes. The research interest is focused on continuous development of the code and its adaptation to an increasingly large series of engines. The thesis work has led to simulate the turbocharger boosting for I.C. engine in Gasdyn to make faster and more accurate simulation of turbocharged engines.

The first and the second chapter of the thesis concerning the thermo-fluid dynamic Gasdyn code, which allows a one-dimensional simulation of the unsteady motion of the fluid inside the engine, by combining the method of characteristics with numerical methods of the second order.

In Third chapter, we discuss the fundamental equations which is the basis of Gasdyn code, it is explained in detail the process which numerically represents turbine and compressor operation starting from their respective maps. Finally, the ways in which the code identifies the matching between the two components are illustrated.

In fourth chapter, turbo-matching of an automotive turbocharger (IHI RHF3) is done using 1D gasdyn simulation software, where experimental results obtained on the University of Genova (UNIGE) test facility were simulated to get turbo-matching of steady state flow.

In fifth chapter, new algorithm to reach convergence for turbocharger simulation is developed and simulation results on two engines "TD-4" and "F1C" were studied to see the effective of new convergence algorithm.

Future development of this thesis work provide the implementation of Gasdyn code for the simulation of unsteady flow through turbocharger and turbo matching of pulsating flow through turbocharger.

Chapter 1

1. Governing Equations

1.1. Equations of dynamic equilibrium indefinite

Given the importance of the replacement process of the working fluid has a volumetric engine, in order to obtain from certain benefits, research has been directed towards the study of models for the calculation of the flow characteristics in intake and exhaust.

Unfortunately, the phenomena in question are so complex (due to mainly their non-stationary in time) that a physically rigorous description by a calculation model of the events suffered from air and flue gases through the various engine components lead to additional complexity of the program and to the calculation of cost management is not always acceptable. Some models therefore introduce appropriate approximations and simplifications, to obtain a fair compromise between the accuracy of the forecast requests, the complexity of the program and the cost of computation.

The models are proposed to solve the equations that express the balance of:

Mass:

$$\frac{\partial \rho}{\partial t} + \frac{\partial(\rho v)_1}{\partial x_1} + \frac{\partial(\rho v)_2}{\partial x_2} + \frac{\partial(\rho v)_3}{\partial x_3} = 0 \quad (1.1)$$

Momentum:

$$\begin{cases} \rho \cdot \left(-\frac{dv_1}{dt}\right) = \frac{\partial \sigma_1}{\partial x_1} + \frac{\partial \tau_3}{\partial x_2} + \frac{\partial \tau_2}{\partial x_3} \\ \rho \cdot \left(-\frac{dv_2}{dt}\right) = \frac{\partial \tau_3}{\partial x_1} + \frac{\partial \sigma_2}{\partial x_2} + \frac{\partial \tau_1}{\partial x_3} \\ \rho \cdot \left(-\frac{dv_3}{dt}\right) = \frac{\partial \tau_2}{\partial x_1} + \frac{\partial \tau_1}{\partial x_2} + \frac{\partial \sigma_3}{\partial x_3} \end{cases} \quad (1.2)$$

Energy:

$$\dot{e} - \dot{q} = \frac{1}{\rho} \sum_{j=1}^3 \sum_{i=1}^3 t_{ij} v_{ij} \quad (1.3)$$

according to the spatial dimensions and time, with the aim of arriving to predict, locally and in time, the conditions of motion of the fluids.

It 'well known that the cyclic operation of reciprocating engines, characterized by the opening and closing of lift valves which connect the cylinder with the ducts, generates in the working of the intense pressure and fluid velocity oscillations, which propagate in the systems of intake and exhaust to the silencers. The processes are highly non-stationary, the temperature gradients and entropy in the gas are considerable, and the fluid manifests significantly its compressibility and viscosity. A detailed simulation of the fluid dynamic phenomena in question is based on integration numerical of the Navier-Stokes equations in three dimensions, with the addition of a model for turbulence. The complexity of this approach makes it impractical for the overall study of the engine and have thus developed one-dimensional models, which have proved of great help in the development of the intake and exhaust systems. Only recently are emerging multidimensional models [1].

1.2. One-dimensional Model

The one-dimensional model used introduces the following assumptions:

1. unsteady motion in time
2. compressible fluid: it adopts the model of ideal gas mixture, with specific variables heat with the temperature and the chemical composition, or perfect gas with constant specific heats.
3. One-dimensional motion, because you believe the longitudinal dimensions the systems studied clearly prevalent than cross.
4. Section of the duct variable assigned with the law.
5. Process non-adiabatic due to heat flows to the walls.
6. Non-isentropic motion for the presence of viscous forces on the walls.

The hypothesis of One-dimensionality implies that all thermodynamic variables such as pressure p , density ρ , fluid velocity u are then considered constant over the cross section of the duct, and variables only in function of a space coordinate x curvilinear, taken generally along the ' x ' axis of the tubes, and the time variable t : then we have $p = p(x, t)$, $\rho = \rho(x, t)$, $u = u(x, t)$, etc .. It also has that, if the entropic level is everywhere uniform, and does not vary with space and time, the flow is said isentropic; if instead the entropy levels are not uniform, the flow is said non-isentropic. Consider an infinitesimal portion of duct with variable section crossed by a compressible fluid [2]:

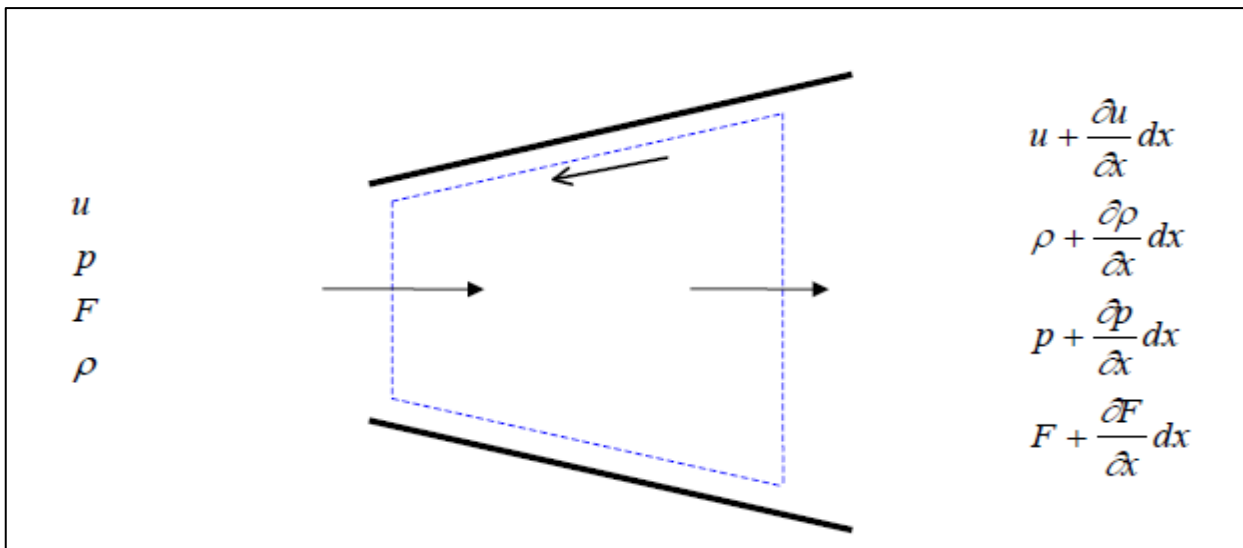


Figure 1:1: One dimensional Scheme.

u = fluid velocity

p = pressure

ρ = density

F = flow section

Based on the newly formulated hypothesis we can derive the equations of continuity, conservation of momentum and energy to the volume of control dashed in figure 1.1.

1.2.1. Mass conservation equation (continuity)

Conservation of mass requires that the speed of the mass within the volume variation is equal to the net mass flow which crosses the contour.

Variation of mass over time within the control volume:

$$\frac{\partial(\rho F dx)}{\partial t} \quad (1.4)$$

Incoming mass flow rate:

$$\rho u F \quad (1.5)$$

Outgoing mass flow rate:

$$\left(\rho + \frac{\partial \rho}{\partial x} dx\right) \left(u + \frac{\partial u}{\partial x} dx\right) \left(F + \frac{\partial F}{\partial x} dx\right) \quad (1.6)$$

The balance shows:

$$\left(\rho + \frac{\partial \rho}{\partial x} dx\right) \left(u + \frac{\partial u}{\partial x} dx\right) \left(F + \frac{\partial F}{\partial x} dx\right) - \rho u F = -\frac{\partial(\rho F dx)}{\partial t} \quad (1.7)$$

and then, developing and considering only the infinitesimal of the first order, we get:

$$\frac{\partial \rho}{\partial t} + \frac{\partial(\rho u)}{\partial x} + \frac{\rho u}{F} \frac{\partial F}{\partial x} = 0 \quad (1.8)$$

1.2.2. Equation of conservation of momentum

The conservation of momentum states that the sum of pressure and frictional forces acting on the surface of the control volume is equal to the sum of the speed of variation of the quantity of motion in its interior and the net flow of the outgoing quantity of motion from it.

Pressure forces:

$$pF - \left(p + \frac{\partial p}{\partial x} dx \right) \left(F + \frac{\partial F}{\partial x} dx \right) + p \frac{\partial F}{\partial x} dx = \left[-\frac{\partial(pF)}{\partial x} dx + p \frac{\partial F}{\partial x} dx \right] \quad (1.9)$$

Friction forces:

$$\tau = f \cdot \frac{1}{2} \rho u^2 \Rightarrow F_{friction} = -f \frac{\rho u^2}{2} (\pi \cdot D \cdot dx) \quad (1.10)$$

Variation in time of the quantity of motion:

$$\frac{\partial(\rho u F dx)}{\partial t} = \frac{\partial(\rho F dx \cdot u)}{\partial t} \quad (1.11)$$

Net outgoing momentum of flow:

$$\left(\rho + \frac{\partial \rho}{\partial x} dx \right) \left(u + \frac{\partial u}{\partial x} dx \right) \left(F + \frac{\partial F}{\partial x} dx \right) - \rho F u^2 = -\frac{\partial(\rho F u^2)}{\partial x} dx \quad (1.12)$$

therefore, by summing these four contributions and taking account of continuity equation, we obtain the following expression:

$$\frac{\partial u}{\partial t} + u \frac{\partial u}{\partial x} + \frac{1}{\rho} \frac{\partial p}{\partial x} + G = 0 \quad (1.13)$$

Where:

$$G = f \frac{u^2}{2} \cdot \frac{u}{|u|} \cdot \frac{4}{D} \quad (1.14)$$

1.2.3. Energy conservation equation

It is determined by applying the first law of thermodynamics to the control volume:

$$\dot{Q} - \dot{L} = \frac{\partial E}{\partial t} + \frac{\partial H_0}{\partial x} dx \quad (1.15)$$

where $\frac{\partial E}{\partial t}$ is the temporal change in internal energy of stagnation, L is the work done by, or on, the system that, for a flow of gas in an element of a conduit of the engine, is zero, Q is the temporal variation of the heat transferred from the gas to the walls of the duct and vice versa, finally $\frac{\partial H_0}{\partial x} dx$ is the net efflux of enthalpy of stagnation through the control surface.

In detail the terms of (1.15) are expressed as follow:

$$\dot{Q} = \dot{q}\rho F dx + \Delta H_{reaction} F dx \quad (1.16)$$

where q is the heat transmitted per unit of mass and time through the walls of the duct, while $\Delta H_{resction}$ is heat, per unit volume and time freed from the reactions that take place in the first section of the exhaust ducts:

$$\frac{\partial E}{\partial t} = \frac{\partial (e_0 \rho F dx)}{\partial t} \quad (1.17)$$

where e_0 is the internal energy of stagnation:

$$e_0 = e + \frac{u^2}{2} \quad (1.18)$$

$$\frac{\partial H_0}{\partial x} dx = \frac{\partial (h_0 \rho F u)}{\partial x} dx \quad (1.19)$$

where h_0 is the enthalpy of the fluid stagnation which is linked to the internal energy of stagnation by the following equation:

$$h_0 = e_0 + \frac{p}{\rho} \quad (1.20)$$

which when combined with the expression of e_0 , it becomes

$$h_0 = c_v T + \frac{p}{\rho} + \frac{u^2}{2} \quad (1.21)$$

The energy equation thus takes the following form:

$$\dot{q}\rho F dx + \Delta H_{reaction} F dx = \frac{\partial(e_0 \rho F dx)}{\partial t} + \frac{\partial(h_0 \rho F u)}{\partial x} dx \quad (1.22)$$

The equations of continuity, momentum and energy constitute a system of partial differential, non-linear, hyperbolic. The closure of the problem (we have four variables p , ρ , u , and, and three equations) is obtained by introducing a fourth equation which expresses the properties of the fluid. Usually it introduces the additional hypothesis of ideal gas at constant specific heats, so that apply the known laws:

$$\frac{p}{\rho} = RT, \quad e = c_v T. \quad (1.23)$$

With the assumption of perfect gas at constant specific heats it is possible to transform the equation of conservation of energy, by removing the fourth associated variable energy specific and internal. The terms of the energy equation, therefore, become:

$$\frac{\partial E}{\partial t} = \frac{\partial}{\partial t} \left[(\rho F dx) \left(c_v T + \frac{u^2}{2} \right) \right] \quad (1.24)$$

$$\frac{\partial H_0}{\partial t} dx = \frac{\partial}{\partial x} \left[(\rho u F) \left(c_v T + \frac{p}{\rho} + \frac{u^2}{2} \right) \right] dx \quad (1.25)$$

Energy equation, after using above expressions, can be rewritten, using the continuity equation and the quantity of motion, in the form:

$$\begin{aligned} \left(\frac{\partial p}{\partial t} + u \frac{\partial p}{\partial x} \right) - a^2 \left(\frac{\partial p}{\partial t} + u \frac{\partial p}{\partial x} \right) - \rho(k-1) \left(q + \frac{\Delta H_{reaction}}{\rho} + uG \right) \\ = 0 \end{aligned} \quad (1.26)$$

where $a = \sqrt{\frac{k \cdot p}{\rho}}$ is the speed of sound, that, for an ideal gas.

$$a = \sqrt{kRT} \quad (1.27)$$

The hyperbolic problem now consists of the equations (1.8), (1.13), (1.26) and the previous $p = \rho RT$; it is written in "non-conservative", a shape suitable to the resolution with the method of characteristics (see Chapter 2).

1.2.4. Formulation of the equations in conservative form.

Substituting equation of motion quantity with the pulse equation, a linear combination of the equation of continuity and that of the quantity of motion, you are obtained:

$$\frac{\partial \rho F}{\partial t} + \frac{\partial (\rho u F)}{\partial x} = 0 \quad \textit{Continuity} \quad (1.28)$$

$$\frac{\partial (\rho u F)}{\partial t} + \frac{\partial (\rho u^2 + p) F}{\partial x} = 0 \quad \textit{Momentum} \quad (1.29)$$

$$\frac{\partial (\rho e_0 F)}{\partial t} + \frac{\partial [\rho u h_0 F]}{\partial x} - \rho q F - \Delta H_{\text{reaction}} F = 0 \quad \textit{Energy} \quad (1.30)$$

This system of equations can be eventually rewritten in matrix form, essential for the implementation and development of numeric type shock-capturing methods that we will study in the next chapters.

We introduce the following carriers:

Conserved variables vector:

$$\mathbf{W} = \begin{bmatrix} \rho F \\ \rho u F \\ \rho e_0 F \end{bmatrix} \quad (1.31)$$

in which there are three groups of independent gas dynamic variables, in turn function of x and t .

Flows vector:

$$\mathbf{F} = \begin{bmatrix} \rho u F \\ (\rho u^2 + p) F \\ \rho u h_0 F \end{bmatrix} \quad (1.32)$$

Source term vector:

$$\mathbf{C} = \begin{bmatrix} 0 \\ -p \frac{dF}{dx} \\ 0 \end{bmatrix} + \begin{bmatrix} 0 \\ \rho G F \\ -(\rho q + \Delta H_{reaction}) F \end{bmatrix} \quad (1.33)$$

So, we can rewrite the hyperbolic system in more compact form:

$$\frac{\partial \mathbf{F}}{\partial t} + \frac{\partial \mathbf{W}}{\partial x} + \mathbf{C} = 0 \quad (1.34)$$

The problem thus posed is not solved, because it consists of a system of three equations in four unknowns represented by the quantities p , ρ , u , and. As has already been done previously, it is introduced the fourth equation is necessary for the closure of the problem and detectable in the fluid behavior.

A first model implemented in computer code, is to perfect gas at constant specific heats. According to this hypothesis, which appears to be very restrictive, the internal energy and the enthalpy of stagnation can be described as follows, as above:

$$e_0 = e + \frac{u^2}{2} = c_v T + \frac{u^2}{2} = \frac{p}{\rho(k-1)} + \frac{u^2}{2} \quad (1.35)$$

$$h_0 = h + \frac{u^2}{2} = c_p T + \frac{u^2}{2} = \frac{kp}{\rho(k-1)} + \frac{u^2}{2} \quad (1.36)$$

the latter allow to rewrite the three vectors \mathbf{W} , \mathbf{F} and \mathbf{C} in the following form:

$$\mathbf{W} = \begin{bmatrix} \rho F \\ \rho u F \\ \left(\frac{p}{k-1} + \rho \frac{u^2}{2} \right) F \end{bmatrix} \quad (1.37)$$

$$\mathbf{F} = \begin{bmatrix} \rho u F \\ (\rho u^2 + p) F \\ u \left(\frac{p}{k-1} + \rho \frac{u^2}{2} \right) F \end{bmatrix} \quad (1.38)$$

$$\mathbf{C} = \begin{bmatrix} 0 \\ -p \frac{dF}{dx} \\ 0 \end{bmatrix} + \begin{bmatrix} 0 \\ \rho G F \\ -(\rho q + \Delta H_{reaction}) F \end{bmatrix} \quad (1.39)$$

A second model implemented in the calculation code, more general than the first, is the one with a mixture of ideal gases. In a real gas, in fact, the specific heat are functions of temperature and chemical composition. The different molecules give different contributions to the specific heat due to the different behavior intramolecular level; the various molecules, in fact, have different vibrational and rotational motions, different electronic motions, different dissociation and ionization. To this is added that the composition of the gas can vary in correspondence of contact discontinuities present in the stream. So, we'll see how the introduction of this model allows the resolution of most of the problems just mentioned, although they should in turn use some restrictive assumptions.

For this type of approach, the system of hyperbolic equations must then be rewritten for each chemical species by replacing the global variables u , p , e , and ρ with those of any chemical species u_j , p_j , e_j , ρ_j , where the partial pressure p_j and the partial density ρ_j are respectively defined as the pressure and density at which you would find the single chemical species j -th if occupied alone the entire volume occupied by the mixture to a prescribed temperature.

Note the equation of the ideal gas state expressions in global terms:

$$P \frac{V}{M} = RT \quad (1.40)$$

and the valid one for each chemical species:

$$P_j \frac{V}{M_j} = RT \quad (1.41)$$

You are obtained by the following relation:

$$\frac{P_j}{P} = X_j = \frac{M_j}{M} \quad (1.42)$$

where X_j is the molar fraction of j-th species.

Proceeding in a similar manner one can derive the definition of the mass fraction Y_j evidently be expressed as:

$$\frac{\rho_j}{\rho} = \frac{M_j}{M} = Y_j \quad (1.43)$$

where M_j is indicated with the mass of the j-th species, and useful to highlight the relationship between the two values, report, however, widely used within the code:

$$X_j = \frac{Y_j / M_{mj}}{\sum_1^{N_s} Y_j M_j} \quad (1.44)$$

It is indicated with N_s the number of chemical species with M_m and their molar mass. For each specie, the value of the pressure is obtained by means of the following report:

$$P_j = \frac{\rho_j}{\sum_1^{N_s} X_j M_j} RT \quad (1.45)$$

The internal energy for each chemical species of a mixture of ideal gases can be defined by an expression of the type:

$$e_j(T) = \sum_{k=1}^N a_{jk} \cdot T^k \quad (1.46)$$

where N is the number of terms of the polynomial development considered to approximate the real evolution of the function and the coefficients a_{jk} are obtained from the literature. The internal energy of the mixture is obtained by a similar interpolation in which the overall coefficients are obtained from a weighted average of the molar fractions of the coefficients relating to each single chemical species:

$$a_{mk} = \sum_{j=1}^{Ns} a_{jk} \cdot X_j \quad (1.47)$$

in which Ns is the number of considered chemical species. After implementation of the code to the second order.

It is therefore evident expression of internal energy:

$$e(T) = a_{1m}T + a_{2m}T^2 \quad (1.48)$$

In differential terms the relationship between internal energy and temperature is:

$$de = c_v(T)dT \quad (1.49)$$

and above equation in integral form becomes:

$$e = \int_0^T c_v(T)dT \quad (1.50)$$

Depending on the model proposed so far you can get the following expressions with which to determine the temperature values and the specific heat at constant volume once known the internal energy value from the hyperbolic system solution (1.28, 1.29, 1.30).

$$T = \left[-a_{1m} + \sqrt{a_{1m}^2 + 4a_{2m}e(T)} \right] \frac{1}{2a_{2m}} \quad (1.51)$$

$$c_v = \frac{de(T)}{dT} = a_{1m} + 2 \cdot a_{2m} \cdot T \quad (1.52)$$

For the determination of the C_v it could also proceed by other means. It 'well known, in fact, that in the case of monatomic gases, this is obtainable according to the following expression:

$$c_{v1D} = \frac{3}{2}R + \frac{n}{2}R + \sum_{j=1}^{N_M} C_{jvibrate} \quad (1.53)$$

where N_M is the number of vibration modes of the molecule.

This expression has been created knowing that in this case the $c_v(T)$ is equal to $3/2R$, where 3 is the number of translational degrees of freedom of the molecule, which we must add $n*(1/2)R$, with n equal to the number of rotational degrees of freedom on which the molecule can distribute their energy. It is finally considered the possibility on the part of the molecule to distribute the energy absorbed in the vibrational modes, function and properties of the temperature determined by the Einstein relationship:

$$C_{jvibrate} = \frac{u^2 e^u}{(e^u - 1)} R \quad (1.54)$$

where:

$$u = \frac{h\nu}{kT} \quad (1.55)$$

$$\nu = \sqrt{\frac{K}{M}} \quad (1.56)$$

where:

e = constant

h = plank constant

k = Boltzmann constant

M = mass associated with the vibration mode

K = stiffness associated to the mode of vibration

ν = natural frequency associated with the mode of vibration

It is however still of an approximate expression in which interactions between the molecules are exclusively of the elastic type and in which it does not consider the dependence on the gas pressure. This dependence, linked to the fact that the molecules have their own volume is not null and that there are of the electromagnetic type relationships between them, becomes

negligible, however, significantly by virtue of high temperatures existing inside the ducts of the engine speed. This simplification allows to greatly relieve the computational cost of the simulations, in fact, in the calculation program are numerous cases in which use the constant $K = \frac{c_v + R}{c_v}$ to switch from internal temperature or vice versa without yet knowing the pressure. In order to take into account the influence of this variable, it should make convergent iterative cycles to the solution every time.

It is also noted that the temperature and pressure fields, in which we operate, allow us to consider the value of the unit of compressibility coefficient, which allows us to use the state equations without any modifications.

In the light of what has been said we could calculate the specific heat c_v making use of views reports for each chemical species, or using polynomial relations, available in the literature, which define the behavior of a real gas as a function of temperature. The current code was developed following the latter possibility, approximating polynomial such relations with relations of the second order, in such a way as not to make excessive the computational burden. So, we can rewrite the hyperbolic problem in the case of mixture of ideal gases. Putting the equations (1.47) and (1.48), written for all chemical species, with (1.45) we obtain the following equations N_s :

$$\begin{cases} e_j(T) = \sum_{k=1}^N a_{jk} \cdot T^k \\ P_j = \frac{\rho_j}{M_{mj}} R \cdot T \end{cases} \Rightarrow P_j = P_j(\rho_j, e_j) \quad j = 1, N_s \quad (1.57)$$

For each chemical species, it will be possible to rewrite the hyperbolic equations but merely refer to the partial quantities.

With this amendment, it is now possible to consider the molecular diffusion of different chemical species. The formula of the conservation of mass becomes:

$$\frac{\partial \rho Y_j F}{\partial t} + \frac{\partial (\rho_j u Y_j F)}{\partial x} = \omega_j \quad (1.58)$$

in which u_j is the velocity of the j th chemical species, while ω_j is the rate of disappearance per unit of volume [kg/m³s] of the j -th species which takes account of chemical reactions. That period is calculated for each species and depends on the kinetics of the various reactions that

take place in the catalyst and in the first exhaust ducts where there is the phenomenon of post oxidation. So, we get:

$$\frac{\partial W_j}{\partial t} + \frac{\partial F_j}{\partial x} + C_j = 0 \quad (1.59)$$

where:

$$W_j = \begin{bmatrix} \rho_j F \\ \rho_j u_j F \\ \rho_j e_0 F \end{bmatrix} \quad (1.60)$$

$$F_j = \begin{bmatrix} \rho_j u_j F \\ (\rho_j u_j^2 + p_j) F \\ \rho_j u_0 h_{0,j} F \end{bmatrix} \quad (1.61)$$

$$C_j = \begin{bmatrix} 0 \\ -p_j \frac{dF}{dx} \\ 0 \end{bmatrix} + \begin{bmatrix} \omega_j \\ \rho_j G_j F \\ -(\rho_j q_j + \Delta H_{reaction,j}) F \end{bmatrix} \quad (1.62)$$

The problem at this point, it would seem closed, having 4Ns equations in 4Ns unknowns ρ_j , u_j , e_j , p_j .

however, it should be introduced into the vector C_j of the sources (via G_j and q_j) the forces and of mechanical origin powers (elastic collisions) and heat exchanging the various gases constituting the mixture, and which are obtainable through a complex model that takes account of the different molecular weights as well as the diffusion of the various chemical species. The powers exchanged for electromagnetic interactions would still be neglected, because the ideal gas model, as already mentioned, does not provide for the existence of such forces. To simplify the problem, then you are using the following approach, based on the estimate of the velocity of the center of mass.

It is not possible to define a velocity 'u' of the mixture, even though there has u_j the speed relating to each component defined.

In the presence of temperature gradients, concentration and pressure along the axis of the duct, each species changes its distribution in space based on convection phenomena, molecular and thermal diffusion governed by different constants for each species and dependent on weight and by molecular complexity.

Neglecting thermal diffusion phenomena, the flow of a component is given by two distinct processes: a convective and a diffusive type.

For the first phenomenon of gas molecule acquires speed due to disturbing external action such as the pressure gradient, the molecule according to the phenomenon moves by the action of internal forces to the mixture, generated by random collisions with other molecules.

The speed of the center of mass can be defined using the following media:

$$u_c = \sum_{j=1}^{N_s} \frac{\rho_j u_j}{\rho} \quad (1.63)$$

One can then define the diffusive flux of the j-th species such as:

$$J_j = \rho_j (u_j - u_c) \quad (1.64)$$

It 'so obvious that the j-th species does not diffuse if its speed coincides with that of the center of mass defined above.

We call Φ_j with the flow of molecules of the j-th species that cross the section A of the duct because of the two distinct processes:

$$\Phi_j = \Phi_j^D + \Phi_j^C = n_j u_j A \quad (1.65)$$

where Φ_j is a flow rate in terms of number of molecules in the unit time and n_j represents the number of molecules per unit volume. And possible to demonstrate that the contributions due to convection and diffusion molecular have the following expressions:

$$\Phi_j^D = C_j \cdot X_j \quad (1.66)$$

$$\Phi_j^C = -D_j \frac{dX_j}{dx} \quad (1.67)$$

where X_j is the molar fraction of j-th species, while:

$$D_j = \mu_j \cdot T \cdot R \cdot N \quad \text{and} \quad C_j = \mu_j \cdot F \cdot N \cdot N_0 \quad (1.68)$$

where:

N = number of moles contained in the control volume;

N_0 = Avogadro constant;

T = temperature in Kelvin;

F = intensity of the external force (given by the pressure gradient);

$$\mu_j \propto \frac{\tau}{M_{mj}} \quad (1.69)$$

τ = mean time between two molecular collisions;

M_{mj} = molecular mass of the species j .

Then comparing the characteristic times of the diffusive phenomenon with those of convective transport, that the first phenomenon occurs much more slowly than the second, so its effects may be neglected. In this way, the speed of each single species is described by the following equality:

$$u_j = \frac{\Phi_j^c}{A n_j} = \mu_j F \quad (1.70)$$

It should be noted that this speed is different from species to species owing to the different m_j mobility. Thus, further simplifying the problem, it was decided to evaluate the speed of each species coinciding with that of the center of mass of the mixture:

$$u_j = u_c = u \quad j = 1, N_s \quad (1.71)$$

This last hypothesis involves neglect of surface forces between the various species as there is no relative motion between them. We can now rewrite the three conservation equations in global terms for the mixture, with the introduction of speed of the center of mass. In vector form:

$$\frac{\partial \mathbf{W}_m}{\partial t} + \frac{\partial \mathbf{F}_m}{\partial x} + \mathbf{C}_m = 0 \quad (1.72)$$

Where:

$$\begin{aligned} \mathbf{W}_m &= \begin{bmatrix} \rho F \\ \rho u_c F \\ \rho e_0 F \end{bmatrix} \quad \mathbf{F}_m = \begin{bmatrix} \rho u F \\ (\rho u_c^2 + p) F \\ \rho u_c h_0 F \end{bmatrix} \quad \mathbf{C}_m \\ &= \begin{bmatrix} 0 \\ -p \frac{dF}{dx} \\ 0 \end{bmatrix} + \begin{bmatrix} 0 \\ \rho G F \\ -(\rho q + \Delta H_{reaction}) F \end{bmatrix} \end{aligned} \quad (1.73)$$

To these three equations are flanked by (N_s-1) scalar continuity equations for the single chemical species, resulting from the writing of the first vector line equation (1.59):

$$\frac{\partial \mathbf{W}_j}{\partial t} + \frac{\partial \mathbf{F}_j}{\partial x} + \mathbf{C}_j = 0 \quad (1.74)$$

where terms \mathbf{W}_j , \mathbf{F}_j and \mathbf{C}_j are:

$$\mathbf{W}_j = [\rho Y_j F] \quad \mathbf{F}_j = [\rho u Y_j F] \quad \mathbf{C}_j = [-\omega_j] \quad (1.75)$$

and correspond to the mass conservation equations for each chemical species to less than one, which is dictated by the other according to the following:

$$\sum_{j=1}^{N_s} Y_j = 1 \quad (1.76)$$

that is the equation of continuity of the global N_s species.

We get then, for incoming carriers in the full matrix system, the following expressions:

$$\mathbf{W}_m = \begin{bmatrix} \rho F \\ \rho u_c F \\ \rho e_0 F \\ \rho Y F \end{bmatrix} \quad \mathbf{F}_m = \begin{bmatrix} \rho u F \\ (\rho u_c^2 + p) F \\ \rho u_c h_0 F \\ \rho u Y F \end{bmatrix} \quad (1.77)$$

$$\mathbf{C}_m = \begin{bmatrix} 0 \\ -p \frac{dF}{dx} \\ 0 \\ 0 \end{bmatrix} + \begin{bmatrix} 0 \\ \rho G F \\ -(\rho q + \Delta H_{reaction}) F \\ -\omega_j \end{bmatrix} \quad \mathbf{Y} = \begin{bmatrix} Y_1 \\ Y_2 \\ \vdots \\ Y_{N_s-1} \end{bmatrix} \quad (1.78)$$

The remaining two vector equation scalar equations (1.59) should not be considered because of the hypothesis made according to which all the chemical species have the same speed equal to that of the center of mass.

Then it is recalled that a mixture of ideal gases can be regarded as a single ideal gas with appropriate molar mass. We will make use of the following equation:

$$p = \rho \frac{R}{\sum_{j=1}^{Ns} X_j M_{mj}} T$$
$$\sum_{j=1}^{Ns} Y_j = 1$$
(1.79)

‘T’ is obtained by the expression of internal energy:

$$e_j(T) = \sum_{k=1}^N a_{jk} \cdot T^k \quad ; \quad X_j = \frac{Y_j / M_{mj}}{\sum_1^{Ns} Y_j M_j}$$
(1.80)

Chapter: 2

2. Numerical Methods

2.1. Introduction:

Generally, it is not possible to determine an analytical solution of the hyperbolic system to the determined partial derivatives in the previous paragraph. The first step in the determination of the solution of similar problems was studied by Riemann in 1858 with the development of the method of characteristics, whose peculiarity lies in the fact of being able to switch from partial differential equations to equations with ordinary derivatives. Over the years the method has been perfected for the treatment of compressible fluids and, in the second half of the 19th century to the present day, has had a wide application in the field of modeling of fluid dynamic processes in internal combustion engines. The main limitations of the method of characteristics are essentially three:

- *Assumption of perfect gas model with constant specific heats;*
- *Linear approximation: the space-time domain is discretized through a calculation grid in the plane (x, t) and the solution is determined between the successive nodes with an accuracy of the first order;*
- *Discontinuities in the solution: the method is unable to grasp properly any discontinuities in the solution, as the typical case of shock waves, distributing the phenomenon on many nodes of the grid.*

Despite these limitations and although passed by the more robust and accurate numerical methods developed subsequently, the method of characteristics is still used in the calculation codes for the modeling of the boundary conditions.

Since the '90s began the application to the computer codes of a new family of methods, called Shock-Capturing. They determine the hyperbolic system solution based on his conservative form and allow you to capture successfully any shockwaves or discontinuities of the chemical/thermal contact in the gas stream.

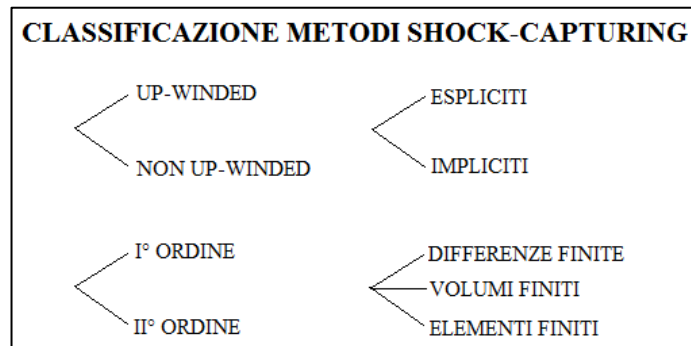


Figure 2.1: Classification of Shock-Capturing numerical methods.

The different pattern of calculation adopted, up-winded or not up-winded, involves achieving significantly different results. The up-winded methods orient the calculation scheme as a function of the direction of flow with excellent results, at the expense of a high computational burden because the Riemann problem is solved in each node of the discretization. Differently, the methods not up-winded always apply the same type of calculation scheme, not realizing the flow direction, but despite this they are obtained with reliable results and is the type of favorite methods if it required a compromise between performance and Rates of limited calculation. Unfortunately, accuracies higher than the first order lead to problems of spurious oscillations in the solution. It is therefore essential to the application of particular algorithm be able to mitigate this phenomenon [2] [3].

2.1.1. The Method of Characteristics:

The method of characteristics is based on the ability to transform partial differential equations into equations to ordinary derived along particular traceable line in the flow field, calls characteristic lines. To directly seize the principle behind the method is appropriate to use a graphical approach. You think you have an equation in the form $c = c(x, t)$, it can represent a generic surface in the space (x, t, c) , as shown in fig. 2.2, and its numerical value is given by the height of the surface above the plane $c=0$.

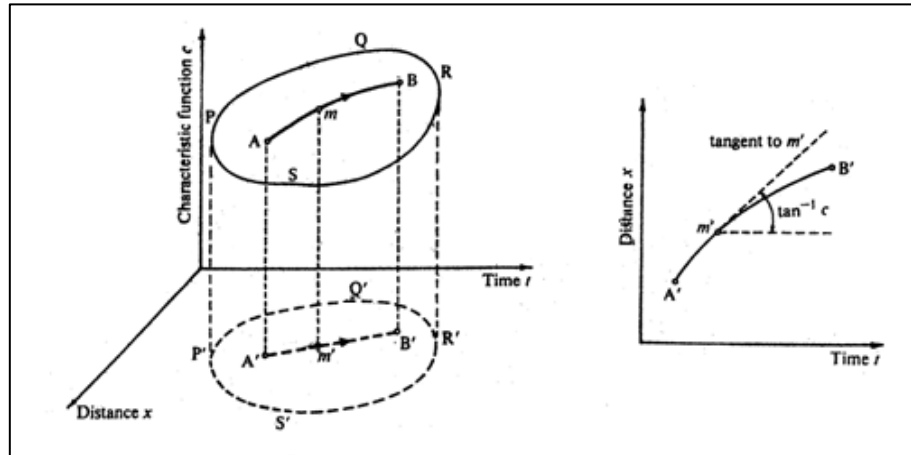


Figure 2:2 Graphical Method of Characteristics interpretation.

Consider a line AB on the surface in question and its projection A'B' on the plane $c = 0$. AB is said characteristic line if, in any of its point, the value of the angular coefficient of the tangent to A'B' is equal to the value assumed by the equation $c = c(x, t)$ in the same point, that is, if:

$$\left(\frac{dx}{dt}\right)_{m'} = \overline{mm'} = c(x, t)_{m'} \quad (2.81)$$

The application of this method to the specific case of the modeling of compressible flow in a conduit, provides for the use of the hyperbolic system of partial differential written in non-conservative form, already introduced in chapter 1 and expressed as following:

$$\frac{\partial \rho}{\partial t} + \frac{\partial(\rho u)}{\partial x} + \frac{\rho u}{F} \frac{dF}{dx} = 0 \quad (2.82)$$

$$\frac{\partial u}{\partial t} + u \frac{\partial u}{\partial x} + \frac{1}{\rho} \frac{dp}{dx} + G = 0 \quad (2.83)$$

$$\left(\frac{\partial p}{\partial t} + u \frac{\partial p}{\partial x}\right) - a^2 \left(\frac{\partial p}{\partial t} + u \frac{\partial p}{\partial x}\right) - (k-1)(\rho \dot{q} - \Delta H_{rec} + \rho u G) = 0 \quad (2.84)$$

Through a suitable linear combination of eq. 2.82-2.83-2.84 that make up the hyperbolic system, it is possible to arrive at a shape that highlights the following quantities: $(u+a)$, $(u-a)$ and u .

$$\begin{aligned} \left(\frac{\partial p}{\partial t} + (u + a) \frac{\partial p}{\partial x}\right) + \rho a \left(\frac{\partial u}{\partial t} + (u + a) \frac{\partial u}{\partial x}\right) \\ - (k - 1)(\rho \dot{q} - \Delta H_{rec} + \rho u G) + a^2 \frac{\rho u}{F} \frac{dF}{dx} + \rho a G = 0 \end{aligned} \quad (2.85)$$

$$\begin{aligned} \left(\frac{\partial p}{\partial t} + (u - a) \frac{\partial p}{\partial x}\right) - \rho a \left(\frac{\partial u}{\partial t} + (u - a) \frac{\partial u}{\partial x}\right) \\ - (k - 1)(\rho \dot{q} - \Delta H_{rec} + \rho u G) + a^2 \frac{\rho u}{F} \frac{dF}{dx} - \rho a G = 0 \end{aligned} \quad (2.86)$$

$$\left(\frac{\partial p}{\partial t} + u \frac{\partial p}{\partial x}\right) - a^2 \left(\frac{\partial p}{\partial t} + u \frac{\partial p}{\partial x}\right) - (k - 1)(\rho \dot{q} - \Delta H_{rec} + \rho u G) = 0 \quad (2.87)$$

To simplify writing, condense the terms source appearing in the equations:

$$\Delta_1 = -(k - 1)(\rho \dot{q} - \Delta H_{rec} + \rho u G) \quad (2.88)$$

$$\Delta_2 = a^2 \frac{\rho u}{F} \frac{dF}{dx} \quad (2.89)$$

$$\Delta_3 = \rho a G \quad (2.90)$$

The terms Δ_1 , Δ_3 are dissipative nature and take on values greater than zero if the flow is not isentropic, with friction and heat exchange with the walls. On the contrary, the term Δ_2 is conservative and depend on the variation of the section along the axis of the duct.

Now you can rewrite the system in a more compact form:

$$\left(\frac{\partial p}{\partial t} + (u + a) \frac{\partial p}{\partial x}\right) + \rho a \left(\frac{\partial u}{\partial t} + (u + a) \frac{\partial u}{\partial x}\right) + \Delta_1 + \Delta_2 + \Delta_3 = 0 \quad (2.91)$$

$$\left(\frac{\partial p}{\partial t} + (u - a) \frac{\partial p}{\partial x}\right) - \rho a \left(\frac{\partial u}{\partial t} + (u - a) \frac{\partial u}{\partial x}\right) + \Delta_1 + \Delta_2 - \Delta_3 = 0 \quad (2.92)$$

$$\left(\frac{\partial p}{\partial t} + u \frac{\partial p}{\partial x}\right) - a^2 \left(\frac{\partial p}{\partial t} + u \frac{\partial p}{\partial x}\right) + \Delta_1 = 0 \quad (2.93)$$

The term in parentheses of Eq. 2.91, 2.92 and 2.93, are nothing more than the ordinary differential of the independent variables p , u , ρ measured along the lines traceable features along the plane (x, t) and with a slope dependent on the properties of the unsteady flow. For example,

if the speed of propagation of a pressure wave within a fluid in movement is defined as $(u+a)$, then the following relation is valid:

$$\frac{dp(x(t), t)}{dt} = \left(\frac{\partial p}{\partial t} + \frac{\partial x}{\partial t} \cdot \frac{\partial p}{\partial x} \right) = \left(\frac{\partial p}{\partial t} + (u + a) \frac{\partial p}{\partial x} \right) \quad (2.94)$$

Clarified this concept, it is easy to determine the slope of the characteristic lines on which it will be possible to transform the above equations in differential equations to ordinary derivatives.

The following equations define the characteristics lines for the equations of the previous system, traceable lines continuously in the plane (x, t) .

$$\frac{dx}{dt} = u + a \text{ absolute velocity of progressive wave} \quad (2.95)$$

$$\frac{dx}{dt} = u - a \text{ absolute velocity of regressive wave} \quad (2.96)$$

$$\frac{\square x}{dt} = u \text{ flow line velocity} \quad (2.97)$$

The first 2 lines are linked to the characteristics propagation nature of the wave motion in the ducts, since the terms $(u+a)$ and $(u-a)$ represent the absolute speed of propagation of pressure waves; the third line is instead correlated to the motion of fluid particles, and provides information on the level of entropy in the ducts. An effective graphic representation is shown in fig. 2.3.

The single feature line represents the separation between two regions of the plan, in which the fluid-dynamic properties differ in infinitesimal quantities; they therefore constitute discontinuities for the derived quantities, for example the speed, but not for the fluid. On the three lines, described by eq. 2.95, 2.96 and 2.97, apply relations (see eq. 2.94) that allow you to transform eq. 2.91, 2.92 and 2.93 in the equations to ordinary derivatives, also known as compatibility equations.

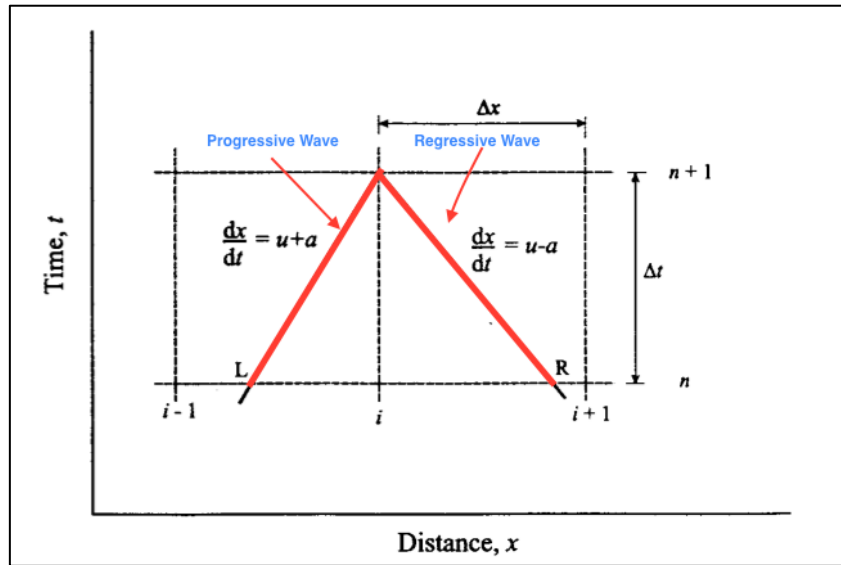


Figure 2:3 Tracking of characteristic lines in the (x, t) discretized.

Without introducing any approximation, you can rewrite the system through compatibility equations, or equations to ordinary derivatives:

$$\frac{dp}{dt} + \rho a \frac{du}{dt} + \Delta_1 + \Delta_2 + \Delta_3 = 0 \quad (2.98)$$

$$\frac{dp}{dt} - \rho a \frac{du}{dt} + \Delta_1 + \Delta_2 - \Delta_3 = 0 \quad (2.99)$$

$$\frac{dp}{dt} - a^2 \frac{d\rho}{dt} + \Delta_1 = 0 \quad (2.100)$$

To simplify the discussion, it develops the case of isentropic flow in ducts with a constant section. In these conditions, the terms source $\Delta_1, \Delta_2, \Delta_3$ is cancel and compatibility equations become:

$$dp + pa \cdot du = 0 \quad (2.101)$$

$$dp - pa \cdot du = 0 \quad (2.102)$$

$$dp - a^2 \cdot d\rho = 0 \quad (2.103)$$

it is also appropriate to the isentropic transformation relations:

$$\frac{p}{\rho^k} = const \quad (2.104)$$

$$\frac{\rho}{a^{2/k-1}} = const \quad (2.105)$$

Differentiating 2.106 relationships, 2.105 and placing them in Eq. 2.101, 2.102 is obtained:

$$du + \frac{2}{k-1} da = 0 \quad (2.106)$$

$$du - \frac{2}{k-1} da = 0 \quad (2.107)$$

From these one obtains the differential of the sound velocity compared to the flow velocity, obtaining:

$$\frac{da}{du} = -\frac{k-1}{2} \quad (2.108)$$

$$\frac{da}{du} = +\frac{k-1}{2} \quad (2.109)$$

The eq. 2.108, 2.109 accompanied of the respective equations of the characteristics lines (eq. 2.95, 2.96) can be represented on the planes (x, t) and (u, a), shown in Fig. 2.4, which are named respectively:

- *Location diagram: on which lines features are represented (eq. 2.95, 2.96);*
- *State diagram: on which the differentials are represented in the speed of sound relative to the flow velocity.*

They introduce 2 families of curves to identify the curves associated progressive wave (λ) and those associated with the regressive (β):

$$\lambda \rightarrow \begin{cases} \frac{du}{dt} = u + a \\ \frac{da}{du} = -\frac{k-1}{2} \end{cases} \quad \beta \rightarrow \begin{cases} \frac{du}{dt} = u - a \\ \frac{da}{du} = +\frac{k-1}{2} \end{cases}$$

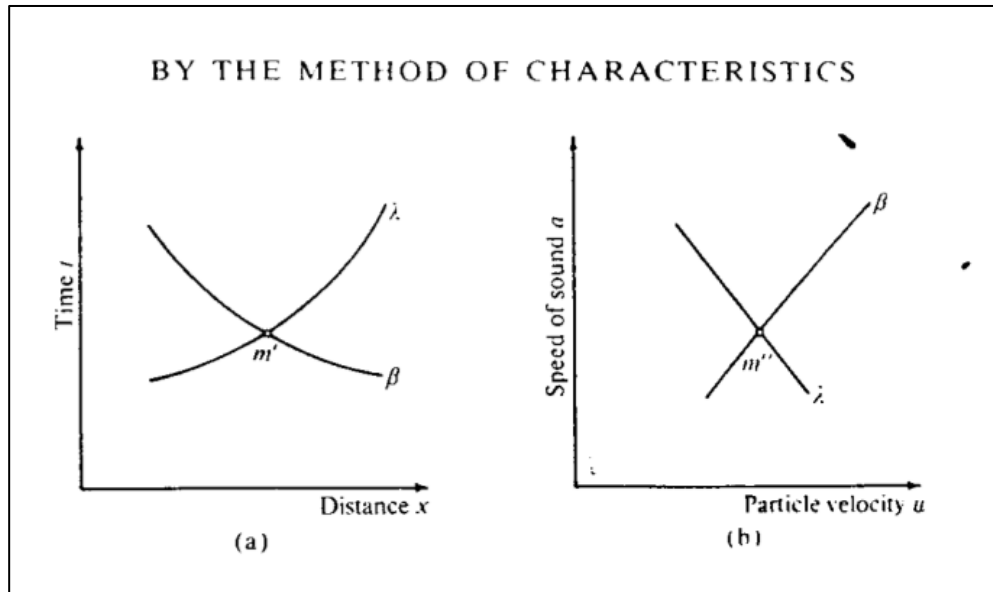


Figure 2:4: Position diagram (a) and state (b) for the families of λ and β curves.

The solution can be determined graphically by the intersection of the two families of characteristic curves.

Rewriting eq. 2.108, 2.109 as:

$$d\left(u + \frac{2}{k-1}a\right) = 0 \rightarrow \lambda \tag{2.110}$$

$$d\left(u - \frac{2}{k-1}a\right) = 0 \rightarrow \beta \tag{2.111}$$

we realize that the words in brackets of 2 equations are constant along the characteristic lines and define the Riemann invariants J_+ and J_- .

$$J_+ = u + \frac{2}{k-1}a \quad \text{cuts down} \rightarrow \lambda \tag{2.112}$$

$$J_- = u - \frac{2}{k-1} a \quad \text{cuts down} \rightarrow \beta \quad (2.113)$$

The terms Δ source assume a non-null value, the invariants of Riemann become the Riemann variables and takes the curvature of the lines drawn on the state diagram.

Up to this point it is not any approximation, but they are only manipulated with the initial equations to arrive at a formulation suitable to the resolution through numerical approach.

Before going into the actual numerical method, we should define new variables:

$$A = \frac{a}{a_{ref}} \quad \text{Non - dimensional speed of sound.} \quad (2.114)$$

$$U = \frac{u}{a_{ref}} \quad \text{Non - dimensional speed of gas.} \quad (2.115)$$

$$A_A = \frac{a_A}{a_{ref}} \quad \text{Non - dimensional speed of sound related to gas} \quad (2.116)$$

$$Z = \frac{a_{ref}}{x_{ref}} \quad \text{Non - dimensional time.} \quad (2.117)$$

$$X = \frac{x}{x_{ref}} \quad \text{Non - dimensional length.} \quad (2.118)$$

where a_{ref} , p_{ref} , x_{ref} are a constant reference values, appropriately chosen for the calculation, whose physical interpretation is instant referring to the following diagram:

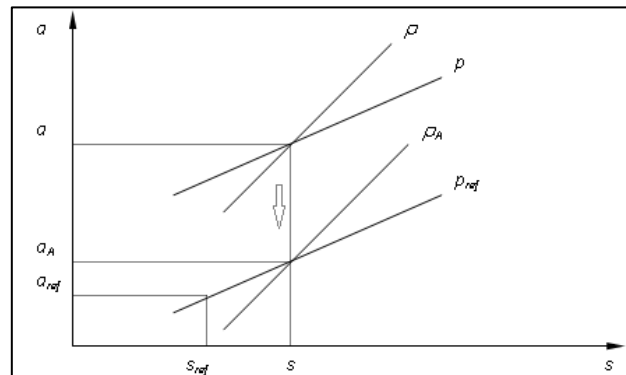


Figure 2.5 :a-s diagram on which it is possible to recognize the reference values of: the speed of sound, pressure and entropy.

On the diagram of Fig. 2.5, you can define the speed of a_A sound. Starting from the local conditions of p , ρ and hence the speed of sound in, it performs an expansion processing (or compression) isentropic up to the reference pressure p_{ref} which corresponds to the speed of sound a_A .

The fictitious transformation is isentropic, so you can write the classic relations:

$$\frac{p}{p_{ref}} = \left(\frac{a}{a_A}\right)^{\frac{2k}{k-1}} \quad (2.119)$$

$$\frac{\rho}{\rho_A} = \left(\frac{p}{p_{ref}}\right)^{\frac{1}{k}} \quad (2.120)$$

In general, for a flow non-isentropic, the value of entropy 's' of the initial state is different from s_{ref} therefore a_A is distinct from a_{ref} isobaric of p_{ref} reference. One senses that the a_A magnitude is related to the entropy of the A_A variable, which represents the entropy level of the gas relative to the reference condition local and especially dynamic gas state, can be immediately related to the entropy variation $\Delta s = s - s_{ref}$.

Isobaric infinitesimal long increment in entropy gives us:

$$ds_{p=const} = \frac{dh}{T} = c_p \frac{dh}{h} \quad (2.121)$$

knowing that the enthalpy and its infinitesimal variation can be expressed in function of the speed of sound:

$$h = c_p T = \frac{kRT}{k-1} = \frac{k}{k-1} \cdot \frac{p}{\rho} = \frac{a^2}{k-1} \quad (2.122)$$

$$\frac{dh}{h} = \frac{2da}{a} \quad (2.123)$$

we obtain a new expression for eq. 2.41:

$$ds_{p=const} = \frac{dh}{T} = 2c_p \frac{da}{a} \quad (2.124)$$

The link between entropy and the speed of sound can be expressed in integral form and dimensionless by:

$$A_A = \frac{a_A}{a_{ref}} = e^{\frac{(s-s_{ref})}{2c_p}} \quad (2.125)$$

Continuing the discussion, they introduce the Riemann variables as dimensionless calling λ and β :

$$\lambda = A + \frac{k-1}{2}U \quad \text{cuts down line } \left(\frac{dX}{dZ}\right)_\lambda = U + A \quad (2.126)$$

$$\beta = A - \frac{k-1}{2}U \quad \text{cuts down line } \left(\frac{dX}{dZ}\right)_\beta = U - A \quad (2.127)$$

In the presence of isentropic flow, λ and β assume constant values, becoming the invariants of Riemann, while in the opposite case their variation along the characteristic lines is expressed as:

$$d\lambda = dA + \frac{k-1}{2}dU \quad (2.128)$$

$$d\beta = dA - \frac{k-1}{2}dU \quad (2.129)$$

The quantities $d\lambda$ and $d\beta$ are determined by the compatibility equations (eq.2.101-102-103), in dimensionless form and rearranged, and the direction of equations.

Following solved equations are applied to the three characteristics families:

- λ Characteristic (traveling wave)

Equation direction:

$$\left(\frac{dX}{dZ}\right)_\lambda = U + A \quad (2.130)$$

Compatibility Equation:

$$\begin{aligned}
 d\lambda = & -\frac{(k-1) \cdot (AU)}{2} \cdot \left(\frac{1}{F} \frac{df}{dX}\right) dZ \\
 & - \frac{(k-1) 2x_{ref} f}{2 D} U^2 \frac{U}{|U|} \left[1 - (k-1) \frac{U}{A}\right] dZ \\
 & + \frac{(k-1)^2 \dot{q}x_{ref}}{2 a_{ref}^3} \frac{1}{A} dZ + \frac{A}{A_A} dA_A
 \end{aligned} \tag{2.131}$$

- β Characteristic (regressive wave)

Equation direction:

$$\left(\frac{dX}{dZ}\right)_{\beta} = U - A \tag{2.132}$$

Compatibility Equation:

$$\begin{aligned}
 d\beta = & -\frac{(k-1) \cdot (AU)}{2} \cdot \left(\frac{1}{F} \frac{df}{dX}\right) dZ \\
 & + \frac{(k-1) 2x_{ref} f}{2 D} U^2 \frac{U}{|U|} \left[1 - (k-1) \frac{U}{A}\right] dZ \\
 & + \frac{(k-1)^2 \dot{q}x_{ref}}{2 a_{ref}^3} \frac{1}{A} dZ + \frac{A}{A_A} dA_A
 \end{aligned} \tag{2.133}$$

- Trajectory Feature (flow line or path line)

Equation direction:

$$\left(\frac{dX}{dZ}\right) = U \tag{2.134}$$

Compatibility Equation:

$$dA_A = \frac{(k-1) A_A}{2 A^2} \left(\frac{2x_{ref} f}{D} |U^3| + \frac{\dot{q}x_{ref}}{a_{ref}^3}\right) dZ \tag{2.135}$$

In the first two compatibility equations (eq. 2.131-2.133) it is observed that changes in variables Riemann, $d\lambda$ and $d\beta$, depend on four basic terms due respectively to the change of section of the pipe, friction, heat exchange and the entropy change.

$$d(\lambda, \beta) = \delta_{section} + \delta_{friction} + \delta_{heat} + \delta_{entropy} \quad (2.136)$$

In the third equation of compatibility, the increase of entropy level depends only from the contributions due to friction and heat exchanges.

$$dA_A = \delta_{friction} + \delta_{heat} \quad (2.137)$$

Now consider the physical features of the *Method of Characteristics*.

In a compressible and unsteady flow, the conditions, in a given section are determined by the mass transport rate and the pressure perturbations that propagate at the speed of sound through the fluid itself. As shown in fig. 2.6, in a generic section of the pipe at time $t+\Delta t$ P of the flow conditions can be influenced only by the states of the gas relative to the previous time t , i.e the points C, D and F. The lines connecting the points P to C, D and F represent characteristic lines in the plane (x,t) and their inclination depends on the absolute speed of sound of the gas in this point

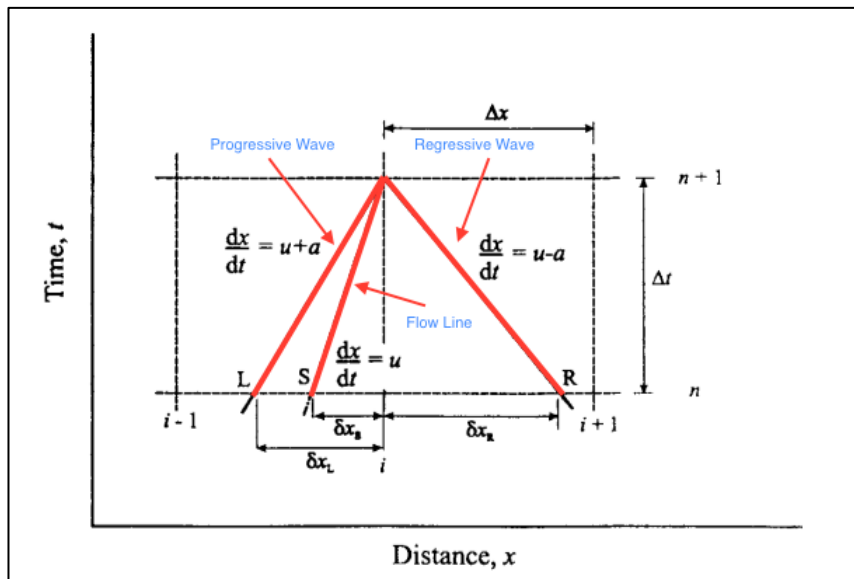


Figure 2:6 Influence of the flow conditions at time $t+\Delta t$ in a given section of the duct.

Operationally, we proceed in the following way: notes the *Riemann variables* at time Z , is the change in entropy through the equation of the flow line 2.135, and then the variations along the lines of the characteristics of *Riemann variables* through the 2.131 compatibility equations and 2.133. It is thus possible to determine the new value of the *Riemann variables* at time $Z + \Delta Z$ in the following way:

$$\lambda_{Z+\Delta Z} = \lambda + \Delta\lambda \quad (2.138)$$

$$\beta_{Z+\Delta Z} = \beta + \Delta\beta \quad (2.139)$$

At this point the solution is determined through deriving from the relations eq 2.126 and 2.127:

$$A = \frac{\lambda + \beta}{2} \quad (2.140)$$

$$U = \frac{\lambda - \beta}{k - 1} \quad (2.141)$$

Is now introduced to the *Method of Characteristics to mesh*, namely it adopts a numerical method for the estimation of the analytical solution.

In the *Method of Characteristics to mesh*, belonging to the family of explicit methods, the points of intersection of the characteristic lines have a known position and defined in the (x, t) . To discretize the space-time domain using a rectangular grid computing with the following features:

SPACE: discretization along the x coordinate is fixed according to the number of mesh, or sub-elements, with which the duct is divided. For a number of the sub-elements correspond $l+1$ compute nodes. Increasing computing nodes, thereby reducing the size of the mesh, you will get more accurate results.

TIME: the size of the time step is determined based on the condition of stability dictated by the policy CFL (*Courant-Friedrichs-Lewy*). Considering the finite propagation velocity of a wave of pressure in a conduit such as the speed of sound in added to the flow velocity u , the distance traveled by the wave in the time of Δt calculation step must be less than the size of the mesh Δx . It therefore introduces the *CFL number*:

$$CFL = (a + |u|) \frac{\Delta t}{\Delta x} \leq 1 \quad (2.142)$$

$$CFL = (A + |U|) \frac{\Delta Z}{\Delta X} \leq 1 \quad (2.143)$$

In order for all the nodes belonging to the grid at the time $Z+\Delta Z$ from falling into the domain of influence the CFL has to assume values ≤ 1 .

The calculation of the *Riemann variables* and tracking features lines are made only in the grid nodes at each time step, as shown in the following figure:

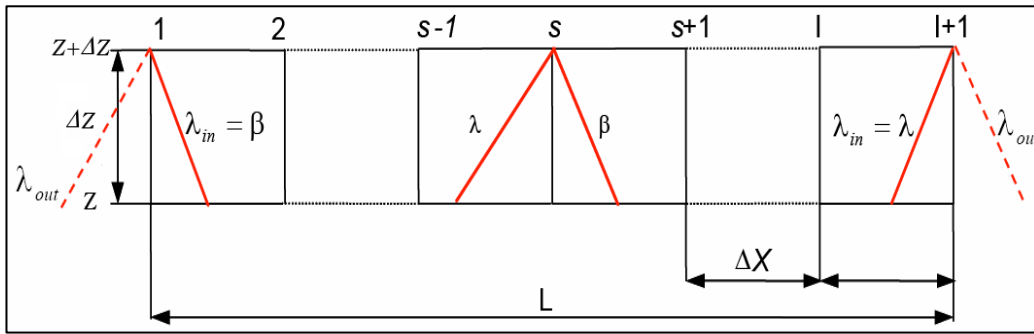


Figure 2.7 Grid space-time used for the calculation of the Riemann variables with the method of characteristics

Now rename the *Riemann variables* as: λ_I corresponding to λ and λ_{II} corresponding to β ; this allows a generalization that simplifies the calculation procedure.

Note the values of the three variables λ_I , λ_{II} , A_A in each mesh point of the duct at the dimensionless time Z , it determines the time step ΔZ , according to the criterion of the CFL so as to define the calculation grid at time $Z + \Delta Z$. For the tracking characteristics of the lines to the new time step we proceed back in time, ie the two families of λ_I and λ_{II} lines are drawn from each node of the mesh at the time $Z + \Delta Z$, as shown in fig. 2.8.

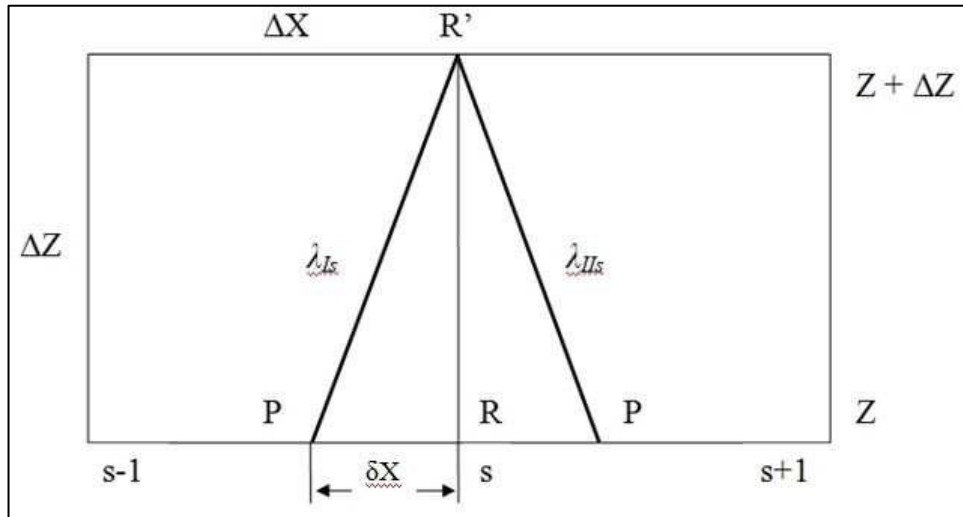


Figure 2.8 Tracking feature lines back in time, starting from the node s in $Z+\Delta Z$ (point R') up to the P points to the time Z .

The two characteristic lines intersect the abscissa axis at the time Z in two points L and R , distinct from the nodes. The slope of the lines is held constant but in reality, they are curved and then introduces an approximation. The smaller is the size of the calculation grid and the lower the numerical error associated with this approximation. In addition to the characteristics lines it is also track the flow line that intersects the axis of the space at the point S .

It is shown that the position of the points L and R on the mesh (Fig. 2.8) can be calculated from the known values of λ_I and λ_{II} in adjacent nodes, for brevity it will only show the calculation of the position of the point L , as regard R is completely analogous process.

λ_I being the progressive characteristic curve, the following relationship:

$$\frac{\delta X_L}{\Delta Z} = U_L + A_L \quad (2.144)$$

Using eq. 2.140 and 2.141 and drifting the 2.144 you get:

$$\frac{\delta X_L}{\Delta Z} = a\lambda_{I_L} + b\lambda_{II_L} \quad (2.145)$$

where a, b represents two constants dependent on the nature of the gas:

$$a = \frac{k + 1}{2(k - 1)} \quad (2.146)$$

$$b = \frac{3 - k}{2(k - 1)} \quad (2.147)$$

- λ_I the point L is determined by linear interpolation between the known values of the same magnitude in the i and i-1 nodes:

$$\lambda_{I_L} = \lambda_{I_i} - \frac{\delta X_L}{\Delta X} (\lambda_{I_i} - \lambda_{I_{i-1}}) \quad (2.148)$$

- λ_{II} at the point L it is determined in a similar manner to λ :

$$\lambda_{II_L} = \lambda_{II_i} - \frac{\delta X_L}{\Delta X} (\lambda_{II_i} - \lambda_{II_{i-1}}) \quad (2.149)$$

Replacing the 2.148 and the 2.149 in 2.145 is finally obtained:

$$\frac{\delta X_L}{\Delta X} = \frac{a\lambda_{I_i} + b\lambda_{II_i}}{\frac{\Delta X}{\Delta Z} + a(\lambda_{I_i} - \lambda_{I_{i-1}}) - b(\lambda_{II_i} - \lambda_{II_{i-1}})} \quad (2.150)$$

At this point the values of the variables are known Riemann and in general all the other quantities in the characteristics of line intersections points with the abscissa axis at the time Z; before you can evaluate Δ_1 and Δ_2 is necessary to calculate the entropy change along the same characteristics.

To do this it uses the equation of the flow line compatibility (2.135) in which the magnitude, A_A , U, q and f must be calculated in the point S to means of a linear interpolation of the neighboring nodes:

$$G_S = G_i - \frac{\delta X_S}{\Delta X} (G_i - G_{i-1}) \quad (2.151)$$

Where G indicates a generic observable and

$$\frac{\delta X_S}{\Delta X} = \frac{\lambda_{I_i} - \lambda_{II_i}}{\frac{\Delta X}{\Delta Z} (k + 1) + (\lambda_{I_i} - \lambda_{I_{i-1}}) - (\lambda_{II_i} - \lambda_{II_{i-1}})} \quad (2.152)$$

The 2.152 is easily obtainable with a similar process to that illustrated previously.

Now it is known the value of A_{AS} and dA_{AS} from which it is possible to calculate the entropy of the point P (A_{AP}) through the equation:

$$A_{AP} = A_{AS} + dA_{AS} \quad (2.153)$$

Known A_{AP} for finding the entropy change along λ_I character line and in a similar manner along λ_{II} , it will be enough to calculate:

$$dA_{AL} = A_{Ap} + A_{AL} \quad (2.154)$$

dA_{AL} and dA_{AR} , are to be inserted respectively in 2.131 and 2.133 to find $\Delta\lambda$ and $\Delta\beta$.

The described numerical method is used to determine the three λ_I variables, λ_{II} , and A_A in all the mesh nodes, except the first and last. In fact, starting from the end nodes we can trace back in time only one of the two characteristic lines because the other falls outside of the duct, in the region bordering contour, as shown in fig. 2.7. It suggests that in the node 1 is possible to know λ'_{II} , directly only while the node $I + 1$ is possible to know λ'_I , because both fall within the duct considered; These two variables are called λ_{in} .

To assess the missing Riemann variable, called λ_{out} , recourse is to the boundary conditions, it conditions that translate the presence of the environment or of a neighboring component with the end of the duct considered. For the modeling of the boundary conditions it is assumed the hypothesis of almost stationarity of the phenomena that take place in the boundary regions, or that is, it is supposed that the gas dynamic processes in these regions can be described by a succession of stationary states, spaced by time intervals ΔZ . These assumptions lead to expressing the boundary conditions as algebraic equations arising from the conservation equations for steady flow and one-dimensional, unsteady neglecting the terms of type $\delta/\delta t$. Numerous situations to the contour can be described with this approach, including: open ends in a constant pressure environment, end partially open, junctions of two ducts with abrupt variation of section, more ducts junctions and others.

In conclusion, please note that, by adopting a linear interpolation technique in the space of the grid, the gate of the Features method to be accurate to the first order in space and time. This characteristic turns out to be a limitation in the very detailed analysis, since they can not be picked by small oscillations of the magnitudes at high frequencies.

2.2. Shock-Capturing methods:

The results of fluid dynamic simulations can be greatly improved by using, for the resolution of hyperbolic system, more robust and accurate than the method of numerical methods to mesh Features. The fundamental merit of the Shock-Capturing methods resides in the ability to grasp correctly any discontinuities in the solution, as for example: shock waves, contact discontinuities due to temperature or chemical composition. Within this family, the methods to the symmetrical finite differences have proved the most efficient, representing a good compromise between: accuracy, the goodness of the solution, simplicity and calculation times. The symmetry of the method consists in applying in each node of the grid the same scheme with finite differences for expressing the terms of the spatial derivatives, irrespective of the flow field characteristics.

The methods described below are explicit and have an accuracy of the II order in the space-time domain. Unfortunately, as is known from the theorem of Godunov, the fact of having an accuracy of higher order at the first port to have problems of spurious oscillations in the solution found, and then is indispensable the use of special algorithms accessories to mitigate this phenomenon.

As described in chapter 1, the Shock-Capturing methods are applied to the hyperbolic system written in conservative form and matrix, complete additional hypothesis on the evolving gas model. Referring to Eq. 1.34 and clearing of the source terms vectors, we obtain the Euler equations describing the isentropic flow in a duct with constant cross section:

$$\frac{\partial \bar{W}(x, t)}{\partial t} + \frac{\partial \bar{F}(\bar{W})}{\partial x} = 0 \quad (2.155)$$

By integrating Eq.2.155 in space x and in time t and applying the divergence theorem of Gauss, we obtained:

$$\int_t^{t+\Delta t} \int_x^{x+\Delta x} \left(\frac{\partial \bar{W}}{\partial t} + \frac{\partial \bar{F}}{\partial x} \right) dx \cdot dt = 0 \quad (2.156)$$

The use of finite difference methods for the solution of eq. 2.156 requires the discretization of the space-time domain through mesh subdivision. The carrier, allows to fully characterize the motion of the flow and can be approximated by the following relationship:

$$\bar{W}(x, t) \cong \bar{W}_i^n(i\Delta x, n\Delta t) \quad (2.157)$$

Introducing the relationship 2.157 Eq. 2.156 is obtained:

$$(\bar{W}_i^{n+1} - \bar{W}_i^n)\Delta x + \left(\bar{F}_{i+\frac{1}{2}}^n - \bar{F}_{i-\frac{1}{2}}^n \right) \Delta t = 0 \quad (2.158)$$

Where the terms \bar{W} and \bar{F} are accessible using the following media expressions in space and time.

$$\bar{W}_i = \frac{1}{\Delta x} \int_{x_{i-\frac{1}{2}}}^{x_{i+\frac{1}{2}}} \bar{W} dx \quad (2.159)$$

$$\bar{F}_{i\pm\frac{1}{2}} = \frac{1}{\Delta t} \int_{t^n}^{t^{n+1}} \bar{F} dt \quad (2.160)$$

The eq. 2.156 allows to disengage from the condition of differentiability, required by the Euler equations, the integral formulation also has the advantage of treating the discontinuities prior to not knowing their localization. appropriately rearranging the terms of Eq. 2.158 you can write:

$$\frac{(\bar{W}_i^{n+1} - \bar{W}_i^n)}{\Delta t} + \frac{\left(\bar{F}_{i+\frac{1}{2}}^n - \bar{F}_{i-\frac{1}{2}}^n \right)}{\Delta x} = 0 \quad (2.161)$$

Now adding the differences along x is obtained:

$$\Delta x \sum_{i_{min}}^{i_{max}} \bar{W}_i^{n+1} = \Delta x \sum_{i_{min}}^{i_{max}} \bar{W}_i^n + \Delta t \left[\bar{F}_{i_{min}+\frac{1}{2}}^n - \bar{F}_{i_{max}+\frac{1}{2}}^n \right] \quad (2.162)$$

Where:

The first member is the total mass, the total momentum and the total amount of energy to the new time instant (n+1);

The first term to the second member represents the total mass, the amount the total momentum and the total amount of energy to time instant n;

The second term to the second member represents the amount of flow preserved through the ends of the conduit.

The well-defined equations constitute a scheme to conservative discretization, feature that guarantees us the validity of the integral properties of differential equations.

In next steps, we will be introducing Shock-Capturing methods Lax-Wendroff and MacCormack, both used in Gasdyn code and belonging to the category of finite difference methods, centered, explicit, with accuracy of the II order.

2.2.1. Lax-Wendroff method:

It is based on the development in Taylor series of the carrier solution, and is used in two forms: schema one step or two steps scheme.

ONE STEP SCHEME

Consider the system of equations in conservative form assuming isentropic stream written in matrix form:

$$\frac{\partial \bar{W}(x, t)}{\partial t} + \frac{\partial \bar{F}(\bar{W})}{\partial x} = 0 \tag{2.163}$$

Since the spatial derivative of the function vector is expressible as:

$$\frac{\partial \bar{W}(x, t)}{\partial t} + \frac{\partial \bar{F}(\bar{W})}{\partial \bar{W}} \frac{\partial \bar{W}}{\partial x} = 0 \tag{2.164}$$

the term $\frac{\partial \bar{F}(\bar{W})}{\partial \bar{W}}$ represents the Jacobian matrix A:

$$A = \frac{\partial \bar{F}(\bar{W})}{\partial \bar{W}} \tag{2.165}$$

whose elements are:

$$a_{ij} = \frac{\partial F_i}{\partial W_j} \tag{2.166}$$

With the introduction of the eq 2.159, Jacobian expression becomes:

$$\frac{\partial \bar{W}(x, t)}{\partial t} + \mathbf{A} \frac{\partial \bar{W}}{\partial x} = 0 \quad (2.167)$$

Consider now the development in a Taylor series arrested to the second order of the vector in the discretized solution \bar{W} domain at time $n+1$ and in the node:

$$\bar{W}_i^{n+1} = \bar{W}_i^n + \left. \frac{\partial \bar{W}}{\partial t} \right|_i^n \Delta t + \frac{1}{2!} \left. \frac{\partial^2 \bar{W}}{\partial t^2} \right|_i^n \Delta t^2 + 0(\Delta t^3) \quad (2.168)$$

Recalling the relationships 2.163 and 2.167:

$$\frac{\partial \bar{W}(x, t)}{\partial t} = -\mathbf{A} \frac{\partial \bar{W}}{\partial x} = -\frac{\partial \bar{F}(\bar{W})}{\partial x} \quad (2.169)$$

one can express the second derivative in time that appears in the development in series:

$$\frac{\partial^2 \bar{W}}{\partial t^2} = -\frac{\partial}{\partial t} \left(\frac{\partial \bar{F}}{\partial x} \right) = -\frac{\partial}{\partial x} \left(\frac{\partial \bar{F}}{\partial t} \right) \quad (2.170)$$

but the time derivative of the vector, using the above relations, it appears to be:

$$\frac{\partial \bar{F}}{\partial t} = \frac{\partial \bar{F}}{\partial \bar{W}} \left(\frac{\partial \bar{W}}{\partial t} \right) = -\frac{\partial \bar{F}}{\partial \bar{W}} \left(\frac{\partial \bar{F}}{\partial x} \right) = \frac{\partial \bar{F}}{\partial \bar{W}} \left(-\mathbf{A} \frac{\partial \bar{W}}{\partial x} \right) = \left(-\mathbf{A} \frac{\partial \bar{F}}{\partial x} \right) \quad (2.171)$$

the eq 2.170 takes the form:

$$\frac{\partial^2 \bar{W}}{\partial t^2} = \mathbf{A} \frac{\partial}{\partial x} \left(\frac{\partial \bar{F}}{\partial x} \right) \quad (2.172)$$

Introducing the 2.169 and 2.172 expressions Taylor series expansion is obtained:

$$\bar{W}_i^{n+1} = \bar{W}_i^n - \mathbf{A} \left. \frac{\partial \bar{W}}{\partial x} \right|_i^n \Delta t + \frac{1}{2!} \frac{\partial}{\partial x} \left(\mathbf{A}^2 \frac{\partial \bar{W}}{\partial x} \right) \Big|_i^n \Delta t^2 + 0(\Delta t^3) \quad (2.173)$$

$$\bar{W}_i^{n+1} = \bar{W}_i^n - \left. \frac{\partial \bar{F}}{\partial x} \right|_i^n \Delta t + \frac{1}{2!} \left. \frac{\partial}{\partial x} \left(A^2 \frac{\partial \bar{F}}{\partial x} \right) \right|_i^n \Delta t^2 + O(\Delta t^3) \quad (2.174)$$

By approximating the partial derivatives in Eq. 2.173 with centered finite differences, we reach the final expression of the one step Lax-Wendroff method:

$$\bar{W}_i^{n+1} = \bar{W}_i^n - A \left(\frac{\bar{W}_{i+1}^n - \bar{W}_{i-1}^n}{2\Delta x} \right) \Delta t + \frac{A^2}{2!} \left(\frac{\bar{W}_{i+1}^n - 2\bar{W}_i^n + \bar{W}_{i-1}^n}{\Delta x^2} \right) \Delta t^2 \quad (2.175)$$

above eq. is valid, where A is constant, otherwise expression is:

$$\begin{aligned} \bar{W}_i^{n+1} = \bar{W}_i^n - \frac{\Delta t}{2\Delta x^2} (F_{i+1}^n - F_{i-1}^n) \Delta t \\ + \frac{\Delta t^2}{2\Delta x^2} \left(A_{i+\frac{1}{2}}^n (F_{i+1}^n - F_i^n) - A_{i-\frac{1}{2}}^n (F_i^n - F_{i-1}^n) \right) \end{aligned} \quad (2.176)$$

where:

$$A_{i\pm\frac{1}{2}}^n = \frac{1}{2} (A_i^n + A_{i\pm 1}^n) \quad (2.177)$$

Or

$$A_{i\pm\frac{1}{2}}^n = A (W_i^n + W_{i\pm 1}^n) \quad (2.178)$$

The eq. 2.175 and 2.176 allow to calculate the \bar{W} solution at time n+1 in i-th node starting from the knowledge of the vector \bar{W} at time n-1 in the nodes, i and i+1.

Unfortunately, the one step Lax-Wendroff method requires a high computational burden, since the need of calculation of the Jacobian matrix A in each node for all the time steps.

TWO STEP SCHEME

Richtmeyer proposed the two step method of Lax-Wendroff. This method avoids the calculation of the Jacobian matrix, by inserting an intermediate step in the calculation of the vector solution in the node and to the desired time, and therefore is particularly suited to implementation in computer codes.

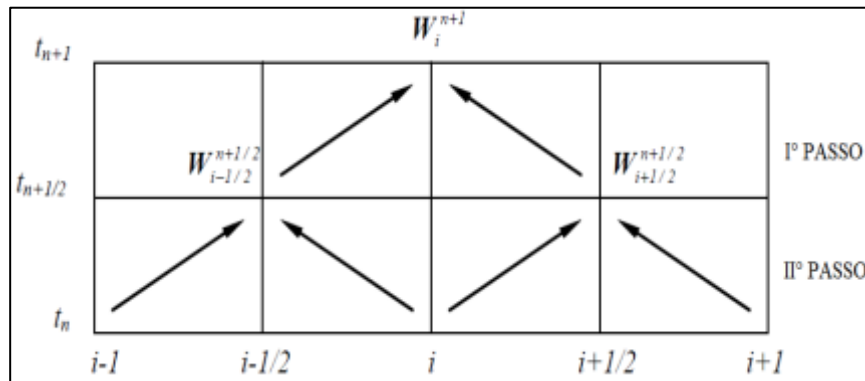


Figure 2:9 Calculation scheme of two step method Lax-Wendroff.

Step I: Note the \bar{W} and \bar{F} vectors in the nodes $i-1, i, i+1$ at time n , one obtains the vector \bar{W} solution, via an expansion in Taylor series stopped at the first order, to the intermediate time $n+1/2$ in intermediate nodes $i+1/2$ and $i-1/2$. Introducing the approximation centered finite difference you get:

$$\bar{W}_{i+1/2}^{n+1/2} = \left(\frac{\bar{W}_{i+1}^n - \bar{W}_i^n}{2} \right) - \left(\frac{\bar{F}_{i+1}^n - \bar{F}_i^n}{2\Delta x} \right) \Delta t \quad (2.179)$$

$$\bar{W}_{i-1/2}^{n+1/2} = \left(\frac{\bar{W}_i^n - \bar{W}_{i-1}^n}{2} \right) - \left(\frac{\bar{F}_i^n - \bar{F}_{i-1}^n}{2\Delta x} \right) \Delta t \quad (2.180)$$

Step II: \bar{W} known you can calculate the vector of \bar{F} flows in the intermediate nodes $i+1/2$ and $i-1/2$ to split time $n+1/2$, then you can determine the vector \bar{W} solution at time $n+1$ in the node.

$$\bar{W}_i^{n+1} = \bar{W}_i^n - \left(\frac{\bar{F}_{i+1/2}^{n+1/2} - \bar{F}_{i-1/2}^{n+1/2}}{\Delta x} \right) \Delta t \quad (2.181)$$

The time step is determined by the stability criterion Courant-Friedrichs-Lewy, previously defined in section 2.1, for which the CFL must assume values ≤ 1 .

2.2.2. MacCormack method:

The novelty introduced by the MacCormack method, compared to the previous method, is to resort to two different phases of calculation: predictor and corrector. Consider the system of

equations in conservative form and in the hypothesis matrix of isentropic flow duct and a constant section:

$$\frac{\partial \bar{W}(x, t)}{\partial t} + \frac{\partial \bar{F}(\bar{W})}{\partial x} = 0 \quad (2.182)$$

- *Phase predictor*: known carriers and in each node at the instant time n, using a scheme of finite difference forward (forward) for the approximation of the derivatives, we calculate the approximate value of the carrier solution \bar{W}^* at the time t^* :

$$\bar{W}_i^* = \bar{W}_i^n - \frac{\Delta t}{\Delta x} (\bar{F}_{i+1}^n - \bar{F}_i^n) \quad (2.183)$$

Determined \bar{W}_i^* can be calculated by the vector amount of flows \bar{F}^* . Finally, we proceed to the calculation of the carrier solution at half time step by the average of the vector estimated at the time t^* and the one at the previous time step.

$$\bar{W}_i^{n+\frac{1}{2}} = \frac{1}{2} (\bar{W}_i^n + \bar{W}_i^*) \quad (2.184)$$

- *Phase corrector*: using finite difference backward (backward) and advancing in the $\Delta t/2$ time to conclude the entire time step, you get the final value of the carrier solution.

$$\bar{W}_i^{n+1} = \bar{W}_i^{n+\frac{1}{2}} - \frac{\Delta t}{2} \left(\frac{\bar{F}_i^* - \bar{F}_{i-1}^*}{\Delta x} \right) \quad (2.185)$$

The diagram of fig. 2.10 summarizes the steps of the method Mac-Cormack:

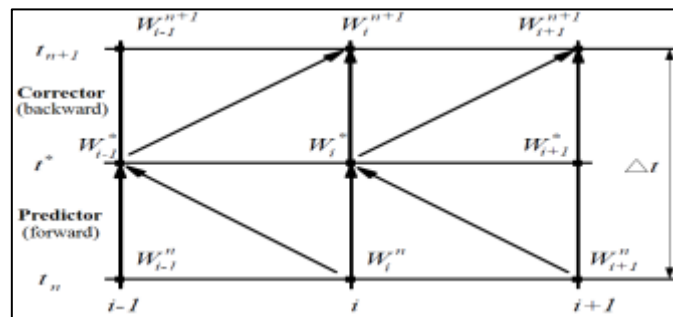


Figure 2:10 Representation of the MacCormack method in the case of forward predictor-backward corrector.

The method is described in the forward-backward predictor corrector shape, but you can reverse the diagram application of finite differences in the two phases getting different results because of the different behavior of the algorithm. It was found by experimental findings that the best solution is achieved by adopting finite difference in the direction of propagation of the discontinuity in the predictor step. If this direction is not known prior, as a rule, you can reverse the scheme of finite difference by making a step forward in the form predictor-corrector backward and the next in the form backward predictor-corrector forward. Also for this method the stability condition is derived from the application of CFL.

2.3. The problem of spurious oscillations:

The Lax-Wendroff and Mac-Cormack methods present the problem of so called spurious oscillations, i.e oscillations of the numerical solution in correspondence of the discontinuities, such as shock or contact discontinuities waves. One reason for this behavior is found in Godunov's theorem, which shows that all the numerical schemes with accuracy higher than the first order and due to a diagram of the constant type coefficients:

$$\bar{W}_i^{n+1} = \sum_k c_k \bar{W}_{i+k}^n \tag{2.186}$$

have non-physical oscillations in the discontinuity of the match solution. The Harten criterion indicates the necessary and sufficient conditions that a numerical method must meet in order to avoid the occurrence of spurious oscillations.

$$TV(\bar{W}^n) = \sum_i |\bar{W}_i^{n+1} - \bar{W}_i^n| \tag{2.187}$$

if, with the advancement of the time step, the TV sum does not grow:

$$TV(\bar{W}^{n+1}) \leq TV(\bar{W}^n) \tag{2.188}$$

then the numerical scheme admits monotonous solution and does not have the problem of spurious oscillations. Methods with this character are called TVD, i.e Total Variation Diminishing.

Through the criterion of Harten you can then show that the methods Lax-Wendroff and TVD Mac-Cormack are not, but you can make such by suitably modifying the calculation schemes so that the coefficients c_k belong to the same solution \bar{W} [1] [2].

The TVD schemes are divided into two classes:

Pre-processing schemes: characterized in that the complex data is modified before updating the solution.

Post-processing schemes: the solution is updated from time to time through the selected numerical method and subsequently modified to meet the requirements of TVD schemes.

Covered in the second group of FCT techniques and flow restrictors, algorithms are implemented in Gasdyn code.

2.4. The FCT technique:

The Corrected Flux Transport, more briefly indicated with the acronym FCT, is a technique of damping of spurious oscillations introduced by Boris and Book in 1973 that includes three basic steps:

- *Transport Stage:* the temporary solution is achieved by the Lax-Wendroff methods or MacCormack represented on the transport operator T .

$$\bar{W}^{n+1} = \bar{W}^n + T(\bar{W}^n) \quad (2.189)$$

- *Diffusion stage:* introduces a numerical diffusion in solution that will dampen the non-physical oscillations. The diffusive flux introduced is defined as:

$$\bar{\theta} \left(\bar{W}_{i+\frac{1}{2}} \right) = \frac{1}{8} (\bar{W}_{i+1} - \bar{W}_i) \quad (2.190)$$

$$\bar{\theta} \left(\bar{W}_{i-\frac{1}{2}} \right) = \frac{1}{8} (\bar{W}_i - \bar{W}_{i-1}) \quad (2.191)$$

which corresponds to a diffusion operator D_i :

$$D_i = \bar{\theta} \left(\bar{W}_{i+\frac{1}{2}} \right) - \bar{\theta} \left(\bar{W}_{i-\frac{1}{2}} \right) \quad (2.192)$$

Now for the calculation of the vector \bar{W} solution there are two different routes of development of the method:

1. *Diffusion via Damping*: diffusion operator in calculating the carrier relative to the time level solution is used n:

$$\bar{W}_D^{n+1} = \bar{W}^{n+1} + D(\bar{W}^n) \quad (2.193)$$

2. *Diffusion via Smoothing*: the operator of diffusion calculation is used in the carrier solution for the new time level n+1:

$$\bar{W}_D^{n+1} = \bar{W}^{n+1} + D(\bar{W}^{n+1}) \quad (2.194)$$

- *Anti-Diffusion Stage*: introduce the non-linear anti diffusive operator "A" that removes, where it is not required, the diffusion introduced in a uniform manner in the previous phase. The operator A is given by:

$$A(\bar{W}^{n+1}) = -\bar{\psi} \left(\bar{W}_{i+\frac{1}{2}}^{n+1} \right) + \bar{\psi} \left(\bar{W}_{i-\frac{1}{2}}^{n+1} \right) \quad (2.195)$$

where $\bar{\psi}$, called anti-diffusive flux (flux limiter), is defined as follow, proposed by *Ikeda and Nakagawa*:

$$\bar{\psi}_{i+\frac{1}{2}}(\bar{W}) = \bar{s} \cdot \max \left[0, \min \left(\frac{5}{8} \bar{s} \Delta \bar{W}_{i-1/2}, \frac{1}{8} |\Delta W_{i+1/2}|, \frac{5}{8} \bar{s} \Delta \bar{W}_{i+3/2} \right) \right] \quad (2.196)$$

with:

$$\bar{s} = \text{sgn} \left(\Delta \bar{W}_{i+\frac{1}{2}} \right) \quad (2.197)$$

$$\Delta \bar{W}_{i+\frac{1}{2}} = \bar{W}_{i+1} - \bar{W}_i \quad (2.198)$$

$$\Delta \bar{W}_{i-\frac{1}{2}} = \bar{W}_i - \bar{W}_{i-1} \quad (2.199)$$

$$\Delta \bar{W}_{i+\frac{3}{2}} = \bar{W}_{i+2} - \bar{W}_{i+1} \quad (2.200)$$

The calculation of the final vector \bar{W}_{DA}^{n+1} solution, depending on the alternatives adopted in the diffusion stages, and defined as:

$$\bar{W}_{DA}^{n+1} = \bar{W}_D^{n+1} + A(\bar{W}^n) \quad \text{Damp case} \quad (2.201)$$

$$\bar{W}_{DA}^{n+1} = \bar{W}_D^{n+1} + A(\bar{W}^{n+1}) \quad \text{Smoothing case} \quad (2.202)$$

The alternative Damping allows almost completely eliminate the spurious oscillations but makes the numerical method unstable, as demonstrated by *Bulaty and Niesser*. To prevent instability, it is necessary that the CFL does not exceed the 0.866 value in place of 1, for the time step Δt this should result in less increased computational burden. The alternative Smoothing however does not completely eliminate the spurious oscillations but does not experience instability, thus leaving time step unchanged.

2.5. Flow restrictors:

The general philosophy of the flow restrictors is applying an anti-diffusive flux only to areas affected by discontinuity, this is to prevent possible non-physical numerical oscillations. *Van Leer* introduced the ϕ parameter, called flow restrictor, able to control the oscillations of the numerical solution. This parameter is a function of the ratio of successive solutions gradients and is defined as:

$$\phi_i = \phi(r_i) \quad (2.203)$$

where:

$$r_i = \frac{\Delta W_{i-\frac{1}{2}}^n}{\Delta W_{i+\frac{1}{2}}^n} \quad (2.204)$$

$$\Delta W_{i+\frac{1}{2}}^n = \Delta W_{i+1}^n - \Delta W_i^n \quad (2.205)$$

$$\Delta W_{i-\frac{1}{2}}^n = \Delta W_i^n - \Delta W_{i-1}^n \quad (2.206)$$

The principle function of the algorithms for the application of the flow restrictors is based on the following concept: when solutions in adjacent points are similar is maintained the accuracy of the second order of the numerical method is used, while in vicinity of a discontinuity the accuracy the method is downgraded to first order for not having the problem of spurious oscillations.

Due to Davi's introduction of the first symmetrical pattern applied method of Lax-Wendroff to make TVD. Following will be briefly illustrated the application of this technique to a linear

partial differential equation, leaving those concerned the most complex application to hyperbolic equations.

Starting from linear differential equation like this:

$$\frac{\partial w}{\partial t} - a \frac{\partial w}{\partial x} = 0 \quad (2.207)$$

the solution at time n+1 determined using the Lax-Wendroff method is:

$$W_i^{n+1} = W_i^n - \frac{v}{2} (\Delta W_{i+1/2}^n + \Delta W_{i-1/2}^n) + \frac{v^2}{2} (\Delta W_{i+1/2}^n + \Delta W_{i-1/2}^n) \quad (2.208)$$

where v represents CFL.

Davis applies a dissipative term in Eq. 1.208 that simulates the effect of an artificial viscosity, using the correct values in each node of the mesh to get the TVD property in the numerical solution. In following table provides additional term, developing the case with constant positive (superscript + to terms G and r):

$$G_{i+1/2}^+(r_i^+) \Delta W_{i+1/2}^n - G_{i-1/2}^+(r_{i-1}^+) \Delta W_{i-1/2}^n \quad (2.209)$$

The eq. 1.208 with the addition of the term 1.209 can be written as:

$$W_i^{n+1} = W_i^n - \Delta W_{i-1/2}^n \left\{ v \left[1 + \frac{1}{2} (1 - v) \left(\frac{1}{r_i^+} - 1 \right) \right] - \left[\frac{G_{i+1/2}^+}{r_i^+} - G_{i-1/2}^+ \right] \right\} \quad (2.210)$$

where:

$$r_i^+ = \frac{\Delta W_{i-1/2}^n}{\Delta W_{i+1/2}^n} \quad (2.211)$$

$$G_{i+1/2}^+(r_i^+) = \frac{v}{2} (1 - v) [1 - \phi(r_i^+)] \quad (2.212)$$

In a similar way, we obtain the variables G^- and r_i^- in case of negative constant:

$$r_i^- = \frac{\Delta W_{i+1/2}^n}{\Delta W_{i-1/2}^n} \quad (2.213)$$

$$G_{i+1/2}^-(r_{i+1}^+) = \frac{v}{2}(1-v)[\phi(r_{i+1}^-) - 1] \quad (2.214)$$

The two different cases can be combined to obtain the following solution:

$$\begin{aligned} W_i^{n+1} = & W_i^n - \frac{v}{2}(W_{i+1}^n + W_{i-1}^n) + \frac{v^2}{2}(W_{i+1}^n - 2W_i^n + W_{i-1}^n) \\ & + [G_{i+1/2}^+(r_i^+) + G_{i+1/2}^-(r_{i+1}^+)]\Delta W_{i+1/2}^n \\ & - [G_{i-1/2}^+(r_i^+) + G_{i-1/2}^-(r_{i-1}^-)]\Delta W_{i-1/2}^n \end{aligned} \quad (2.215)$$

where:

$$G_{i+1/2}^+(r_i^+) = \begin{cases} \frac{v}{2}(1-v)[1 - \phi(r_i^+)], & a > 0 \\ 0, & a \leq 0 \end{cases} \quad (2.216)$$

$$G_{i+1/2}^-(r_{i+1}^+) = \begin{cases} 0, & a > 0 \\ \frac{v}{2}(1-v)[\phi(r_{i+1}^-) - 1], & a \leq 0 \end{cases} \quad (2.217)$$

The evaluation of the terms 1.216-1.217 preclude the knowledge of the direction of flow, being to the coefficient that determines the sign of the shipping term. Davis solves this problem, so as to obtain a non-up-wind scheme and avoid the high computational effort required, redefining the terms G:

$$G_{i+1/2}^+(r_i^+) = \frac{|v|}{2}(1-|v|)[1 - \phi(r_i^+)] \quad (2.218)$$

$$G_{i+1/2}^-(r_{i+1}^-) = \frac{|v|}{2}(1-|v|)[1 - \phi(r_{i+1}^-)] \quad (2.219)$$

To make the TVD of the flow restrictor ϕ method cannot assume any values, in the Davis diagram eligibility region is defined by:

$$\phi(r) = \begin{cases} \min(2r, 1), & r > 0 \\ 0, & r \leq 0 \end{cases} \quad (2.220)$$

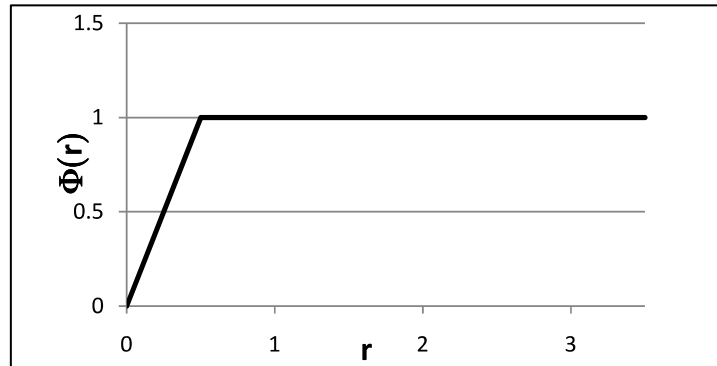


Figure 2:11: Davis scheme of the flow restrictor eligibility region of ϕ .

This limit leads to consequences on the CFL, by imposing its value to 0.7.

The scheme is extended to the solution of certain hyperbolic equations with numerical methods of Lax-Wendroff and Mac-Cormack.

Chapter 3

3. Modeling of turbocharger in Gasdyn

The instrument used in the performance of this thesis was the Gasdyn software, a code developed in-house at the Politecnico di Milano from Motors group. Gasdyn is a thermo-1D computational fluid dynamics model, able to simulate the operation of internal combustion engines in their entirety. With greater ease than the 3D software and the ability to calculate the properties of air and flue gas at every point of the engine, the Gasdyn code allows to reach an optimization of the parameters of interest such as torque, power, fuel consumption, noise and emissions in a short time.

The numerical model is based on the fluid dynamic equations of conservation of the one-dimensional flow, unsteady, compressible, reagent flowing inside ducts of variable section. The available numerical methods for solving the equations, are the Method of Characteristics to mesh, which has an accuracy of one order, and methods Shock-Capturing, which have an accuracy of the second order. It is preferred to use the Shock-Capturing methods able, thanks to their order of accuracy, to grasp the possible discontinuity of the resulting solution, for example, to the presence of shock waves. Within this family, the methods including Gasdyn lets you choose are those of Lax-Wendroff and Mac-Cormack, both finite difference methods, focused and explicit.

A problem which appears in the use of methods with greater accuracy of order unity is that of spurious oscillations, numerical oscillations in correspondence of the discontinuity. This problem is solved using the Flow restrictors applying an anti-diffusive flux in those areas affected by discontinuities thus limiting any non-physical oscillations.

And necessary to define the boundary conditions to represent what is located at the ends of the conduits, as the external environment, or, as we will see below, the turbine and the compressor. Although the flow inside the ducts is strongly unsteady, the edge phenomena are represented as a succession of stationary states, defined by the conservation equations for steady flow and one-dimensional. When you can't ignore the model as correctly as possible a few unsteady phenomena, you can enter the boundary conditions derived from 3D simulations, performed with other software [1] [2].

3.1. Modeling turbines:

The approach followed in Gasdyn for modeling of the turbine consists in receiving as input the characteristic curves of steady flow and extract from them the boundary conditions that best represent their operation in unsteady conditions. The representation of the turbine is translated in terms of quantities such as pressures, temperatures, flow and speed in the ducts connected to it. The Gasdyn code also calculates the power and torque developed by it to go then to define its matching with the compressor.

For the fact that our interest in turbochargers of the processed flow rates are low, the choice falls on radial rather than axial geometries. The results obtained from modeling of a centripetal turbine with a quasi-static approach is not exactly consistent with the data obtained experimentally as the non-stationariness of the inside flow. it is high and is expanded by the volute of negligible volume. There is not yet 1D computational models available that describe properly the magnitudes of the unsteady flow without increasing the complexity of the problem and with it the calculation time. For this reason and for the fact that the results are still acceptable, the turbine is described as operating under quasi-static conditions.

3.1.1. Features of the radial turbine steady stream:

The magnitudes of the steady stream, from which we start to model the turbine, are defined as follows:

$$\text{Expansion ratio} = \frac{p_{01}}{p_2}$$

$$\text{Flow parameter} = \frac{\dot{m}\sqrt{T_{01}}}{p_{01}}$$

$$\text{Speed parameter} = \frac{N}{\sqrt{T_{01}}}$$

$$\text{Total to static efficiency} = \eta_{TS} = \frac{h_{01} - h_2}{h_{01} - h_{2s}}$$

$$\text{Ratio of peripheral speed} = \frac{u}{C_{is}}$$

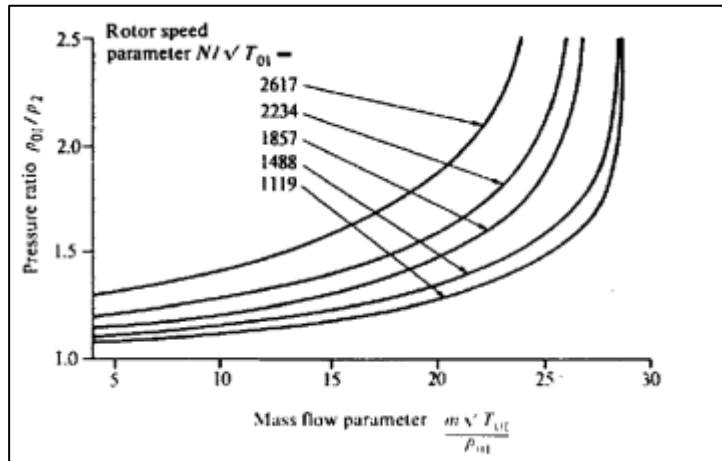


Figure 3.1 Characteristic curve of expansion ratio - flow parameter of a radial turbine for various speed parameters.

where the subscript 01 means the total quantities in the inlet section and 2 with the static variables in the output section. The representation of the performance curves through dimensionless parameters is useful in the design phase because it allows to identify among several machines that is coupled to the better system.

The first characteristic curve describes the trend of the expansion ratio as a function of the flow parameter, is shown in fig.3.1. The single characteristic curve, for a given rate parameter, outlines a growing trend of the flow with the expansion ratio up to a value beyond which no longer increases with it, this as the speed of sound within the machine has been reached. Unlike the axial turbines, the curves are strongly dependent on the speed of the impeller and the total inlet temperature and can't be approximated by a single curve independent from them. For the same expansion ratio, the processed flow rate decreases with increasing speed, this is because it is closest to the flow block.

The other feature of our interest is the efficiency curve trend η_{TS} as a function of the speed ratio (fig.3.2). It is noted that it too is dependent on the speed parameter, the maximum efficiency point moves to the grow of the speed parameter to the relationship between the peripheral speed of the blades and speed of increasing gas.

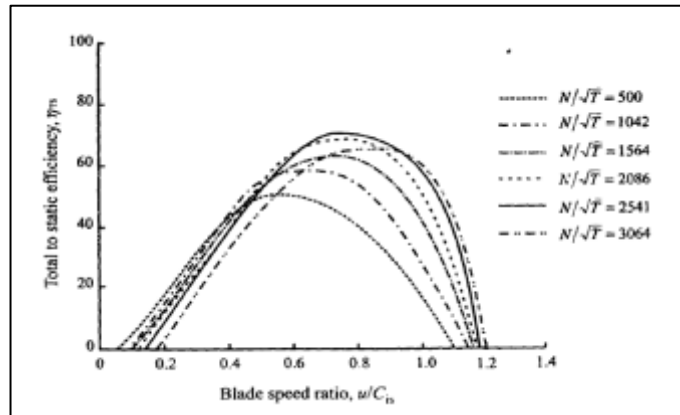


Figure 3.2 Characteristic curve performance - the speed ratio of a radial turbine for various speed parameters

The Gasdyn model requires these curves input and need to set the entire flow range, from no flow conditions to the choked flow. Maps are provided by the manufacturers as a series of experimental data only in vicinity of the point of maximum efficiency, was then developed by the group of a Matlab tool motors that allows the fitting of the maps on entire range of flow rates. It can thus represent operating conditions that fall outside the range of maximum efficiency, as can happen in a typical turbocharger.

3.1.2. Performance of turbines with variable outlet pressure:

The method used by Gasdyn consists in expressing the performance curves of the stationary flow into a form compatible with the equations of the waves which describe the gas flowing in the ducts. In this way, it is possible to evaluate the influence of the presence of the turbine on what is located upstream and downstream of it. The pressure downstream of the turbine can't be assumed constant for the fact that it does not vented directly into the atmosphere, there are in fact the exhaust pipes, the catalytic converter and the muffler. Are indicated with 1 and 2 the upstream and downstream of the turbine sections (fig.3.3). The starting point is the characteristic curve represented in fig. (3.4).

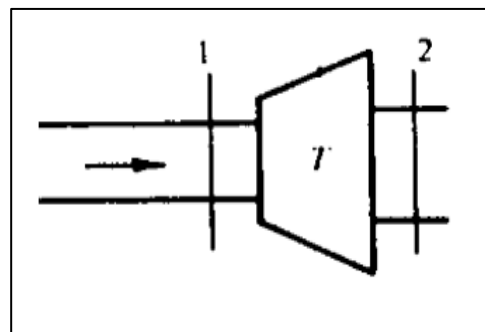


Figure 3.3 Schematic view of a representative turbine.

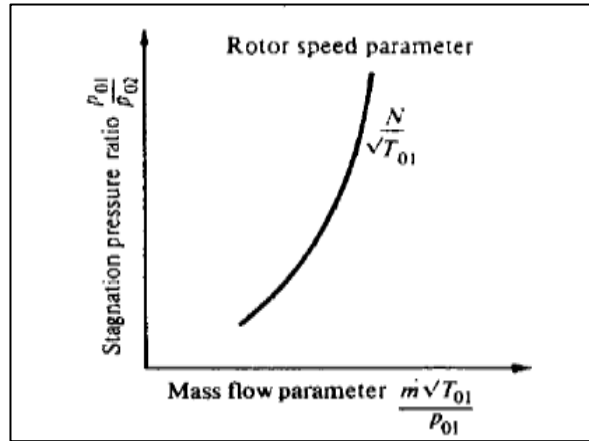


Figure 3:4 Characteristic curve of expansion ratio - flow parameter of a radial turbine

To make the expression of the turbine consistent with the wave equations, Gasdyn expresses the operating maps in terms of the Mach number on the upstream section M_1 , starting from the flow parameter:

$$\frac{\dot{m}\sqrt{T_{01}}}{p_{01}F_{01}} = \left(\frac{k}{R}\right)^{\frac{1}{2}} \frac{M_1}{\sqrt{\left\{1 + \frac{k-1}{2}M_1^2\right\}^{\frac{k+1}{2(k-1)}}}} \quad (3.221)$$

Through an iterative process, it is possible to know the value of M_1 to the fact that, of the known flow rate parameter, is only of itself function:

$$M_1 = \left(C + \frac{k-1}{2}CM_1^2\right)^{\frac{k+1}{2(k-1)}} \quad (3.222)$$

with:

$$C = \left\{\left(\frac{R}{k}\right)^{\frac{1}{2}} \left(\frac{\dot{m}\sqrt{T_{01}}}{p_{01}F_{01}}\right)\right\}^{\frac{2(k-1)}{k+1}} \quad (3.223)$$

Once known M_1 are defined reports (p_{01}/p_1) and (T_{01}/T_1) between stagnation variables and static variables upstream of the turbine:

$$\frac{p_{01}}{p_1} = \left(1 + \frac{k-1}{2} M_1^2\right)^{\frac{k}{k-1}} \quad (3.224)$$

$$\frac{T_{01}}{T_1} = \left(1 + \frac{k-1}{2} M_1^2\right) \quad (3.225)$$

Through eq. 3.224 and 3.225 are defined quantities that describe the operation of the turbine:

$$\frac{p_1}{p_2} = \frac{p_1}{p_{01}} \frac{p_{01}}{p_2} \quad (3.226)$$

$$\frac{T_2}{T_1} = 1 - \eta_{TS} \left\{1 - \frac{p_2}{p_{01}} \frac{k-1}{k}\right\} \frac{T_{01}}{T_1} \quad (3.227)$$

$$G_1 = \frac{\dot{m} \sqrt{T_{01}}}{p_{01}} \left(\frac{p_{01}}{p_1}\right) \left(\frac{T_1}{T_{01}}\right)^{\frac{1}{2}} \quad (3.228)$$

The next step consists in tying (p_1/p_2) , (T_1/T_2) and G_1 to the flow conditions in the discharge pipes and the turbine exhaust. To make this step it is necessary to first introduce the wave propagation equations that correctly model the behavior of the gas inside the ducts. For the definition of the boundary conditions, as mentioned above we utilized the method of characteristics, so the wave equations are expressed in terms of the Riemann λ_{in} and λ_{out} variables.

- Upstream of turbine:

$$\lambda_{in,1} = A_1 + \frac{k-1}{2} U_1 \quad (3.229)$$

$$\lambda_{out,1} = A_1 - \frac{k-1}{2} U_1 \quad (3.230)$$

- Downstream of turbine:

$$\lambda_{in,2} = A_2 - \frac{k-1}{2} U_2 \quad (3.231)$$

$$\lambda_{out,2} = A_2 + \frac{k-1}{2} U_2 \quad (3.232)$$

where U and A respectively are the velocity of the gas and the speed of sound.

$$\lambda_{in,1}^* = \frac{\lambda_{in,1}}{A_{A1}} \quad (3.233)$$

$$\lambda_{in,2}^* = \frac{\lambda_{in,2}}{A_{A2}} \quad (3.234)$$

with $A_{AN} = (a_A/a_{ref})$ representing the entropy level of gas compared to the reference state.

- Upstream of turbine:

$$\lambda_{in,1}^* = A_1^* + \frac{k-1}{2} U_1^* \quad (3.235)$$

$$\lambda_{out,1}^* = A_1^* - \frac{k-1}{2} U_1^* \quad (3.236)$$

- Downstream of turbine:

$$\lambda_{in,2}^* = A_2^* - \frac{k-1}{2} U_2^* \quad (3.237)$$

$$\lambda_{out,2}^* = A_2^* + \frac{k-1}{2} U_2^* \quad (3.238)$$

The generic Mach number can be seen as, $M=(U^*/A^*)$ and it is possible to express the Riemann variables marked in function of it.

- Upstream of turbine:

$$\lambda_{in,1}^* = A_1^* \left(1 + \frac{k-1}{2} M_1 \right) \quad (3.239)$$

$$\lambda_{out,1}^* = A_1^* \left(1 - \frac{k-1}{2} M_1 \right) \quad (3.240)$$

- Downstream of turbine:

$$\lambda_{in,2}^* = A_2^* \left(1 - \frac{k-1}{2} M_2 \right) \quad (3.241)$$

$$\lambda_{out,2}^* = A_2^* \left(1 + \frac{k-1}{2} M_2 \right) \quad (3.242)$$

The size (A_1^*/A_2^*) expresses the relationship between the entropy of the gas input and the entropy of the outlet gas, as the internal processing machine is adiabatic it is led back to the expansion ratio as follows:

$$\frac{A_1^*}{A_2^*} = \left(\frac{p_1}{p_2} \right)^{\frac{k-1}{2k}} \quad (3.243)$$

Now we can rewrite the equations of propagation of the waves so that it also contains the characteristics of the turbine.

- Upstream of turbine:

$$\lambda_{in,1}^* = A_1^*(1 + C_1 G_1) \quad (3.244)$$

$$\lambda_{out,1}^* = A_1^*(1 - C_1 G_1) \quad (3.245)$$

- Downstream of turbine:

$$\lambda_{in,2}^* = A_2^*(1 - C_2 G_2) \quad (3.246)$$

$$\lambda_{out,2}^* = A_2^*(1 + C_2 G_2) \quad (3.247)$$

having defined the flow parameter G and the constant C in the input and output sections, respectively, as:

$$G_n = \frac{\dot{m} \sqrt{T_n}}{p_n} \quad n = 1, 2 \quad (3.248)$$

$$C_n = \frac{k-1}{2} \sqrt{\frac{R}{k} \frac{1}{F_n}} \quad n = 1, 2 \quad (3.249)$$

Now they express the relationship between the Riemann variables as a function of the variables (p_1/p_2) , (T_1/T_2) and G_1 :

$$\frac{\lambda_{in,1}^*}{\lambda_{in,2}^*} = \left(\frac{p_1}{p_2}\right)^{\frac{k-1}{2k}} \left(\frac{1 + C_1 G_1}{1 - C_2 G_1 \left(\frac{p_1}{p_2}\right) \left(\frac{T_2}{T_1}\right)^{\frac{1}{2}}} \right) \quad (3.250)$$

$$\frac{\lambda_{out,1}^*}{\lambda_{in,1}^*} = \frac{(1 - C_1 G_1)}{(1 + C_1 G_1)} \quad (3.251)$$

$$\frac{\lambda_{out,2}^*}{\lambda_{out,1}^*} = \left(\frac{p_1}{p_2}\right)^{\frac{k-1}{2k}} \left(\frac{1 - C_2 G_1 \left(\frac{p_1}{p_2}\right) \left(\frac{T_2}{T_1}\right)^{\frac{1}{2}}}{1 - C_1 G_1} \right) \quad (3.252)$$

The last step of the translation of the maps in the boundary conditions is the collection of the starting values in the set of data in the form $(x, p_1/p_2, T_1/T_2$ and $G_1)$, having defined as x :

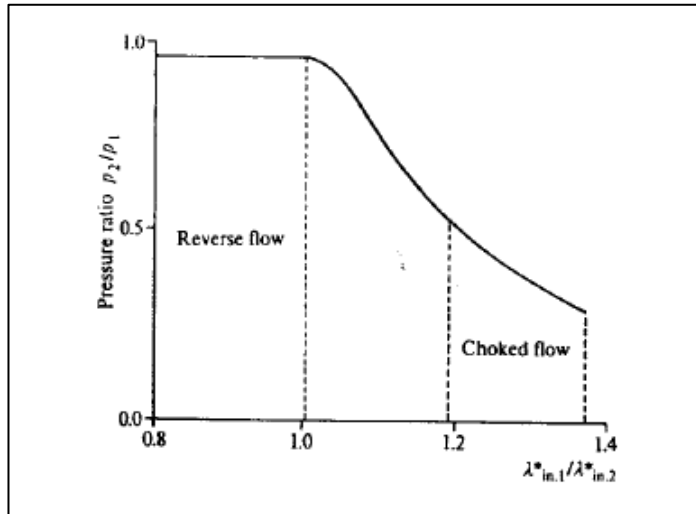


Figure 3:5 Boundary condition in terms of the pressures of a radial turbine

$$x = \frac{\lambda_{in,1}^*}{\lambda_{in,2}^*} \quad (3.253)$$

The boundary conditions have to be tabulated for any point of the turbine operation. They are then identified x_{min} and x_{max} , which assumes x values when the processed flow is zero or maximum respectively:

$$x_{min} = \left(\frac{p_1}{p_2}\right)^{\frac{k-1}{2k}} \quad (3.254)$$

$$x_{max} = \left(\frac{p_1}{p_2}\right)^{\frac{k-1}{2k}} \left(\frac{1 + C_1 G_{1,max}}{1 - C_2 G_{1,max} \left(\frac{p_1}{p_2}\right) \left(\frac{T_2}{T_1}\right)^{\frac{1}{2}}} \right) \quad (3.255)$$

If $x_{min} \geq x$ the flow will flow in the opposite direction inside the turbine, reports (T_1/T_2) and (p_1/p_2) will be uniform and algorithm cycle will be increasing the flow rate of the G_1 until you have the ΔG incoming flow positive. If $x_{max} \leq x$ G_1 will reach the maximum, and the program cycle will increase (p_1/p_2) of $\Delta(p_1/p_2)$ until you identify the maximum expansion ratio. They are shown in fig.3.5 and fig.3.6 representations of boundary conditions of the turbine.

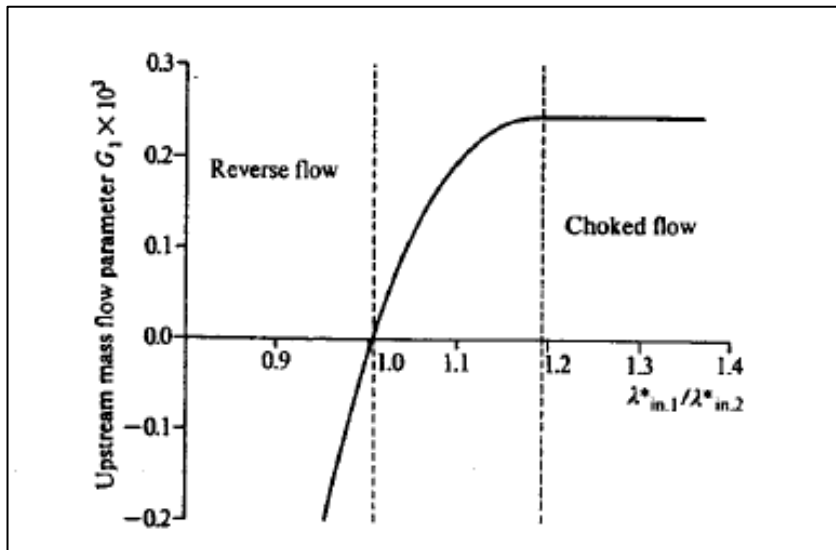


Figure 3:6: Boundary state in terms of the scope of a radial turbine

The complete algorithm implemented in Gasdyn is an iterative procedure, starting from the values of the variables Riemann input to the turbine, will define the new flow conditions inside the ducts. The steps are:

1. Calculation of the Riemann variables $\lambda_{in,1}^*$ $\lambda_{in,2}^*$ from $\lambda_{in,1}$, $\lambda_{in,2}$, A_{A1} and A_{A2} ;
2. Calculation of the speed parameter from the characteristics curves and x from eq. (3.253);
3. Determination of (p_1/p_2) , (T_1/T_2) and G_1 by extrapolation from the curves $(x, N/\sqrt{T_{01}})$;
4. Calculation of the Riemann variables $\lambda_{out,1}^*$ $\lambda_{out,2}^*$, from equations. (3.251) and (3.252);
5. Calculation of the new A_{A1} and A_{A2} from the initial values and the equation:

$$\frac{A_2}{A_1} = \left(\frac{T_1}{T_2}\right) \left(\frac{P_1}{P_2}\right)^{\frac{k-1}{2k}} \quad (3.256)$$

6. Calculating the values of $\lambda_{in,1}$, $\lambda_{in,2}$, $\lambda_{out,1}$ and $\lambda_{out,2}$.
7. If the difference between the initial values of $\lambda_{in,1}$ and $\lambda_{in,2}$, and calculated values is less than a given tolerance, the solution is the final one, in case it is not so, the algorithm starts from the calculation of $\lambda_{in,1}^*$ $\lambda_{in,2}^*$ and repeat the process as long as this does not happen.

the calculated values of $\lambda_{in,1}$, $\lambda_{in,2}$, $\lambda_{out,1}$ and $\lambda_{out,2}$, it is now possible to derive the flow characteristics that determine the turbine inside the ducts in terms of pressures, flows, temperatures, speed and other variables of interest.

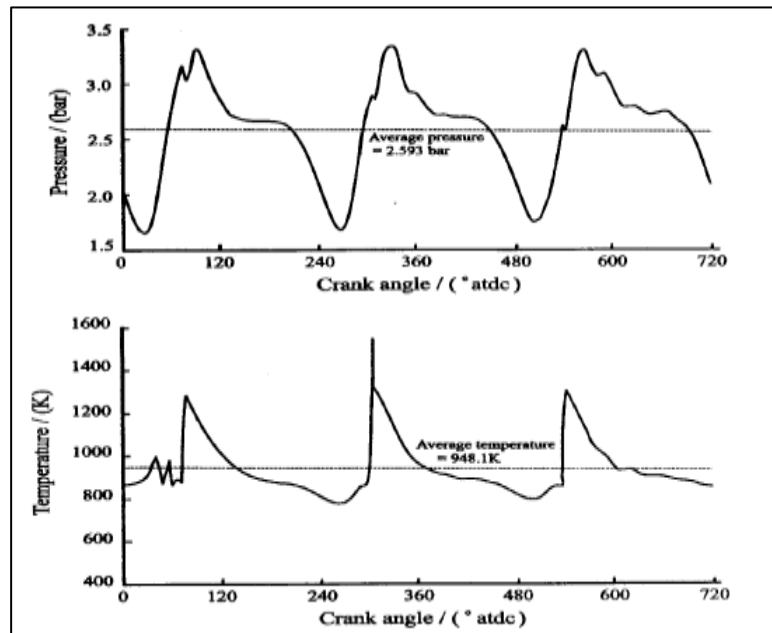


Figure 3:7 Pressure profile and the temperature upstream of the turbine.

3.1.3. Work and Efficiency of turbines:

The pressure oscillations and temperature upstream of the turbine, represented in fig.3.7, cause fluctuations of the instantaneous work and the processed mass flow rate. You can see this from the fact that these oscillations ranging in continuously change the speed parameter ($N/\sqrt{T_{01}}$) and the expansion ratio (p_{01}/p_2) as shown in fig.3.8.

Actual power will be given by the product between flow rate and enthalpy difference horse of the machine:

$$W_{is,T} = \dot{m}\eta_{TS}(h_{01} - h_{2S}) = \dot{m}\eta_{TS} \frac{C_{is}^2}{2} \quad (3.257)$$

and the maximum theoretically available will be:

$$e_T = \dot{m}(h_{01} - h_{2S}) = \dot{m} \frac{C_{is}^2}{2} \quad (3.258)$$

You notice that in fig.3.9 η_{TS} performance and theoretical power e_T oscillate in phase. The theoretical power has in fact its best to high expansion ratios while η_{TS} for limited amounts. L' of the actual instantaneous power trend is in phase with respect to the theoretical one and, as said, is more damped for high values of it.

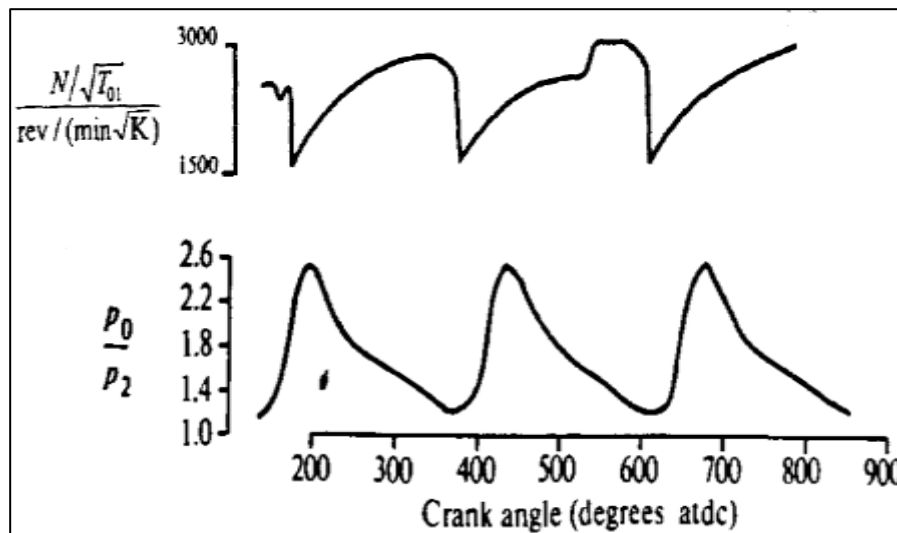


Figure 3:8 results of the rate parameter and the expansion ratio with the crank angle

For the calculation of the instantaneous effective power from Eq. (3.258), the Gasdyn code solves, once again, by translating the equations through the method of characteristics. The flow rate, defined as $\dot{m} = \rho u F$ can be derived for any instant of time 't' from equation that expresses the function of Riemann variables:

$$\dot{m} = \frac{4k}{k-1} \left(\frac{p_{ref}}{a_{ref}} \right) \left\{ \frac{(\lambda_{in} - \lambda_{out})}{(\lambda_{in} + \lambda_{out})^2} \right\} \left(\frac{\lambda_{in} + \lambda_{out}}{2A_A} \right)^{\frac{2k}{k-1}} \quad (3.259)$$

and the same applies to the term $(\eta_{TS} \frac{C_{is}^2}{2})$, seen as enthalpy difference between inlet and outlet of the turbine:

$$\eta_{TS} \frac{C_{is}^2}{2} = \frac{A_0^2}{k-1} \left\{ 1 - \left(\frac{A_2}{A_1} \right)^2 \right\} a_{ref}^2 \quad (3.260)$$

The total mass flow processed by the turbine will be obtained by integrating the instantaneous value of the engine cycle, and multiplying the whole by the number of cycles N_C :

$$\dot{m}_T = N_C \int \dot{m} dt \quad (3.261)$$

and similarly, the power produced will be given by:

$$\dot{W}_{TA} = N_C \int W_{is,T} dt \quad (3.262)$$

with N_C indicating the number of cycles per second.

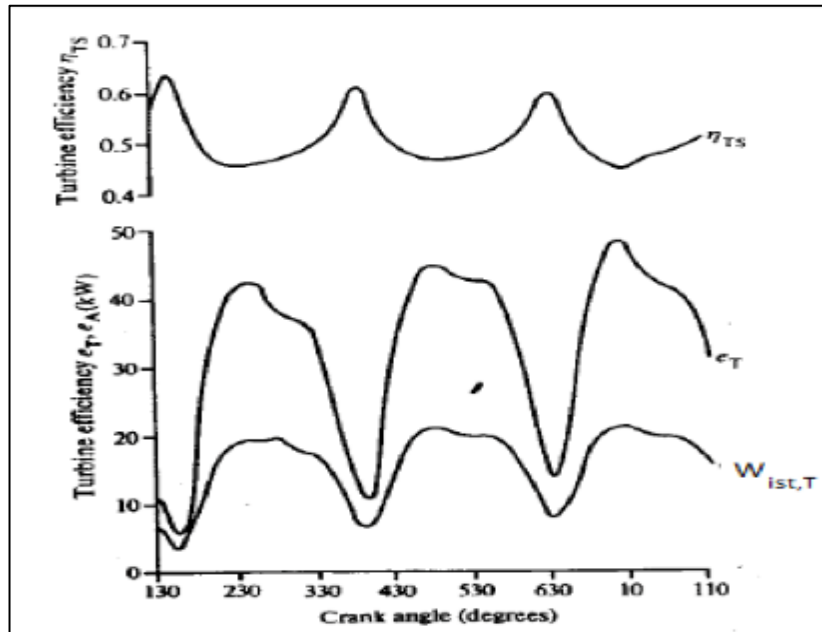


Figure 3:9 Power Performance and efficiency with the crank angle.

3.2. Modeling of centrifugal compressors:

The aerodynamics of the blades of centrifugal compressors is very complex and it is difficult to understand the totality of the fluid dynamic phenomena even in steady flow conditions. The centrifugal compressor, the same way of the turbine, is modeled using the operation curves of the steady-flow analysis as the basis for the non-stationary. The model implemented in Gasdyn allows to identify the boundary conditions of a compressor, considering wave effects in the flow or exhaust.

3.2.1. Characteristics of centrifugal compressors steady stream:

Similarly, to what was done for the turbine also for the compressor performance curves it is described by variables calculated in stationary conditions. These dimensionless parameters can be defined in several ways depending on whether they refer to static or total quantities:

$$\text{Compressor ratio} = \frac{p_{02}}{p_{01}}, \frac{p_2}{p_{01}}, \frac{p_2}{p_1}$$

$$\text{Flow parameter} = \frac{\dot{m}\sqrt{T_{01}}}{p_{01}}, \frac{\dot{m}\sqrt{T_1}}{p_1}$$

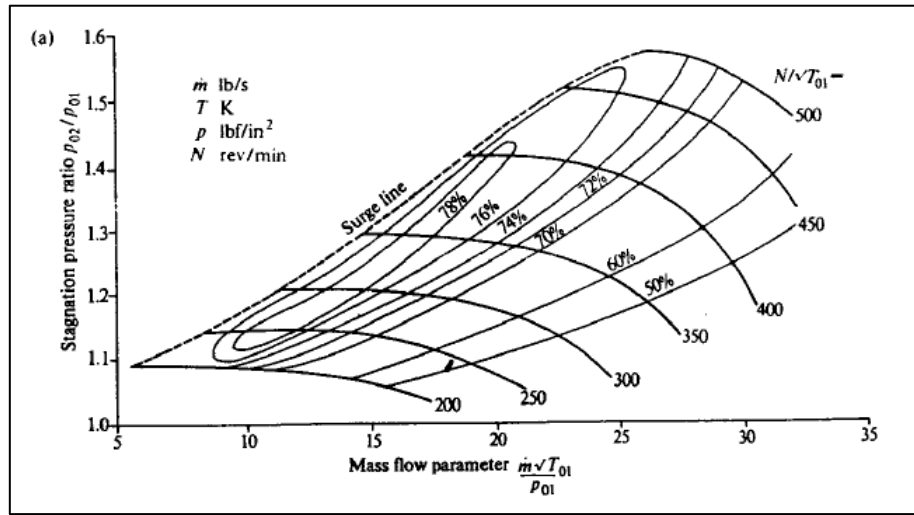


Figure 3:10 Characteristic curve of the total compression ratio - flow parameter of a centrifugal compressor.

$$\text{Speed parameter} = \frac{N}{\sqrt{T_{01}}}, \frac{N}{\sqrt{T_1}}$$

$$\text{Compressor efficiency} = \eta_c = \frac{h_{2S} - h_{01}}{h_{02} - h_{01}}$$

where subscript 01 and 02 will indicate the total quantities on the input section and the output of the compressor and with the subscript 2 the static quantities on the output section.

The characteristic curve that describes the operating conditions of a centrifugal compressor (fig.3.10) shows the trend of the compression ratio with respect to the flow parameter. They also represent the iso-efficiency curves that define the efficiency of the machine in every operating point. The curves are strongly influenced by the flow parameter, if efficiency increases, at equal flow parameter, that could arise in pumping phenomenon, if instead at one of its growth corresponds to an increase of the flow parameter greater compression ratios than are obtainable without problems. From fig.3.11 you can see how the maximum yield point is very close to the choked conditions, therefore much attention must be paid to the fact that in unsteady conditions, the compressor does not work in this area for a prolonged time, else it may result in damage.

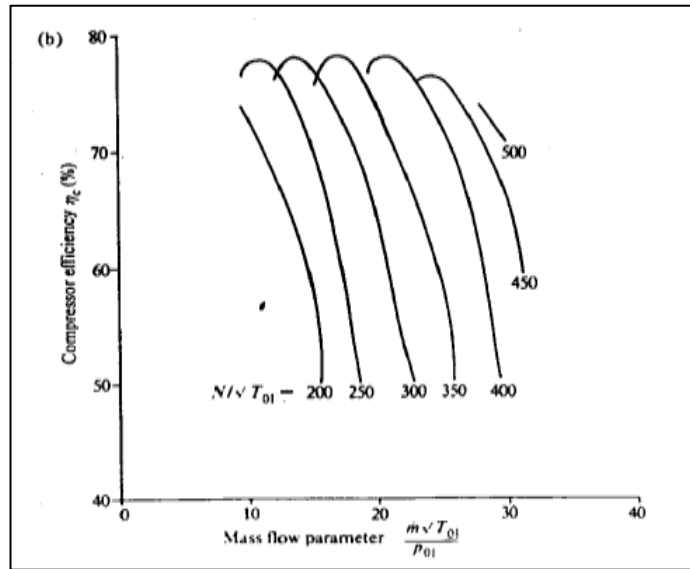


Figure 3:11 Efficiency characteristic curve - flow parameter of a centrifugal compressor.

3.2.2. Performance of centrifugal compressors with variable inlet pressure:

The centrifugal compressor but does not suck directly from the atmosphere through a discharge pipe, the inlet pressure should be considered variable for wave effects in the duct. The procedure for the determination of the boundary equations is analogous to the case of the turbine with variable exhaust pressure, described in section 3.1.2. The resulting equations are in fact identical to the previous case:

$$\frac{\lambda_{in,1}^*}{\lambda_{in,2}^*} = \left(\frac{p_1}{p_2}\right)^{\frac{k-1}{2k}} \left(\frac{1 + C_1 G_1}{1 - C_2 G_1 \left(\frac{p_1}{p_2}\right) \left(\frac{T_2}{T_1}\right)^{\frac{1}{2}}} \right) \quad (3.263)$$

$$\frac{\lambda_{out,1}^*}{\lambda_{in,1}^*} = \left(\frac{1 - C_1 G_1}{1 + C_1 G_1} \right) \quad 3.44$$

$$\frac{\lambda_{out,2}^*}{\lambda_{out,1}^*} = \left(\frac{p_1}{p_2}\right)^{\frac{k-1}{2k}} \left(\frac{1 - C_2 G_1 \left(\frac{p_1}{p_2}\right) \left(\frac{T_2}{T_1}\right)^{\frac{1}{2}}}{1 - C_1 G_1} \right) \quad (3.264)$$

having indicated with 1 and 2 respectively, the upstream and downstream sections of the compressor (fig.3.12).

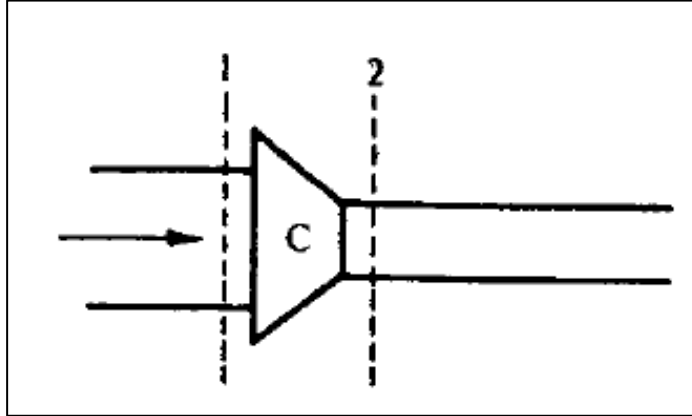


Figure 3:12 representative diagram of a compressor.

The only difference is in the calculation of the (T_2/T_1) ratio due to the different definition of efficiency, the turbine being a driving machine and the compressor a user machine:

$$\frac{T_2}{T_1} = 1 - \frac{1}{\eta_c} \left\{ \left(\frac{P_2}{P_1} \right)^{\frac{k-1}{k}} - 1 \right\} \quad (3.265)$$

The computational method implemented by Gasdyn code is as follows:

1. Calculation of the Riemann variables $\lambda_{in,1}^*$ $\lambda_{in,2}^*$ from $\lambda_{in,1}$, $\lambda_{in,2}$, A_{A1} and A_{A2} ;
2. Calculation of the speed parameter from the characteristics curves and x from eq. (3.253);
3. Determination of (p_1/p_2) , (T_1/T_2) and G_1 by extrapolation from the curves $(x, N/\sqrt{T_{01}})$. Because of the shape of the boundary conditions in correspondence of the reverse flow zone (fig.3.13) is possible for certain values that dx obtain three values of the flow parameter G_1 , in this case, the program takes the value closest to the one previous calculated iteration.
4. Calculation of the Riemann variables $\lambda_{out,1}^*$ $\lambda_{out,2}^*$, from equations (3.251) and (3.252);
5. Calculation of the new A_{A1} and A_{A2} from the initial values and the equation:

$$\frac{A_{A2}}{A_{A1}} = \left(\frac{T_1}{T_2} \right) \left(\frac{P_1}{P_2} \right)^{\frac{k-1}{2k}} \quad (3.266)$$

6. Calculating the values of $\lambda_{in,1}$, $\lambda_{in,2}$, $\lambda_{out,1}$ and $\lambda_{out,2}$.
7. If the difference between the initial values of $\lambda_{in,1}$ and $\lambda_{in,2}$, and calculated values is less than a given tolerance, the solution is the final one, in case it is not so, the algorithm starts from the calculation of $\lambda_{in,1}^*$ $\lambda_{in,2}^*$ and repeat the process as long as this does not happen.

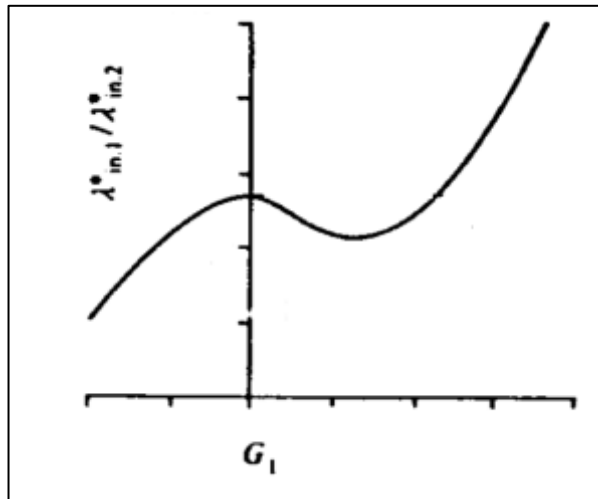


Figure 3:13 Boundary conditions of a centrifugal compressor

3.2.3. Work and Efficiency for centrifugal compressors:

The instantaneous power absorbed by the compressor is obtained as the product between flow rate and enthalpy difference horse of the machine:

$$W_{is,C} = \frac{1}{\eta_c} \dot{m}(h_{01} - h_{2s}) = \frac{1}{\eta_c} \dot{m} c_p T_{01} \left\{ \left(\frac{P_2}{P_1} \right)^{\frac{k-1}{k}} - 1 \right\} \quad (3.267)$$

It's also useful to determine the instantaneous torque that moves the compressor:

$$L_{C,is} = \frac{W_{CI}}{2\pi N} \quad (3.268)$$

The mass flow, the static pressure upstream P_1 and the upstream static temperature T_1 are obtained for each instant of time 't' from the equations which express them as a function of Riemann variables as in the case of the turbine:

$$\dot{m} = \frac{4k}{k-1} \left(\frac{p_{ref}}{a_{ref}} \right) \left\{ \frac{(\lambda_{in} - \lambda_{out})}{(\lambda_{in} + \lambda_{out})^2} \right\} \left(\frac{\lambda_{in} + \lambda_{out}}{2A_A} \right)^{\frac{2k}{k-1}} \quad (3.269)$$

$$p_1 = \left(\frac{\lambda_{in,1} + \lambda_{out,1}}{2A_{A1}} \right)^{\frac{2k}{k-1}} p_{ref} \quad (3.270)$$

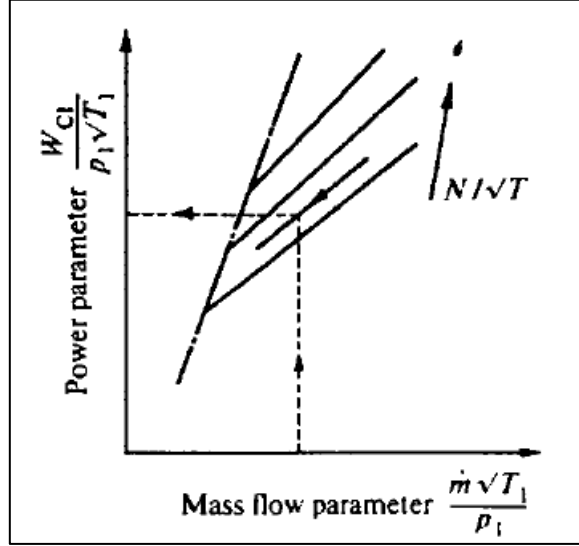


Figure 3:14 Characteristic curve of the total compression ratio - flow parameter of a centrifugal compressor.

$$T_1 = \left(\frac{\lambda_{in,1} + \lambda_{out,1}}{2A_{A1}} \right)^2 T_{ref} \quad (3.271)$$

The power and torque parameters are defined as follows:

$$\frac{W_{is,C}}{\sqrt{T_1} p_1} = \left(\frac{\dot{m} \sqrt{T_1}}{p_1} \right) c_p \left\{ \left(\frac{P_{02}}{P_{01}} \right)^{\frac{k-1}{k}} - 1 \right\} \quad (3.272)$$

$$\frac{L_{C,is}}{p_1} = \left(\frac{\dot{m} \sqrt{T_1}}{p_1} \right) \left(\frac{\sqrt{T_1}}{N} \right) \frac{c_p}{2\pi} \left\{ \left(\frac{P_{02}}{P_{01}} \right)^{\frac{k-1}{k}} - 1 \right\} \quad (3.273)$$

For each instant of time 't', knowing the flow parameter and the speed parameter, it is possible to derive instantaneous power and torque as shown in fig.3.14 and 3.15.

The power ratings and total torque is finally calculated from the integration of the respective parameters on the engine cycle:

$$W_c = \frac{\int \left(\frac{W_{is,c}}{\sqrt{T_1 p_1}} \right) \sqrt{T_1 p_1} dt}{\int dt} \quad (3.274)$$

$$L_c = \frac{\int \left(\frac{L_{c, is}}{p_1} \right) p_1 dt}{\int dt} \quad (3.275)$$

as well as the total incoming mass flow rate in the compressor:

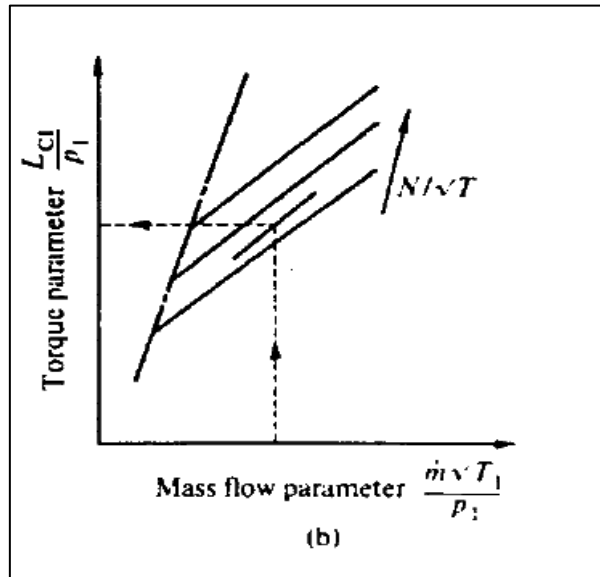


Figure 3:15 Characteristic curve of the total compression ratio - flow parameter of a centrifugal compressor.

$$\dot{m}_c = N_c \int \dot{m} dt \quad (3.276)$$

3.3. Turbo-Matching in Gasdyn:

The turbo-matching is the process by which power balance is achieved on the turbocharger, all the power produced by the turbine is absorbed by the compressor and by any internal components such as the bearings. The mass flow rate processed by the two machines (compressor and turbine) can be different. Also, if waste-gate valve is open then some of the mass flow is by-passed by it and in this case work produced by turbine would be correspond to the fraction of mass flowing through turbine. The Gasdyn Code provides two different analytical methods for turbo-matching between the turbine and compressor. The most simplistic method, called Cyclic Matching, implements a power balance every engine cycle, when the power produced by the turbine is equal to that absorbed by the compressor bearings and hence matching is reached. The second method, called Instantaneous Matching, is more precise as it calculates each time step the instantaneous torque provided and accelerates or decelerates the turbocharger as a function of it.

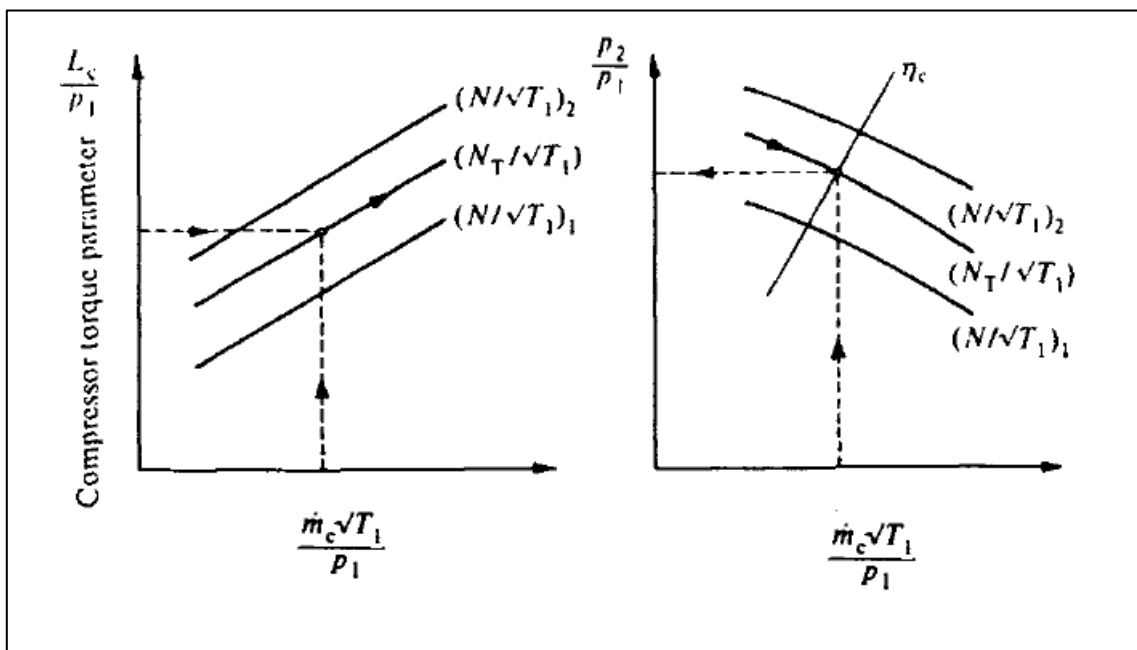


Figure 3:16 characteristic curves of centrifugal compressor

3.3.1. Cyclic Matching:

The Cyclic Matching process implements a power balance on the shaft of turbocharger each engine cycle:

$$\eta_M W_T - W_C = 0 \quad (3.277)$$

Initially the boost pressure p_2 , the temperature T_2 and the turbocharger speed N_T are estimated by characteristic curves. Power produced by the turbine mediated on cycle is calculated from eq. 3.262. It expresses the total flow rate of the compressor, as a product of the flow corresponding to one cycle and the number of cycles (eq. 3.277), to determine the flow parameter ($\dot{m}_c \sqrt{T_1/p_1}$). Knowing the turbine power and the speed of the group, the compressor torque parameter is calculated as:

$$\frac{L_C}{p_1} = \eta_M \frac{L_T}{p_1} \quad (3.278)$$

From the characteristic curves shown in fig.3.5 it is possible to derive the new speed N_T and, by means of it, the new boost pressure p_2 .

The energy balance on the compressor is possible, to calculate the new value of temperature T_2 , by entering the new value of the torque parameter in new equation, which is also obtained from the operation maps:

$$2\pi N_T L_C = \dot{m}_c c_p (T_2 - T_1) \quad (3.279)$$

The iterative process is repeated at the end of each cycle as long as Eq.3.278 is not verified. To reduce the jitter caused by this procedure it is useful to introduce a damping factor D , the lower unit, and define the value of the new turbocharger speed as follows:

$$N_T = N_{T,old} + D(N_{T,new} - N_{T,old}) \quad (3.280)$$

in this way, the convergence of speed is strongly linked to the initial value estimated N_T , p_2 and T_2 .

3.3.2. Instant Matching:

The Instant Matching is more accurate, it is not exactly in fact to consider the constant speed of the turbocharger over the entire engine cycle, it will rise and fall because of the available instantaneous torque variation. If a generic time step of the simulation arises, we can express the torque generated by the turbine and that absorbed by the compressor and bearings as:

$$W_{ist,T} = \frac{L_{ist,T}}{2\pi N_T} \quad (3.281)$$

$$W_{ist,C} = \frac{L_{ist,C}}{2\pi N_T} \quad (3.282)$$

$$W_{ist,B} = (1 - \eta_M) \frac{L_{ist,T}}{2\pi N_T} \quad (3.283)$$

Whist having denoted by the instantaneous powers and η_M the mechanical efficiency of the turbocharger that evaluates the power produced by the turbine less than that absorbed from the bearings. Instant torque available will then be the one developed by the turbine less than that absorbed by the compressor and bearings:

$$L_{ist} = L_{ist,T} - L_{ist,C} - L_{ist,B} \quad (3.284)$$

The turbocharger acceleration is proportional to the instantaneous torque and inversely proportional to the polar moment of inertia of the rotating parts:

$$\frac{dN_T}{dt} = \frac{1}{2\pi I} (\eta_M L_{ist,T} - L_{ist,C}) \quad (3.285)$$

You can define the turbocharger speed N_{T2} at time step following the one in which the speed N_{T1} is as:

$$N_{T_2} = N_{T_1} + \left(\frac{1}{2\pi I} \frac{x_{ref}}{a_{ref}} \right) (\eta_M L_{ist,T} - L_{ist,C}) \quad (3.286)$$

expressing the time difference dt in terms of dimensionless time $dZ = dt (a_{ref}/x_{ref})$. In this way, the turbo-matching is reached instant by instant, if dt is suitably chosen then it is possible to describe the oscillating nature of the turbocharger speed during an engine cycle.

Chapter: 4

4. Turbo-matching Steady state

Turbocharging technique will play a fundamental role in the future not only to improve automotive engine performance, but also to reduce fuel consumption and exhaust emissions both in Spark Ignition and diesel automotive applications. To achieve excellent engine performance for road application, it is necessary to overcome some typical turbocharging drawbacks i.e., low end torque level and transient response. Experimental studies, developed on dedicated test facilities, can supply a lot of information to optimize the engine-turbocharger matching, especially if tests can be extended to the typical engine operating conditions (unsteady flow). A specialized component test rig (particularly suited to study automotive turbochargers) has been operating since several years at the University of Genova. The test facility allows to develop studies under steady or unsteady flow conditions both on single components and subassemblies of engine intake and exhaust circuit.

In the chapter, preliminarily, the measurement of the turbine steady flow performance map is carried out. In a second step the same component is tested under unsteady flow conditions. Instantaneous inlet and outlet static pressure, mass flow rate and turbocharger rotational speed are measured, together with average inlet and outlet temperatures.

The integration of the experimental activity with the numerical analysis represents a methodology that can be helpfully employed during the design process of internal combustion engine intake systems [4].

4.1. Introduction:

It is widely recognized that turbocharging is a very useful technique commonly applied in both Spark-Ignition and Compression Ignition engines to improve engine efficiency. Advanced technologies, such as variable geometry and multi-stage turbocharging, high and low pressure loop EGR systems, assisted turbocharging and turbo-compounding, are emerging to control emissions and maintain fuel economy in both diesel and gasoline engines. Moreover, an effective management of the turbocharging system gives the possibility to achieve a suitable engine torque curve and an excellent vehicle drivability.

The engine-turbocharger matching can be successfully carried out by means of one-dimensional (1D) models. The classical quasi-steady approach, based on the employment of compressor and turbine characteristic maps (provided by the manufacturers or directly measured) is usually followed. Anyway, in many cases, a limited operating domain of the turbocharger device is

available, and mathematical techniques for the extrapolation of the performance maps are commonly utilized in commercial software products. In addition, due to various phenomena, the actual compressor and turbine behavior may differ from the one expressed by the characteristic map. First of all, performance data refer to a steady operation of the devices, while the turbocharger, due to the pressure pulsations caused by the engine, always operates under unsteady conditions. This is particularly true in the case of small S.I engines fitted with a reduced number of cylinders, determining a wide mass flow rate and pressure ratio oscillations during each engine cycle. Moreover, heat transfer through the casing and heat radiated by the turbine and the engine may affect the efficiency values derived at the test-bench.

To analyze the steady and unsteady behaviors, since several years, a specialized component test facility has been operating at the University of Genova. Under Assistant Professor Silvia Marelli (Department of Mechanical, Energy, Management and Transportation Engineering) University of Genova, The test rig is fitted with specific devices which allow for investigations to be performed under steady and unsteady flow operation both on single components and engine subassemblies [5].

4.2. Experimental Rig:

The experimental investigation is carried out on the University of Genova (UNIGE) test facility. Three electrical screw compressors provide a total mass flow rate of about 0.6 kg/s at a maximum pressure of 8 bar. Two independent feeding lines allow to supply turbocharger turbine and compressor with air at controlled pressure thus allowing to measure steady flow maps over an extended range. Main feature of the test rig is the availability of two different systems to generate the unsteady flow typically occurring in the intake and exhaust automotive engine circuit. In a first configuration, diametric slot rotating valves are adopted in order to perform parametric studies by properly controlling the main characteristics of generated pressure pulses (i.e. mean value, amplitude, shape and pulse frequency). The second layout, including a Variable Valve Actuation cylinder head (Fiat Multiair system) makes it possible to analyze the interactions between the engine circuit and both turbocharger turbine and compressor. Measurement of different parameters under steady and unsteady flow conditions is performed by an automatic data acquisition system using dedicated procedures developed in Lab VIEW® environment.

The experimental investigation was performed on a small automotive turbocharger (IHI RHF3) matched to a small-size spark ignition engine. Initially, the reference compressor steady flow maps, expressed in terms of both total-to-total pressure ratio and total-to-total efficiency versus corrected mass flow rate, were measured at different corrected rotational speed levels. Secondly, the compressor performance was evaluated under unsteady flow conditions by integrating the turbocharger in a current production automotive engine intake circuit [6].

4.2.1. Features of the IHI turbo RHF3:

The supercharging unit object of study is characterized by very small dimensions and can reach high engine speeds, in the order of 220000 revolutions per minute.



Figure 4.1: Exploded IHI turbo RHF3.

This unit is manufactured according to the typical architecture of the exhaust-gas turbocharger systems for automotive application, which involves the use of a radial turbine mixed flow and a centrifugal radial compressor.

Fig. 4.1 shows a picture of the turbo group disassembled: the rotors of the two machines, the intermediate casing are visible which encloses the shaft support bearing and the compressor (left) and turbine (right). In the case of mounting on the turbine engine it is also equipped with a tire handling system of the waste-gate by-pass valve of the flue gas in the turbine, for the boost pressure adjustment. This system is not present in Fig. 4.1 as the experimental tests conducted have been carried out with the waste-gate valve in the fully closed position, therefore without the adjustment possibility of the flow of exhaust gas in the turbine involutes.

4.3. Modelling of Steady flow through Turbocharger in Gasdyn.

4.3.1. Duct: Duc

It is the element that allows the modeling of the ducts. The single component is often modeled as a set of conduits and joints, then this tool turns out to be essential. Through the graphical interface, you can set the main features that simulate the actual ducts, such as geometric dimensions, physical characteristics of the material, wall temperature, surface roughness. In addition, you can set the size of the mesh, fundamental parameter for numerical methods introduced in Ch. 1.

4.3.2. Constant pressure junction: Jun

junction is a model that allows you to connect two or more ducts regardless of total pressure losses. It is widely used whenever there is a variation of a limited extent of section diameter (in the order of 1-2 mm on diameter) and in the case of joints with negligible losses, for example, the branching of the intake plenum into the individual ducts. This tool is indispensable in the one-dimensional modeling, in fact the use of dissipative connections in correspondence with each small geometric discontinuity would lead to systematic over estimation of losses.

4.3.3. Sudden diameter variation: Sud

This element allows to model the sudden area changes (contractions and enlargements) along the duct-system, including the evaluation of the consequent concentrated pressure losses. In the case of sudden contractions, a “vena contracta” arises in the restriction, followed by a subsequent expansion of the fluid flow. The effective flow area in the contraction is determined by means of a discharge coefficient ($C_d = A_{\text{effective}}/A_{\text{geometrical}}$ in the contraction), which can be assigned manually or evaluated automatically (C_d auto). Otherwise, an isentropic contraction can be selected, which involves no stagnation pressure loss.

In the case of sudden enlargements, it is supposed that no “vena contracta” arises in the abrupt enlargement ($C_d=1.0$). The model adopted is non-isentropic, allowing for the calculation of the stagnation pressure loss across the enlargement.

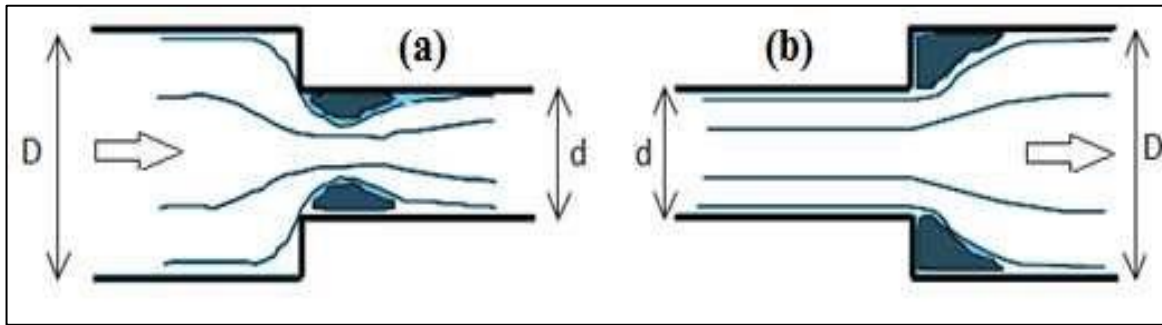


Figure 4:2 (A) Brusco shrinkage resulting contracted vein; (B) abrupt enlargement characterized by a zone of dead water in the first section of the duct of larger cross-section.

Isoentropic

This option allows to treat the sudden contraction of the flow as an isoentropic process, with no stagnation pressure loss.

C_d auto

This option allows to calculate the discharge coefficient ($C_d = A_{\text{effective}}/A_{\text{geometrical}}$ in the contraction) for the sudden contraction automatically, in order, to determine the effective flow area in the restriction. The semi-empirical formula adopted is the following:

$$C_d = 1 - 0.2 \left[1 - \left(\frac{d}{D} \right)^4 \right] \quad (4.287)$$

where D is the large diameter and d the small diameter of the contraction.

C_d [non-dimensional]

This is the discharge coefficient ($C_d = A_{\text{effective}}/A_{\text{geometrical}}$ in the contraction) adopted in the case of sudden contractions to determine the effective flow area due to the “vena” contraction. Typical values are in the range $0.6 \div 0.98$.



4.3.4. Volume:

This zero-dimensional element allows to model a capacity and thus lends itself to be used as a backwater tank in the case of stationary flushing. Assigning a sufficiently high volume it is possible to break down the velocity of flow and then to obtain a static pressure approximately equal to the total pressure, less than a kinetic contribution negligible.

4.3.5. Orifice:

This element allows to model an orifice separating two ducts with different (or equal) diameters. A “vena contracta” arises in the orifice, so that a discharge coefficient is adopted to determine the effective flow area in the restriction. The stagnation (and static) pressure loss in the component is evaluated.

This element can be used also to simulate an EGR valve. Different diameters D1 and D2 upstream and downstream of the orifice can be assigned. The effective flow area is calculated on the basis of semi-empirical formula:

$$C_d = 1 - \left[1 - \left(\frac{d}{D_1} \right)^4 \right] \cdot \left[0.2 + 0.2 \cdot \left(1 - \left(\frac{d}{D_2} \right)^4 \right) \right] \quad (4.288)$$

Where D1 and D2 are the upstream and downstream (large) diameters, and d is the (small) diameter of the contraction.

In our case, orifice is introduced to chock the flow in downstream of compressor line, to simulate the valve in the experimental rig.

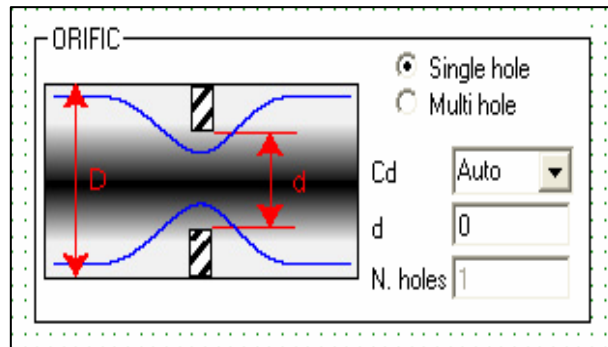


Figure 4:3 Orifice modelling in Gasdyn.

4.3.6 Air Injection:

It is the tool that enables you to impose the desired conditions in the boundary regions of a conduit. In the case of different inlet boundary conditions for turbine inlet side and compressor inlet, among the various possible solutions, mass flow and temperature boundary conditions are imposed on the turbine and compressor inlet sides, so as, to do the turbo-matching.

4.3.7. Y junction: ,

This element allows to model “Y” junctions of three pipes with pressure loss. The concentrated static pressure loss (or pressure recovery) depends on the geometry (angles, diameters) of the

concurrent ducts and on the flow regimes and types. In a “Y” junction two symmetric (equal) pipes are joined to a main duct, with an angle within the two ducts generally in the range 0°-120° (but 60° and 120° are the only values acceptable in this element).

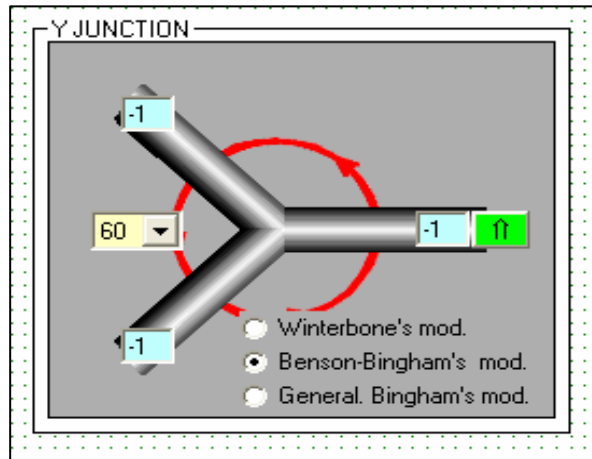


Figure 4:4 Y junction modelling in Gasdyn.



4.3.8. Outlet:

Data for the open termination. This is the tailpipe outlet of the exhaust system. It is modelled as an open end, with the typical acoustical transmission and reflection characteristics of this element. This kind of termination is required to calculate the sound field and the noise radiated at a fixed distance from the outlet. A constant outlet pressure (equal to the ambient pressure or back-pressure) is assumed in the “vena contracta”.

Outflow area ratio:

This coefficient is used to fix the tailpipe outlet effective flow area. If the outlet is a fully open end, the coefficient is in the range 1.0-0.98. If it is a partially open end, the coefficient is given by the ratio between the open flow area and the duct cross-section area. In this case, typical values may be 0.1, 0.5, 0.7, etc.



4.3.9. Output pick-up:

They are virtual sensors that allow the relief of thermo-fluid-dynamic and acoustic magnitudes based on the chosen settings. In the specific case, transducers are placed in the schematic to measure the pressure, temperature and mass flow rate through the ducts at various locations like upstream and downstream of turbine and compressor.

4.4. Turbine: Tur

This element allows to model a single-entry or multi-entry turbine with its fluid dynamic characteristics. In the case of a turbocharged I.C. engine, it is possible to connect this component to the exhaust manifold, to simulate the unsteady flows upstream and downstream of the turbine, the upstream and downstream average pressures, the turbine work and speed on the basis of the turbine map data.

Generally, one-entry or two-entry turbines are adopted on most I.C. engines. The compressor, driven by the turbine, can be also modelled, but this is not strictly necessary. In fact, it is possible to simulate the turbine alone (if the main interest is focused on the pressure pulses in the exhaust system, to optimize the manifold geometry and the silencer), taking into account the turbocharging effect, by means of suitable intake conditions (on the basis of reasonable data or experimental measurements).

Mass flow factor [a_{dim}]:

This factor multiplies the mass flow parameter (m_{T01}/p_{01}) of the turbine map curves. The suggested value is 1.0, when the fluid dynamic characteristics of the turbine matched to the engine are available. For our case, turbine experimental data is available.

Rotor diameter [m]:

This is the max. diameter of the turbine rotor, which is, 0.033 m.

Rotor speed [rps]:

This is the input turbine rotor speed in revolution per second [rps]. A typical value can be in the range 400÷1200 rps. If the compressor is not modelled, this value remains fixed during the calculation, hence it must be assigned carefully. Conversely, if also the compressor is included in the simulation, the matching process of the complete turbocharger to the engine allows to adjust the turbocharger speed during the calculation, on the basis of the turbine and compressor performance maps. In this second case, the rotor speed represents only an initial value.

The graph included in the turbine data window can show two kinds of curves:

4.4.1. Chart type – Map:

The graph included in the map window shows the turbine expansion ratio (p_{01}/p_2) versus the mass flow parameter ($m\sqrt{T_{01}}/p_{01}$), for different values of the speed parameter ($n/\sqrt{T_{01}}$).

The fluid dynamic characteristics of the turbomachine (turbine map) must be assigned for the simulation of the component. The curves of expansion ratio (p_{01}/p_2) versus mass flow parameter ($m\sqrt{T_{01}}/p_{01}$), for different values of the speed parameter ($n/\sqrt{T_{01}}$), must be given in input as a

set of data. So, based on the experimental data gathered at Genova site, below we can see the plotted results for 3 distinctive RPM of turbine.

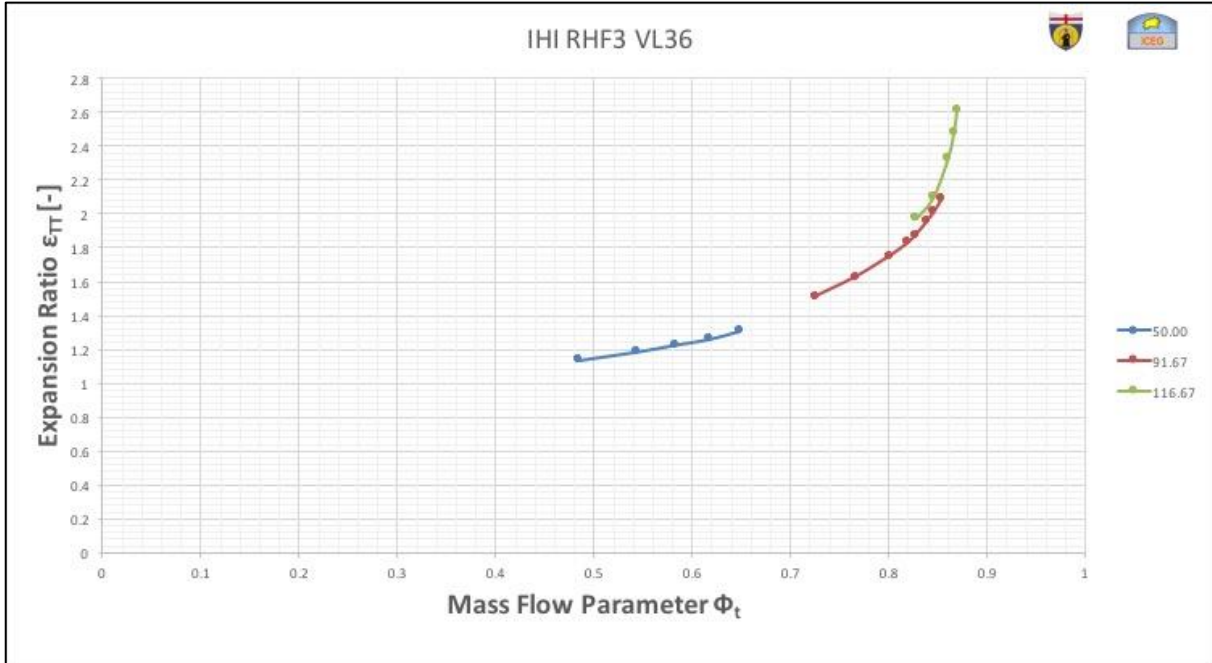


Figure 4:5 Experimental results of turbine (Expansion ratio v/s Mass flow parameter).

Speed (parameter) = Turbine speed parameter ($n/\sqrt{T_{01}}$ [rps/K^{0.5}]).

Mass par = Turbine mass flow parameter ($m\sqrt{T_{01}}/p_{01}$ [kg s⁻¹K^{0.5}/bar]).

Expansion ratio = Turbine expansion ratio (p_{01}/p_2 non-dimensional).

Each curve, corresponding to a certain speed parameter value, must be described by a prefixed number of experimental data couples, on the basis of the experimental map provided by the turbine manufacturer.

4.4.2. Chart type – Efficiency:

The graph included in the efficiencies window shows the turbine fluid dynamic efficiency (η_{ts} , total-to-static) versus the velocity ratio (u/c_{is} , where u is the turbine blade speed, c_{is} is the ideal gas velocity due to an isentropic expansion), for different values of the speed parameter ($n/\sqrt{T_{01}}$).

The fluid dynamic characteristics of the turbomachine (turbine efficiency) must be assigned for the simulation of the component. The curves of efficiency (η_{ts} , total-to-static) versus the velocity ratio. (u/c_{is} , where u is the turbine blade speed, c_{is} is the ideal gas velocity due to an isentropic expansion), for different values of the speed parameter ($n/\sqrt{T_{01}}$) must be given in input as a set of data. All input data are expressed in the S.I. system.

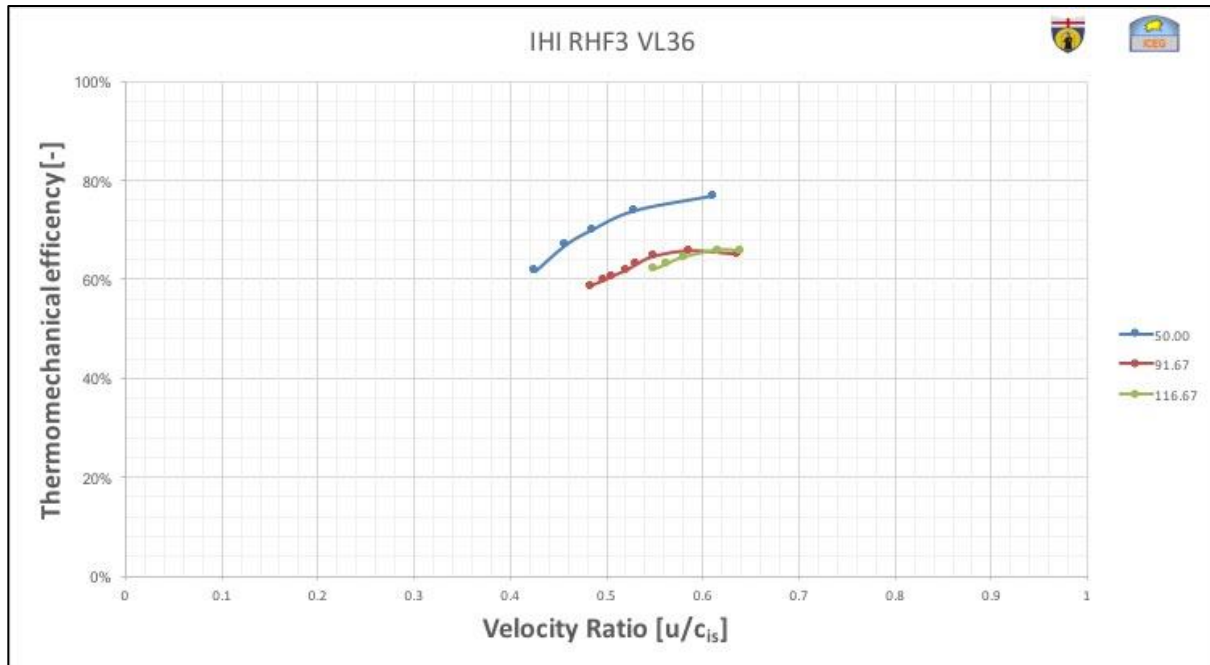


Figure 4:6 Experimental results of turbine (Efficiency v/s velocity ratio).

Speed (parameter) = Turbine speed parameter ($n/\sqrt{T_{01}}$ [rps/ $K^{0.5}$]).

Velocity R = Turbine velocity ratio (u/c_{1s} non-dimensional).

Efficiency = Turbine efficiency (η_{ts} non-dimensional).

Each curve, corresponding to a certain speed parameter value, must be described by a prefixed number of experimental data couples, on the basis of the experimental measurements provided by the turbine manufacturer. Each curve must leave from the origin.

4.5 Compressor: Com

This element allows to model a centrifugal, axial or volumetric compressor driven by the turbine to supercharge the engine, by considering its fluid dynamic characteristics.

In the case of a turbocharged i.c. engine, it is possible to connect this component to the intake manifold as the first element of the intake. The model adopted currently allows to simulate the unsteady flows downstream of the compressor, the air delivery pressure and temperature, the compressor work and speed on the basis of performance map data.

Mass flow factor [adim.]

This factor multiplies the mass flow parameter ($m\sqrt{T_{01}/p_{01}}$), of the compressor map curves. The suggested value is 1.0, when the fluid dynamic characteristics of the compressor matched to the engine are available. If the data refer to a different compressor (larger/smaller), it is possible to couple it to the engine by adjusting the mass flow factor (generally in the range 0.1÷10.0).

Rotor momentum of inertia [kg/m²]:

This is the momentum of inertia of the turbocharger rotor 4.226e-06 [kg/m²]. It is necessary to calculate the new turbine and compressor operating conditions by means of the turbocharger model with rotor inertia.

Mechanical efficiency [%]:

This is the mechanical efficiency of the turbocharger, expressed in [%]. It is necessary to calculate the shaft energy balance of the turbocharger; a typical value lies in the range 95÷98 %.

Accuracy limit [%]:

It is necessary to fix a tolerance or accuracy limit [%] to determine when the turbocharger has been matched to the engine (with the required accuracy), i.e. a stable operating point has been achieved for both the engine and the turbocharger. In this situation, after a certain number of simulation cycles, the turbocharger speed is stable, within the assigned accuracy limit, which can be in the range 1÷15%. The suggested value for a reasonable result is 5 %. The smaller (larger) the accuracy limit, the larger (smaller) the number of cycles required to achieve a stable turbocharger operating point, i.e. a satisfactory matching of the turbocharger to the engine
The graph included in the compressor data window can show two kinds of curves:

4.5.1. Chart type – Map:

The compressor compression ratio (p_{02}/p_{01}) versus the mass flow ($m\sqrt{T_{01}/p_{01}}$), for different values of the speed parameter ($n/\sqrt{T_{01}}$);

Surge line:

The map is limited on the left by the surge line. This is the limitation of the air flow at the compressor inlet. If the pressure ratio is too high and the volume flow is too small, the air no longer sticks to the suction side of the blades, then the discharge process is interrupted. The air flow stops going through the compressor and is reversed until the pressure is stabilized and the positive volume flow rate is reached again, then the pressure builds up again and the cycle

repeats. This flow instability creates a pulsation and the resulting noise is known as "surging" [7].

Choke line:

The cross section of the compressor inlet is normally the limitation of the maximum centrifugal compressor volume flow rate. When the flow at the inlet reaches it's maximum velocity the flow rate can no longer be increased. The choke line is the rapidly descending line on the right of the compressor map [7].

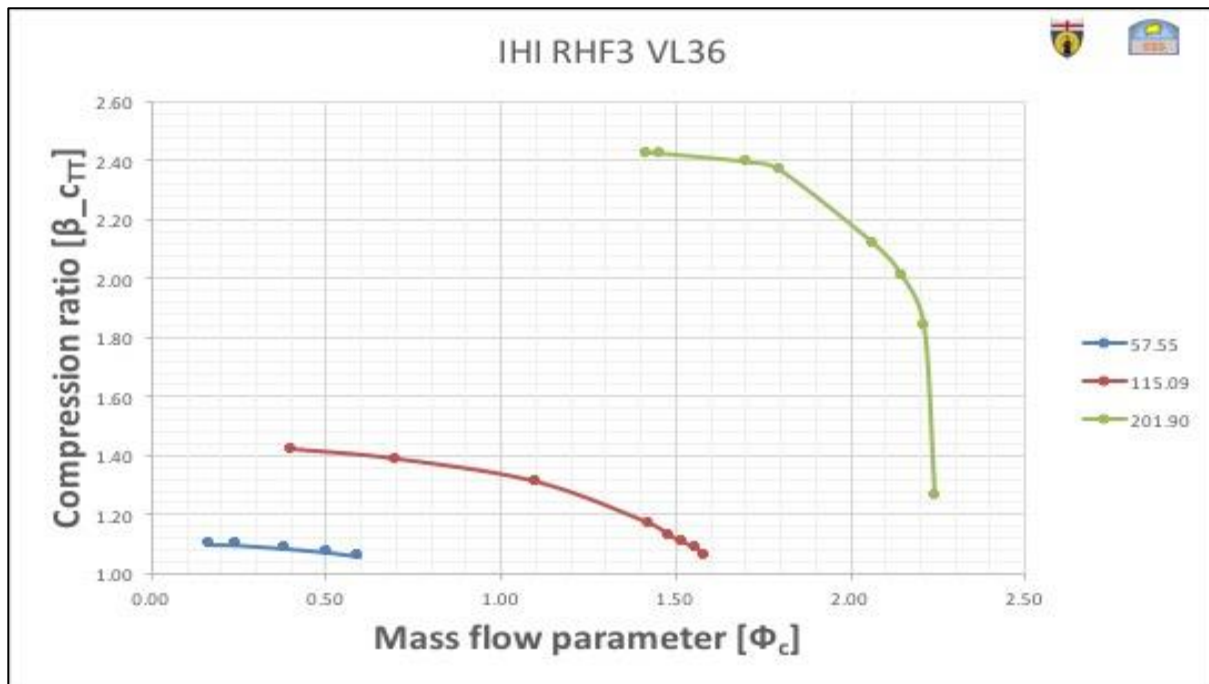


Figure 4:7 Experimental results of compressor (Compression ratio v/s Mass flow parameter).

4.5.2. Chart type - Efficiency:

The compressor fluid dynamic efficiency (η_{TT} , total-to-total, or η_{TS} , total-to-static) versus the mass flow parameter ($m\sqrt{T_{01}/p_{01}}$), for different values of the speed parameter ($n/\sqrt{T_{01}}$).

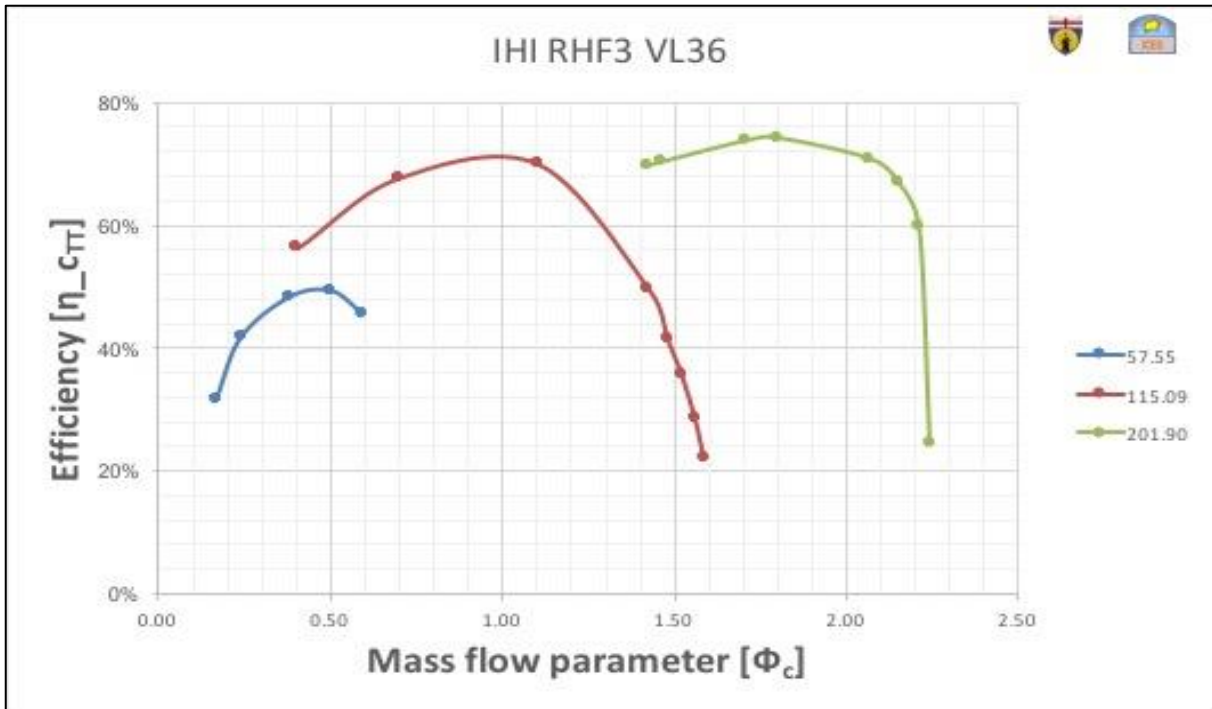


Figure 4:8 Experimental results of compressor (Efficiency v/s Mass flow parameter).

4.6. Smoothing and Extrapolating of Compressor and Turbine Curves:

It is necessary to extrapolate the compressor curves beyond the surge limit to allow a safe simulation, without interruptions. In fact, during the turbocharger matching process, sometimes a provisional operating point could lay into the compressor surge region, to finally achieve a realistic operating point at the end of the simulation (providing the turbocharger matched to the engine within the required accuracy limit). Hence, the compressor curves (compression ratio and efficiency vs. mass flow parameter) and turbine curves (expansion ratio vs. mass flow parameter and efficiency vs. velocity ratio) must be extrapolated for different speed parameter values.

In order to do that, we use Matlab tool (spline function) to extrapolate and fit the curves. Usually because the maps are listed with different values of Speed parameter, we used the Matlab program interpolating "spline" data on an interval sets of Speed Parameter, from the point of view of the modeling of a motor is necessary to have the greatest number of points as possible. In fact, for a correct interpolation of the maps during the simulation of the transient turbocharger, you must have the full curves. Resulting curves are shown in figures [8].

4.6.1. Extrapolated and smooth Turbine curves:

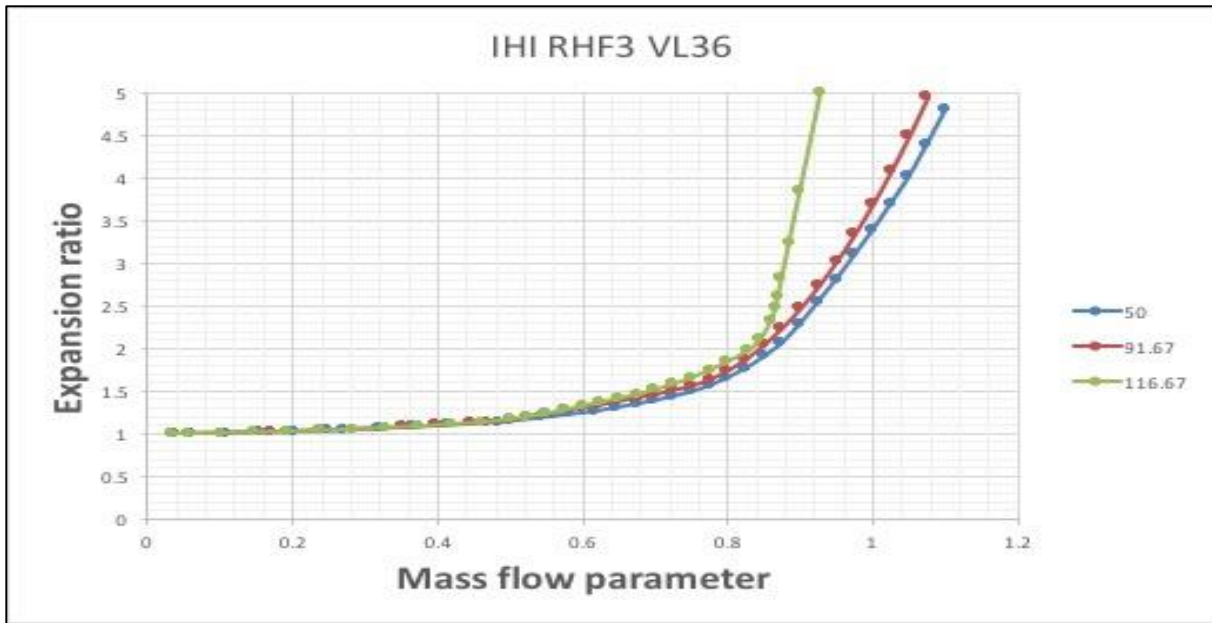


Figure 4:9 Extrapolated result of turbine's Expansion ratio v/s Mass flow parameter curve.

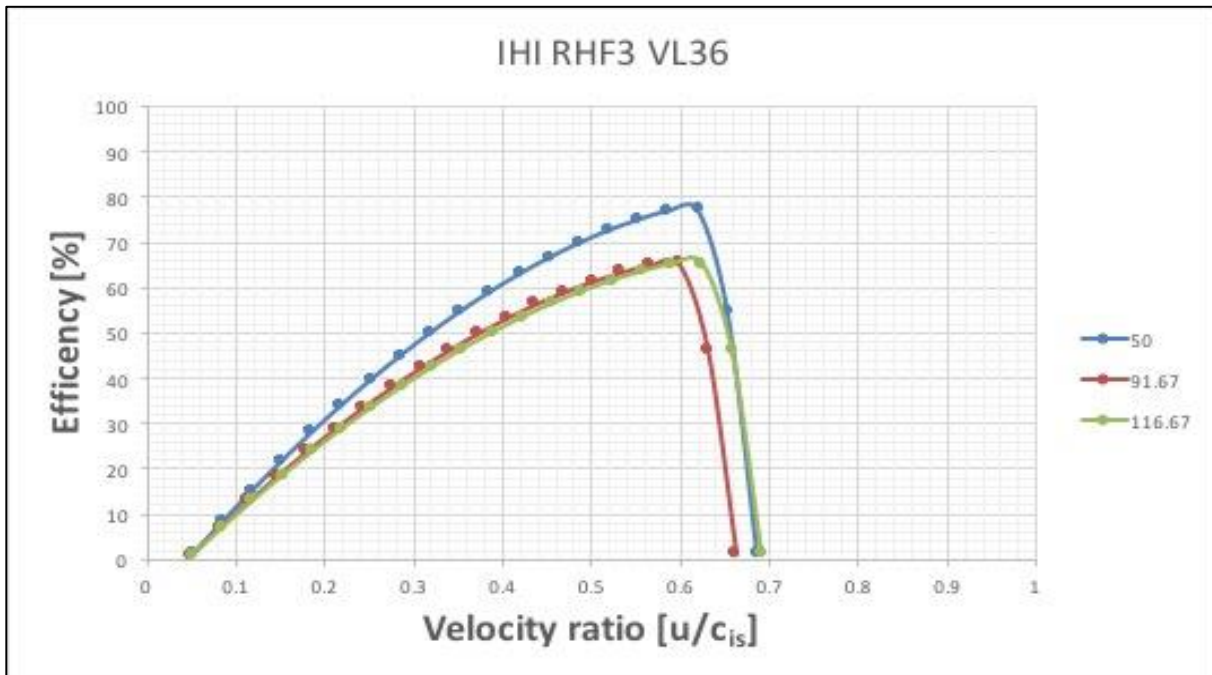


Figure 4:10 Extrapolated result of turbine's efficiency v/s velocity ratio curve.

4.6.2 Extrapolated and smooth Compressor curves:

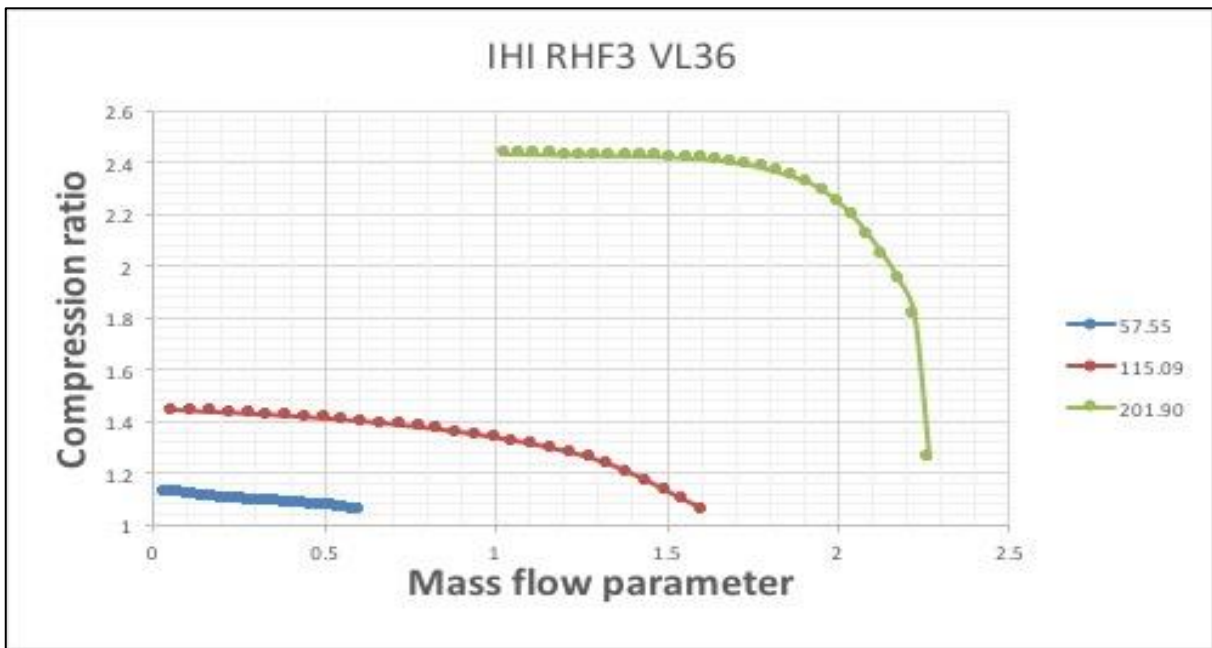


Figure 4:11 Extrapolated result of compressor's Compression ratio v/s Mass flow parameter curve.

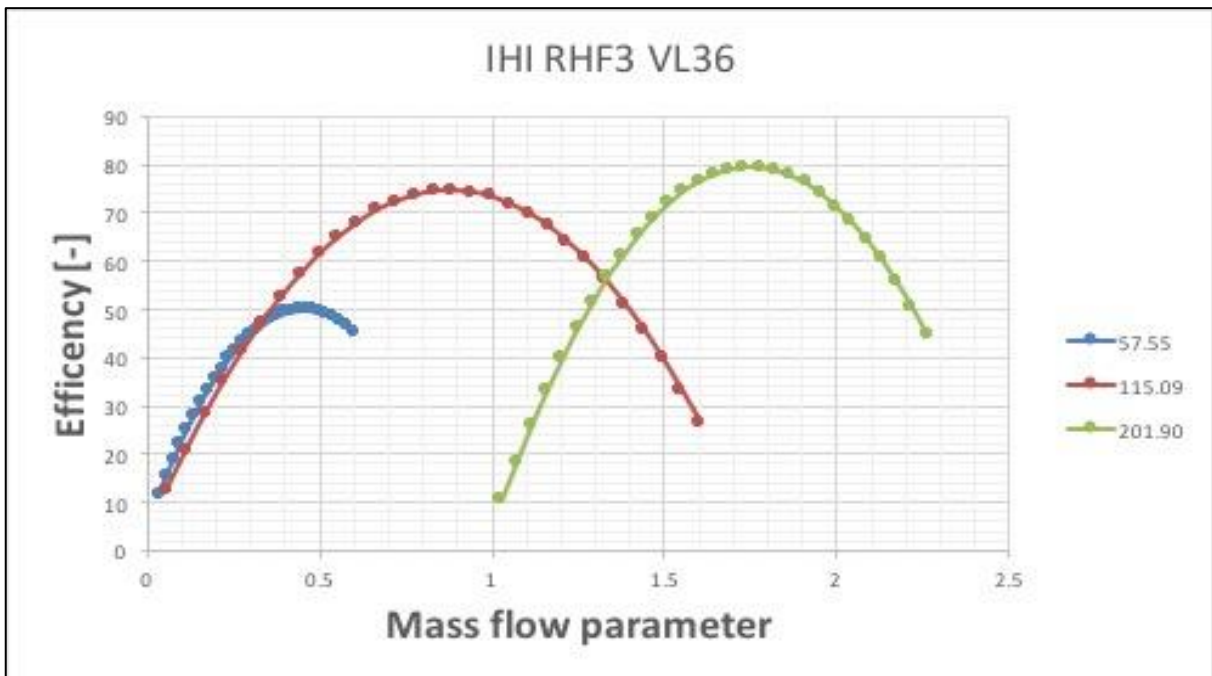


Figure 4:12 Extrapolated result of compressor's efficiency v/s Mass flow parameter curve.

4.7. Gasdyn Modelling and Simulation for steady state:

Based on the experimental rig setup, a schematic of experimental rig is prepared in 1D Gasdyn simulation software as shown in figure 4.13 with following circuits and dimensions:

4.7.1. Input circuit of the turbine:

An injector “Injector-1” is introduced in the modelling upstream of turbine side to impose the boundary conditions on the Inlets T-1, T-2, T-3 and T-4.

Symmetric Inlets T-1 and T-3 are taken with following pipe lines dimensions:

pipeY_noRV-1 ($D_{in}=69$ mm, $D_{out}=69$ mm, $L=155$ mm)
 pipeY_noRV-5 ($D_{in}=69$ mm, $D_{out}=69$ mm, $L=385$ mm)
 pipeY_noRV-7 ($D_{in}=41$ mm, $D_{out}=41$ mm, $L=53$ mm)
 curve 1-4 (flow-split) ($Vol=3563.202943$ mm³)
 pipeY_noRV-11 ($D_{in}=41$ mm, $D_{out}=41$ mm, $L=185$ mm)
 partValve-1 (ball valve) $D=41$ mm
 pipeY_noRV-9 ($D_{in}=41$ mm, $D_{out}=41$ mm, $L=105$ mm)
 Y-2 (flow-split) ($Vol=123575.8037$ mm³)
 pipeY-1 ($D_{in}=41$ mm, $D_{out}=41$ mm, $L=80$ mm)

Symmetric Inlets T-2 and T-4 are taken with following pipe lines dimensions:

metal tubing ($D_{in} = 52.5$ mm, $D_{out} = 52.5$ mm, $L = 313$ mm)
 converging portion ($D_{in} = 52.5$ mm, $D_{out} = 45.5$ mm, $L = 44$ mm)

4.7.2. Output circuit of the turbine:

Converging adaptor ($D_{in} = 70$ mm, $D_{out} = 54$ mm, $L = 100$ mm)
 2 identical adapters ($D_{in} = D_{out} = 54$ mm, $L = 356$ mm)
 PipeT-Out-1 ($D_{in}=70,3$ mm, $D_{out}=70,3$ mm, $L=575$ mm)
 PipeT-Out-2 ($D_{in}=70,3$ mm, $D_{out}=106,3$ mm, $L=115$ mm)
 PipeT-Out-3 ($D_{in}=106,3$ mm, $D_{out}=106,3$ mm, $L=190$ mm)
 PipeT-Out-4 ($D_{in}=106,3$ mm, $D_{out}=158,3$ mm, $L=130$ mm)
 PipeT-Out-5 ($D_{in}=158,3$ mm, $D_{out}=158,3$ mm, $L=545$ mm)
 PipeT-bend-1 (curve 90°, $D_{in}=158,3$ mm, $D_{out}=158,3$ mm, radius of curvature = 229 mm)
 PipeT-Out-6 ($D_{in}=158,3$ mm, $D_{out}=158,3$ mm, $L=3644$ mm)
 PipeT-bend-2 (curve 90°, $D_{in}=158,3$ mm, $D_{out}=158,3$ mm, radius of curvature = 229 mm)
 PipeT-Out-7 ($D_{in}=158,3$ mm, $D_{out}=158,3$ mm, $L=3475$ mm)
 Outlet T-1

4.7.3. Input circuit of the Compressor:

Inlet C-1

PipeC-In-3 ($D_{in}=106,3$ mm, $D_{out}=106,3$ mm, $L=445$ mm)

PipeC-bend-1 (curve 90° , $D_{in}=106,3$ mm, $D_{out}=106,3$ mm, radius of curvature =152 mm)

PipeC-In-4 ($D_{in}=106,3$ mm, $D_{out}=106,3$ mm, $L=1020$ mm)

PipeC-bend-2 (curve 90° , $D_{in}=106,3$ mm, $D_{out}=106,3$ mm, radius of curvature =152 mm)

PipeC-In-5 ($D_{in}=106,3$ mm, $D_{out}=106,3$ mm, $L=245$ mm)

PipeC-bend-3 (curve 90° , $D_{in}=106,3$ mm, $D_{out}=106,3$ mm, radius of curvature =152 mm)

PipeC-In-8 ($D_{in}=106,3$ mm, $D_{out}=50$ mm, $L=110$ mm)

Pipe in plastic material (curve 90° , $D_{in} = D_{out} = 51$ mm, radius of curvature = 430 mm)

Portion of metal tubing ($D_{in} = 44.3$ mm, $D_{out} = 44.3$ mm, $L = 300$ mm)

adapter tube (plastic) ($D_{in} = 44.3$ mm, $D_{out} = 51$ mm, $L = 90$ mm)

4.7.4. Output circuit of the Compressor:

Rubber sleeve ($D_{in} = D_{out} = 36$ mm, $L = 80$ mm)

Portion of metal tubing ($D_{in} = D_{out} = 38$ mm, $L = 300$ mm)

Rubber sleeve ($D_{in} = D_{out} = 36$ mm, $L = 220$ mm)

Metal conduit ($D_{in} = D_{out} = 36$ mm, $L = 200$ mm)

PipeT-Out-1 ($D_{in}=70,3$ mm, $D_{out}=70,3$ mm, $L=575$ mm)

PipeT-Out-2 ($D_{in}=70,3$ mm, $D_{out}=106,3$ mm, $L=115$ mm)

PipeC-Out-1 ($D_{in}=90$ mm, $D_{out}=90$ mm, $L=880$ mm)

PipeC-bend-7 (curve 90° , $D_{in}=90$ mm, $D_{out}=90$ mm, radius of curvature =26 mm)

PipeC-Out-2 ($D_{in}=90$ mm, $D_{out}=90$ mm, $L=3970$ mm)

Outlet C-1

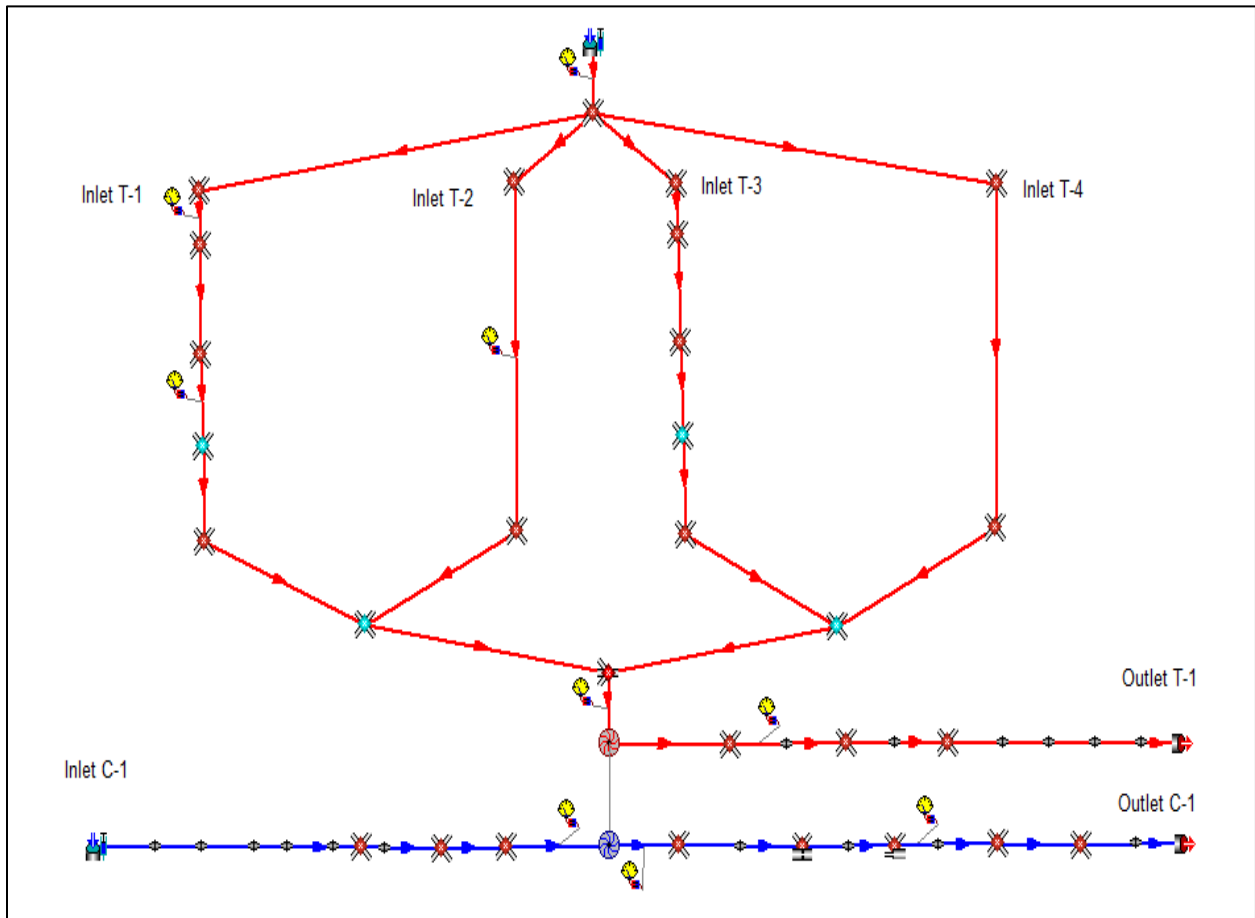


Figure 4:13 Gasdyn schematic of steady-state flow through Turbo-charger.

4.7.5. Boundary conditions:

As there is no cylinder in the model, so the RPM and no. of cycles sets only gives us the time of simulation for steady state to get the convergence. Which in our case is set to 4000 RPM and 50 cycles, gives us 1.5 seconds, in order to get the results, which is fair time to get the steady state convergence and turbo-matching.

An injector is placed upstream of Inlet T-1, T-2, T-3 and T-4 with mass and temperature boundary conditions, to regulate the mass flow, temperature and pressure entering the turbine inlet.

Same Concept is applied in the upstream of compressor inlet C-1, with temperature and mass flow boundary conditions. Though inlet of compressor should be kept as ambient condition but for some experimental readings, pressurized conditions upstream of the compressor, necessary to control the power absorbed by the compressor.

C-Valve-1 (in experimental rig setup) represents the motorized valve to the delivery side of the compressor, which is modelled as an orifice in the upstream of compressor with different chocked diameter, to achieve the desired boost pressure upstream of compressor.

Ambient conditions are maintained at the outlet T-1 and outlet C-1, which are present at the experimental site.

4.7.6. Results:

Once schematic of the experimental rig is modelled in Gasdyn with the specification provided in sections 4.7.1 to 4.7.4 along with the boundary conditions mentioned in section 4.7.5. Simulations for 4 different operating points is run (picked from experimental data) to match and compare the results obtained from simulation and experiment. The results from the simulation and experiments are plotted below in figures 4.14 to 4.18.

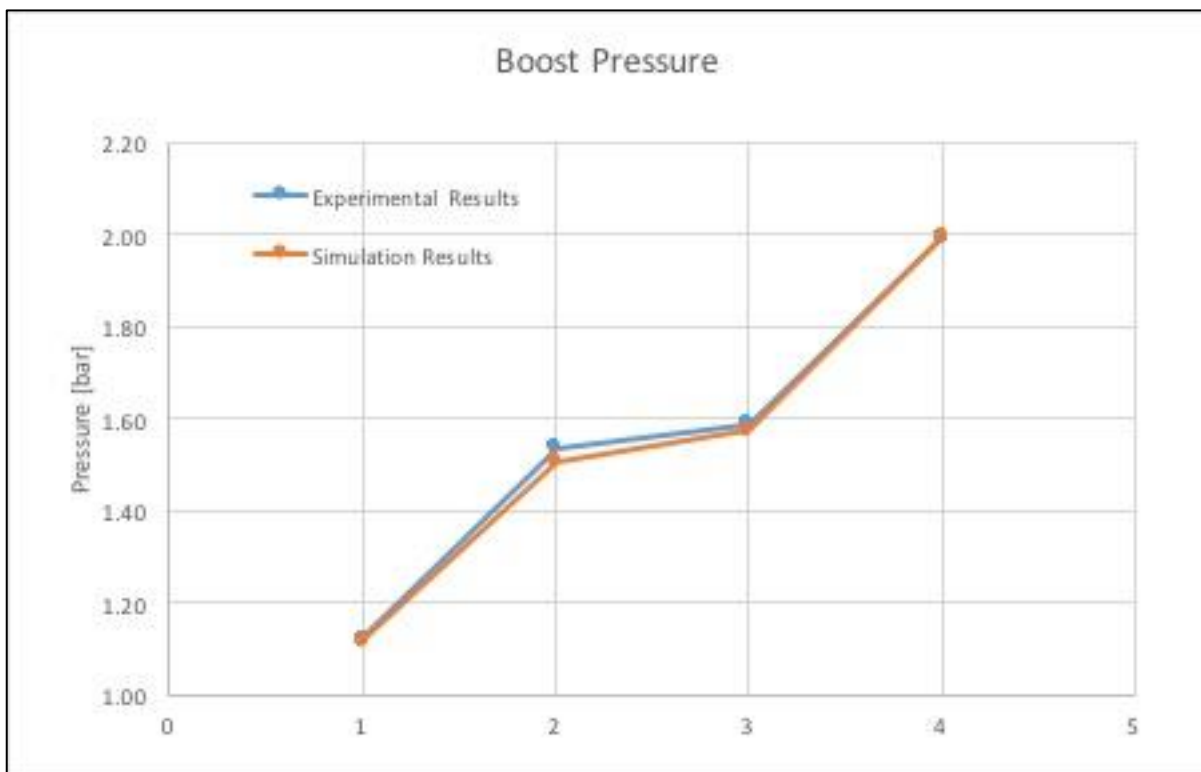


Figure 4.14: Comparison of boost pressure (Experimental v/s simulation) at the downstream of compressor.

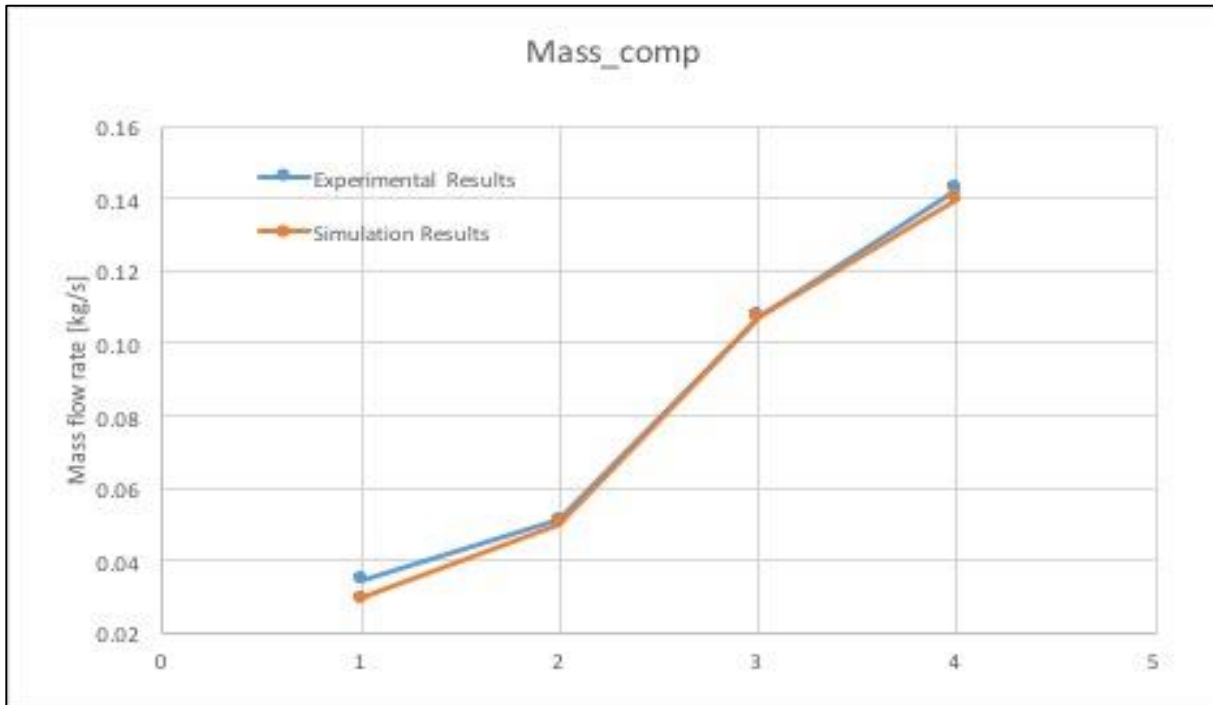


Figure 4:15: Comparison of mass flow through compressor line (Experimental v/s simulation).

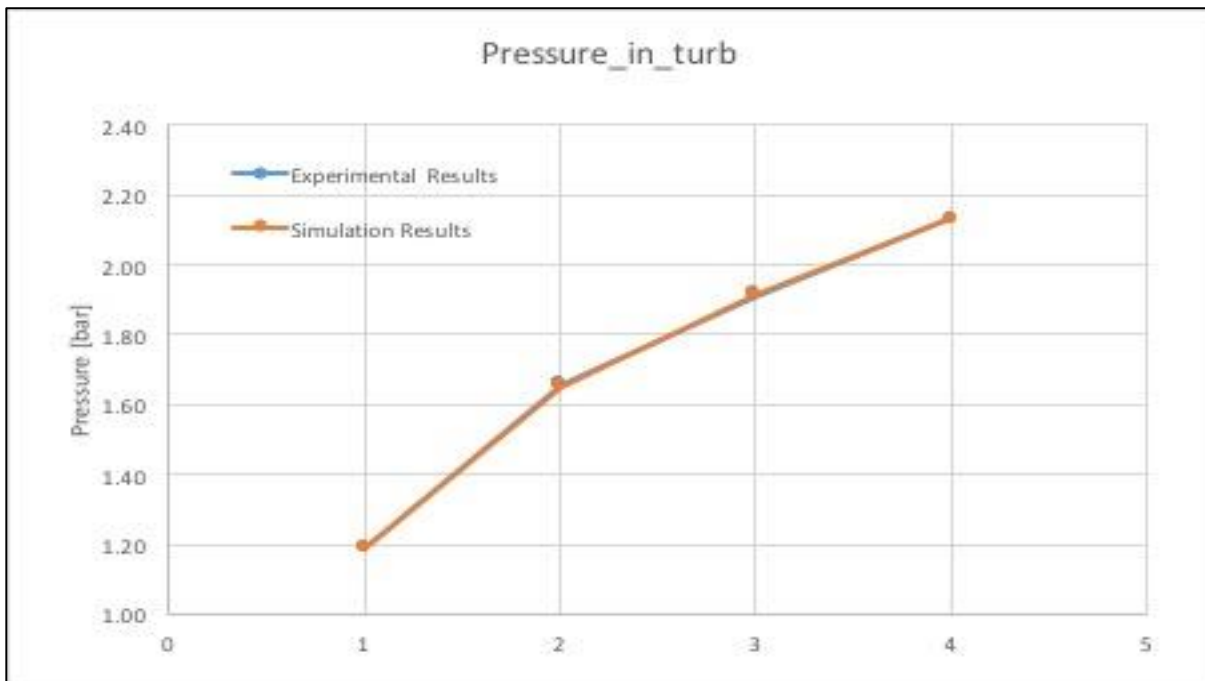


Figure 4:16: Comparison of pressure upstream of turbine (Experimental v/s simulation).

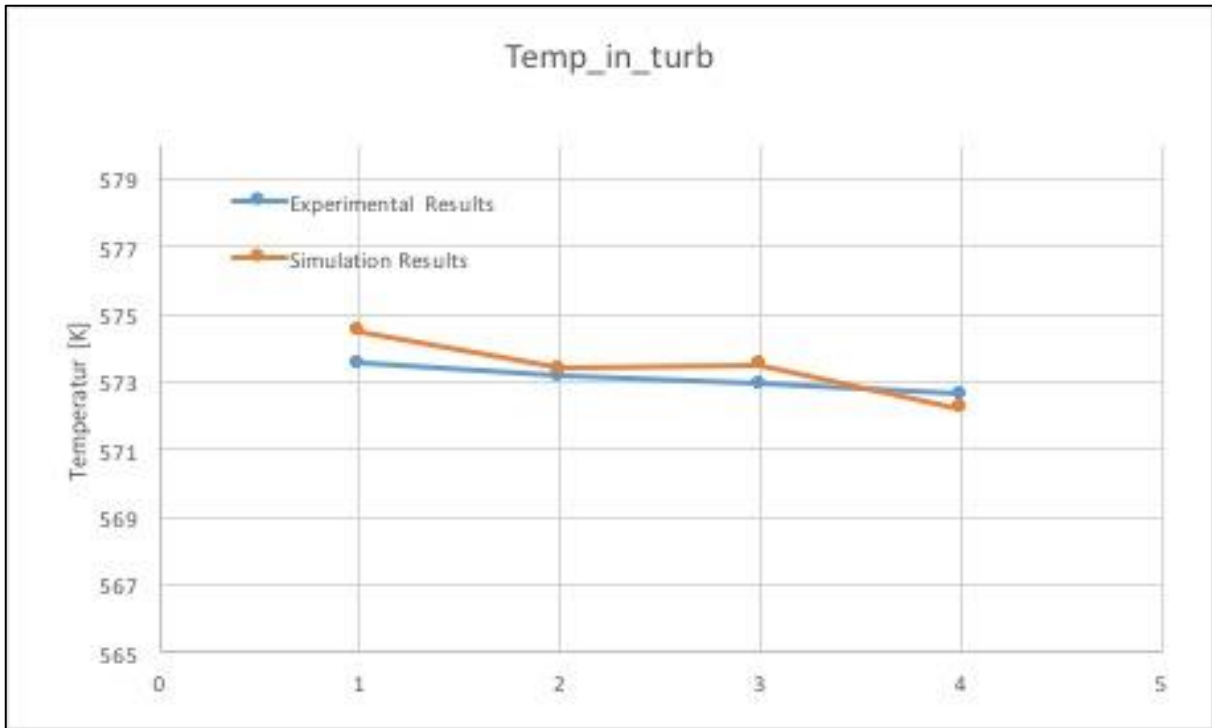


Figure 4:17: Comparison of Flow Temperature at the inlet of turbine (Experimental v/s simulation).

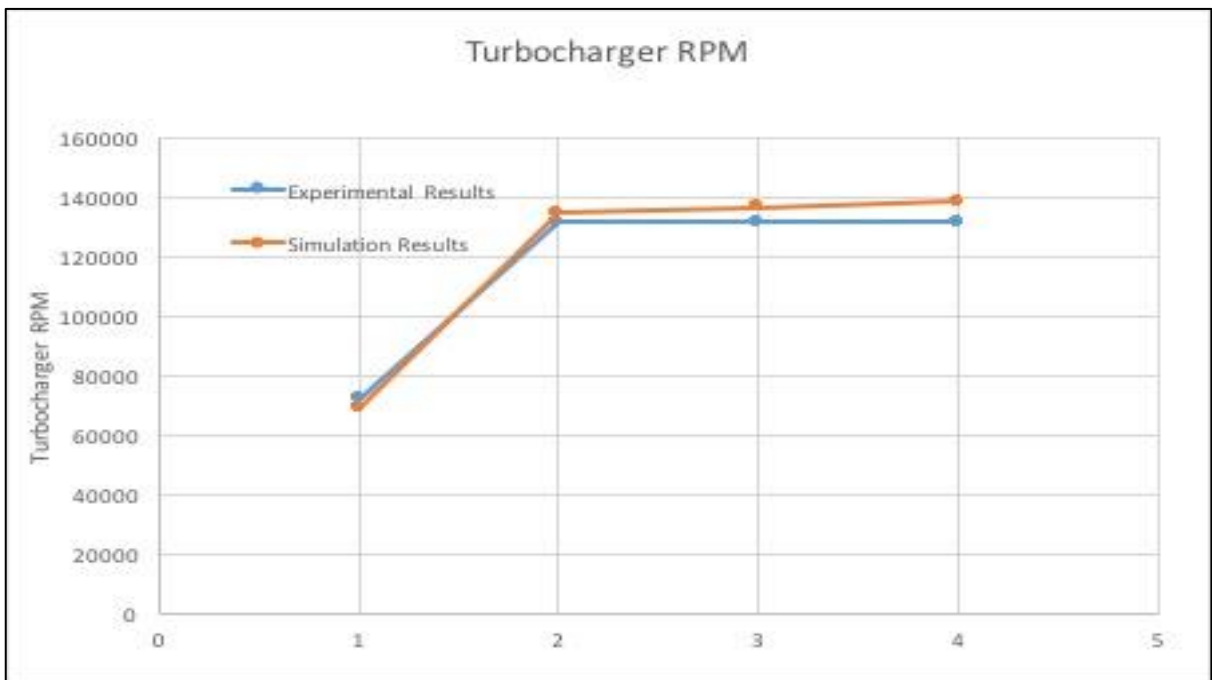


Figure 4:18: Comparison of Turbocharger speed (Experimental v/s simulation RPM).

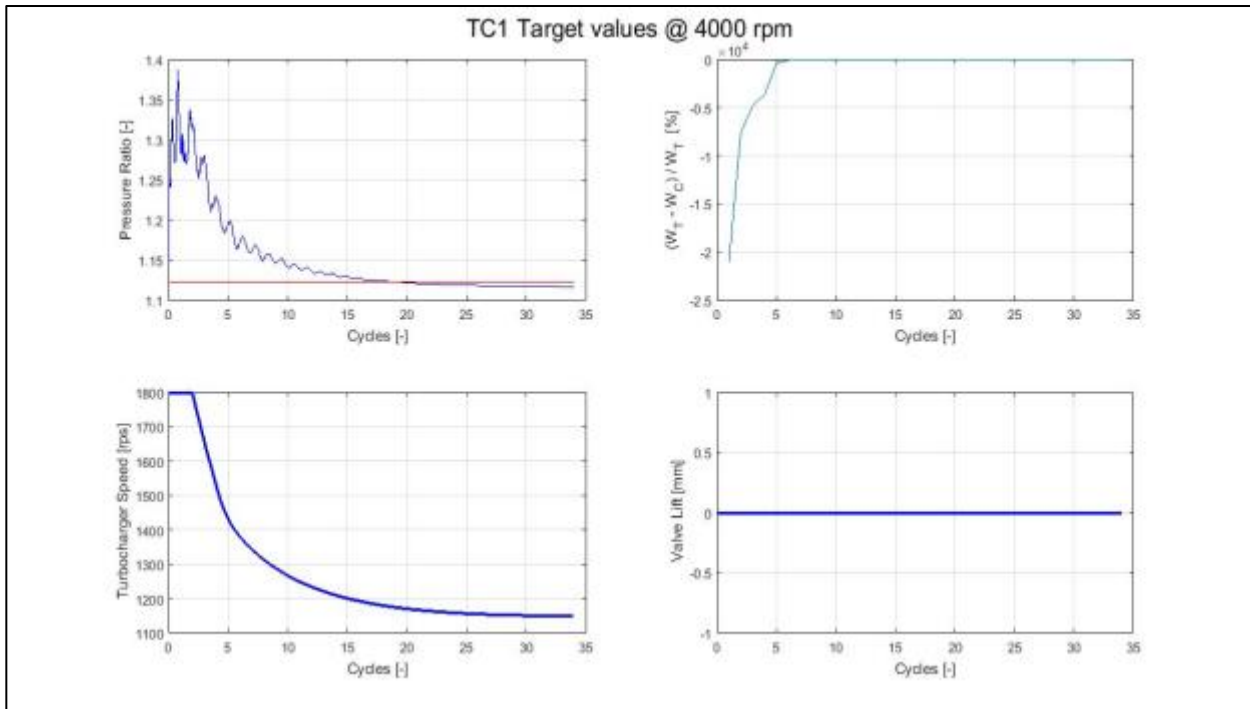


Figure 4:19: Plot of boost pressure, turbocharger speed and power balance of 1st simulated point.

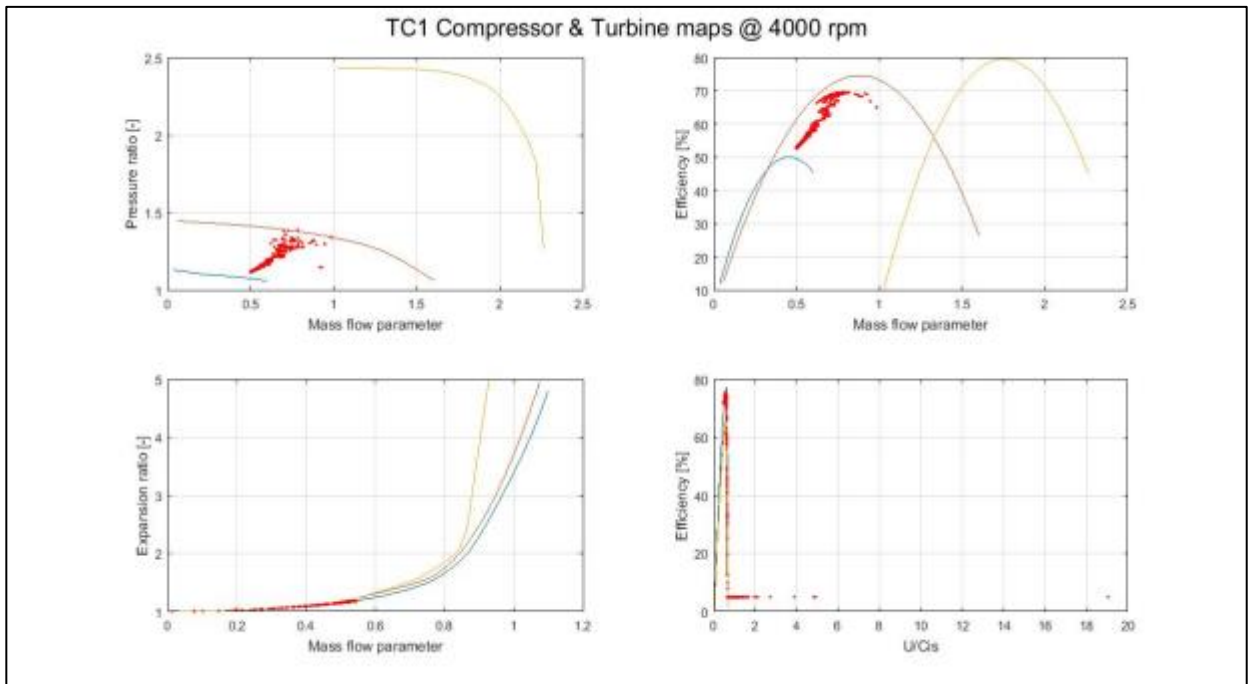


Figure 4:20: Plot of Iterative step's value for 1st simulated point during simulation cycles.

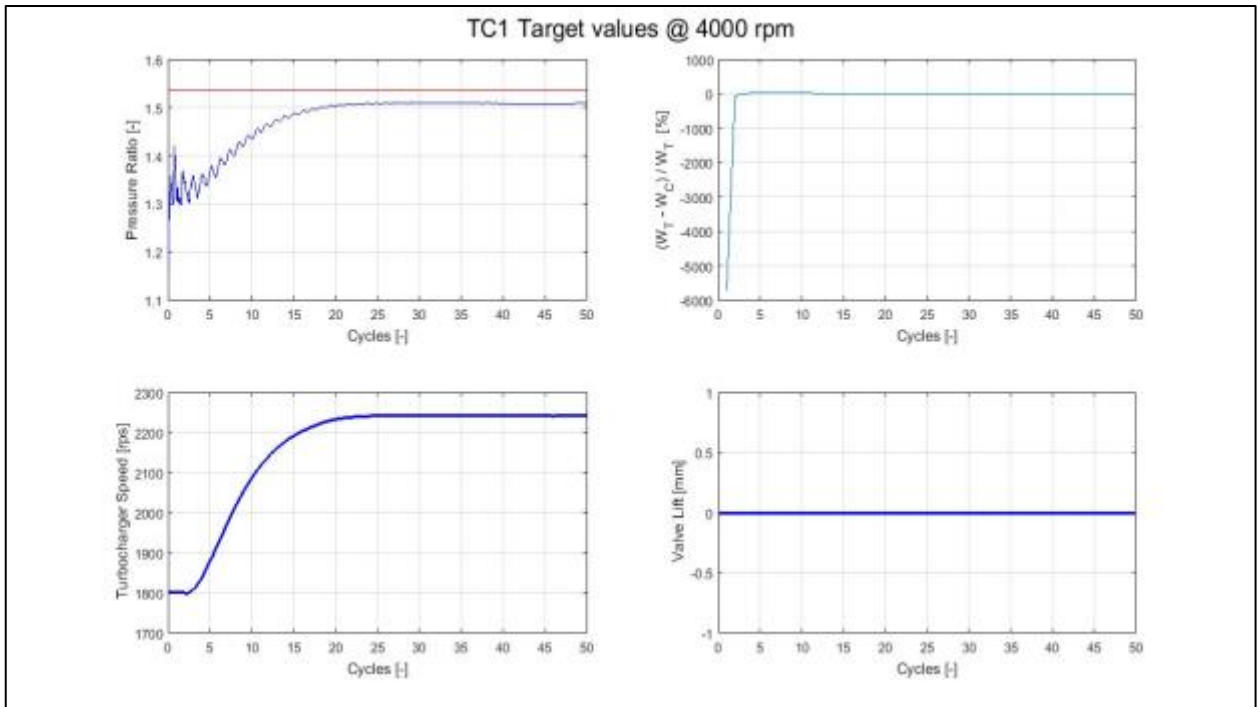


Figure 4:21: Plot of boost pressure, turbocharger speed and power balance of 2nd simulated point.

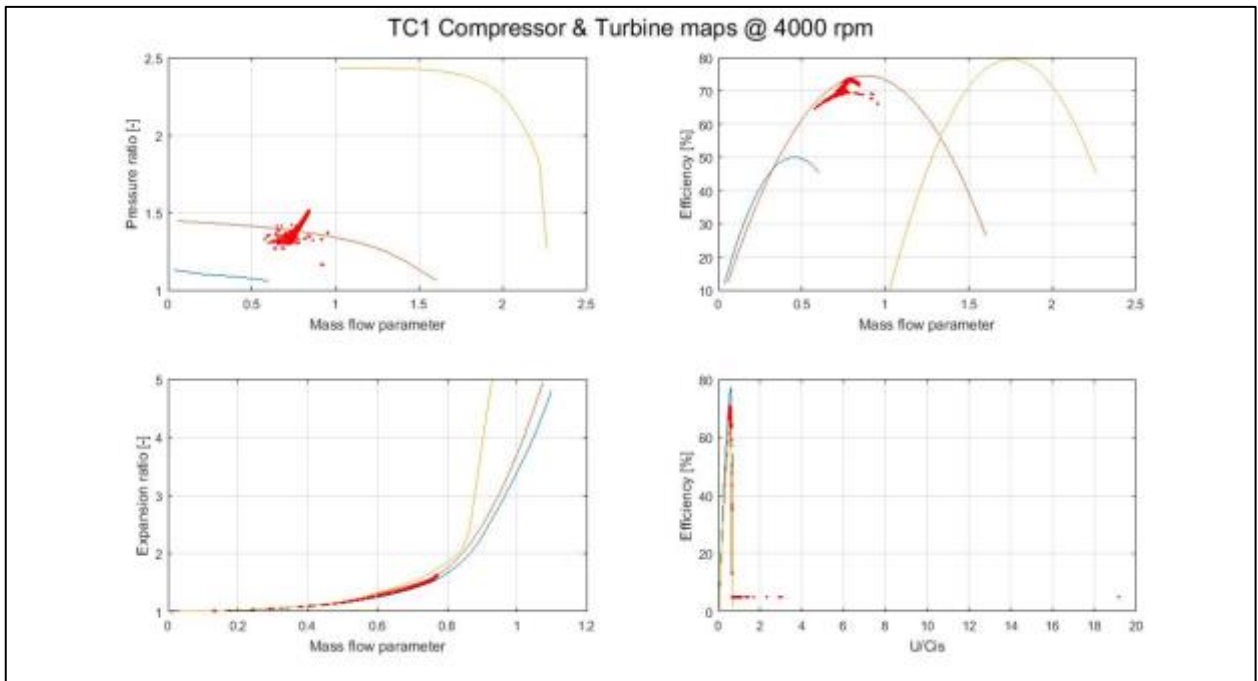


Figure 4:22: Plot of Iterative step's value for 2nd simulated point during simulation cycles.

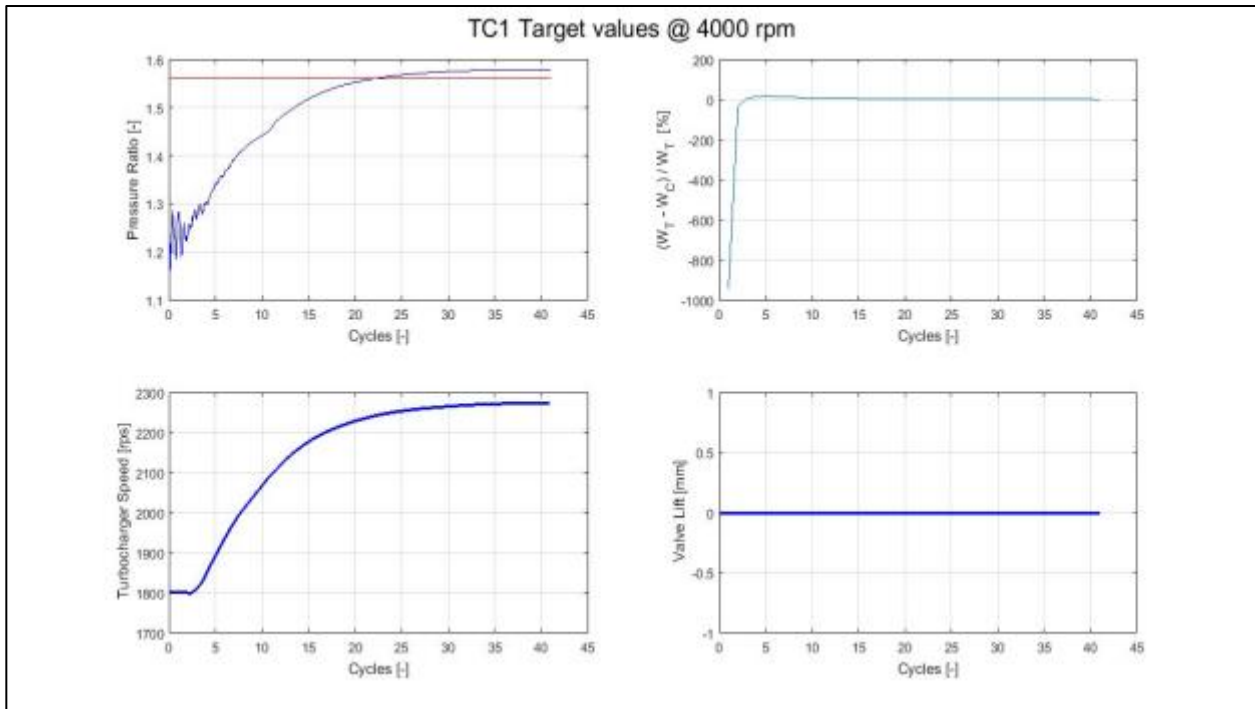


Figure 4:23: Plot of boost pressure, turbocharger speed and power balance of 3rd simulated point.

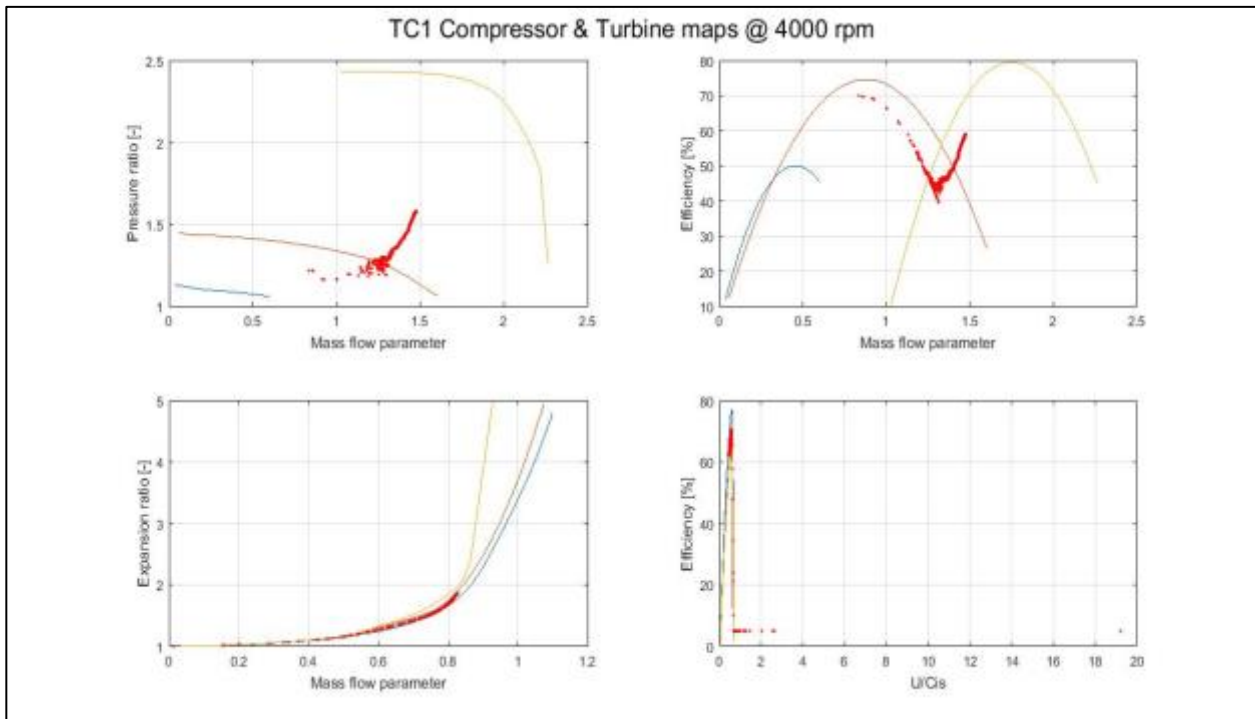


Figure 4:24: Plot of Iterative step's value for 3rd simulated point during simulation cycles.

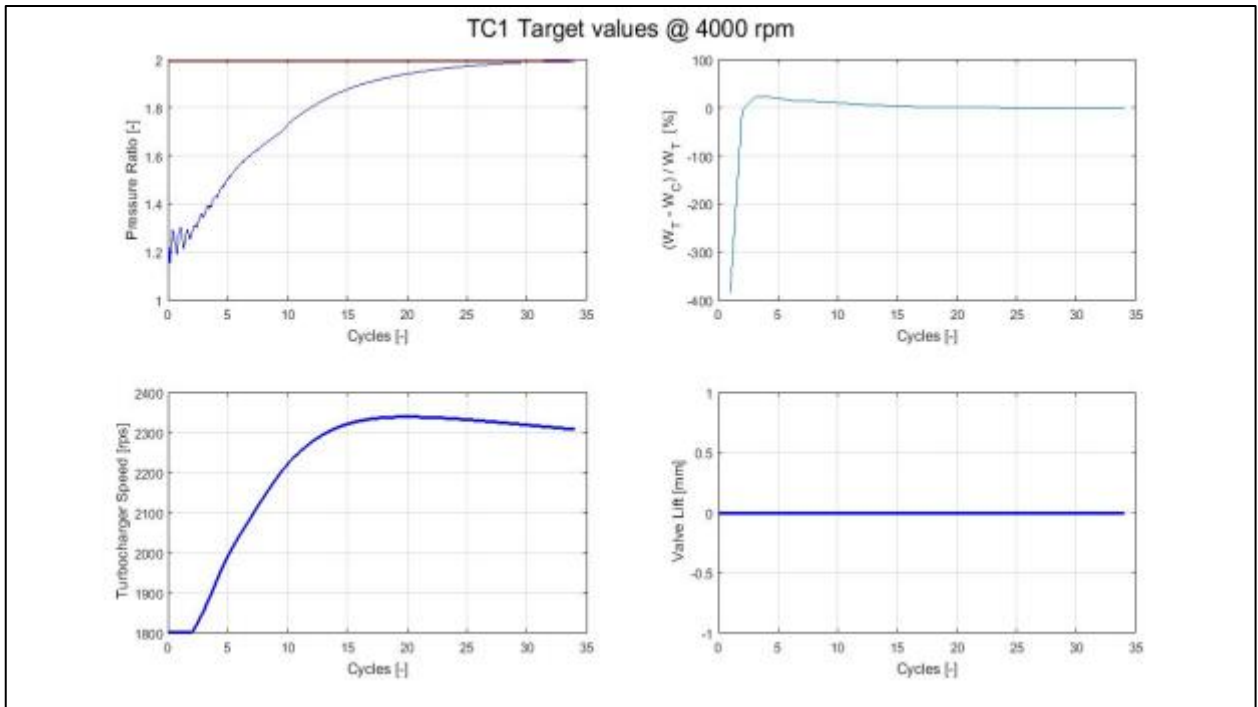


Figure 4:25: Plot of boost pressure, turbocharger speed and power balance of 4th simulated point.

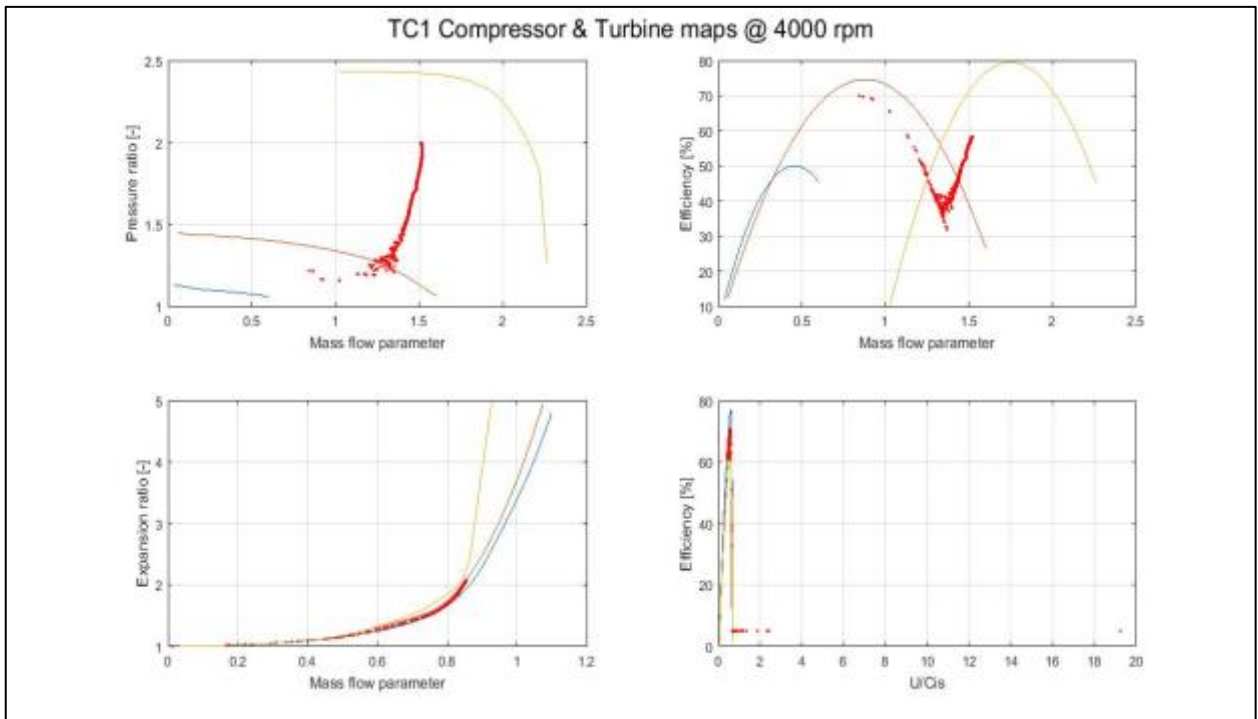


Figure 4:26: Plot of Iterative step's value for 4th simulated point during simulation cycles.

4.8. Conclusion and Future Work:

A good match of experimental data and simulation results can be seen in figures 4.14 to 4.18. This shows the good ability of Gasdyn software to simulate the turbocharger for steady flow.

For future work, Gasdyn can be used to simulate unsteady flow through turbocharger. To simulate the pulsating flow produced by motorized rotating valve, we can introduce a cylinder (with no piston movement but intake and outlet poppet valves in action) in upstream of turbine line to simulate the pulsating flow.

Chapter: 5

5. Convergence Algorithm for Turbocharger:

The correct study of turbocharger and its characteristic demands necessitates to reach a condition of "stability", in which its operating conditions between a cycle and the next can be considered almost unchanged: this means that the average speed of turbocharger must not vary appreciably. Once you reach this stability it is possible to determine on the turbine and compressor maps a region of instantaneous operating points which corresponds to a single point of cyclic operation: in these conditions the matching condition was obtained, which is the equality of the work in a cycle between turbine and compressor.

Previously in the older version of Gasdyn, the convergence condition was represented by the value of the percentage deviation of the oscillation speed of the turbocharger, which had to be lower than a set limit value. As a first approximation compliance with this condition may have seemed effective: in reality, it had problems due to the fact that the turbocharger speed fell within the set tolerance despite this was still accelerating or decelerating. Precisely for this reason it is an alternative model of convergence been implemented.

5.1. Old Condition for Turbocharger convergence (v.10.2.1):

When the simulation for turbocharger is run with some predefined no. of simulation cycles for each engine rpm and with tolerance limit, to stop the simulation, we put some conditions/constraints on various parameters to achieve the convergence and hence stop the simulation for that rpm. At first, we check the below mentioned conditions only after some certain no. of cycles for example (5 cycles), so that we don't stop the simulation in early stage where for first few cycles we can easily be mistaken for the convergence tolerance criteria. So for the same reason, all the below conditions are active after 5 cycles of the simulation. Then following conditions, as explained below, apply.

5.1.1. Condition 1:

As anticipated the main parameter is represented by the gradient of the average speed of the turbocharger, boost pressure, Power balance b/w compressor and turbine to be compared with a reference tolerance value set in an "input file" usually equal to 0.03%; The calculation of the gradient can be easily traced to the calculation of the derivative:

$$\frac{\text{Mean speed } (n + 1) - \text{Meanspeed}(n)}{\text{cycangle}} \leq \text{Toll_acc} \quad (5.289)$$

Where:

- Cycangle = angle of rotation necessary to achieve a complete cycle, 720 ° for a four-stroke.
- Mean Speed (n + 1) = average speed of the next cycle (+ 720 °);
- Mean Speed (n) = average speed of the previous cycle, taken as a reference.
- Toll_acc = is the acceptable tolerance for convergence on turbo speed.

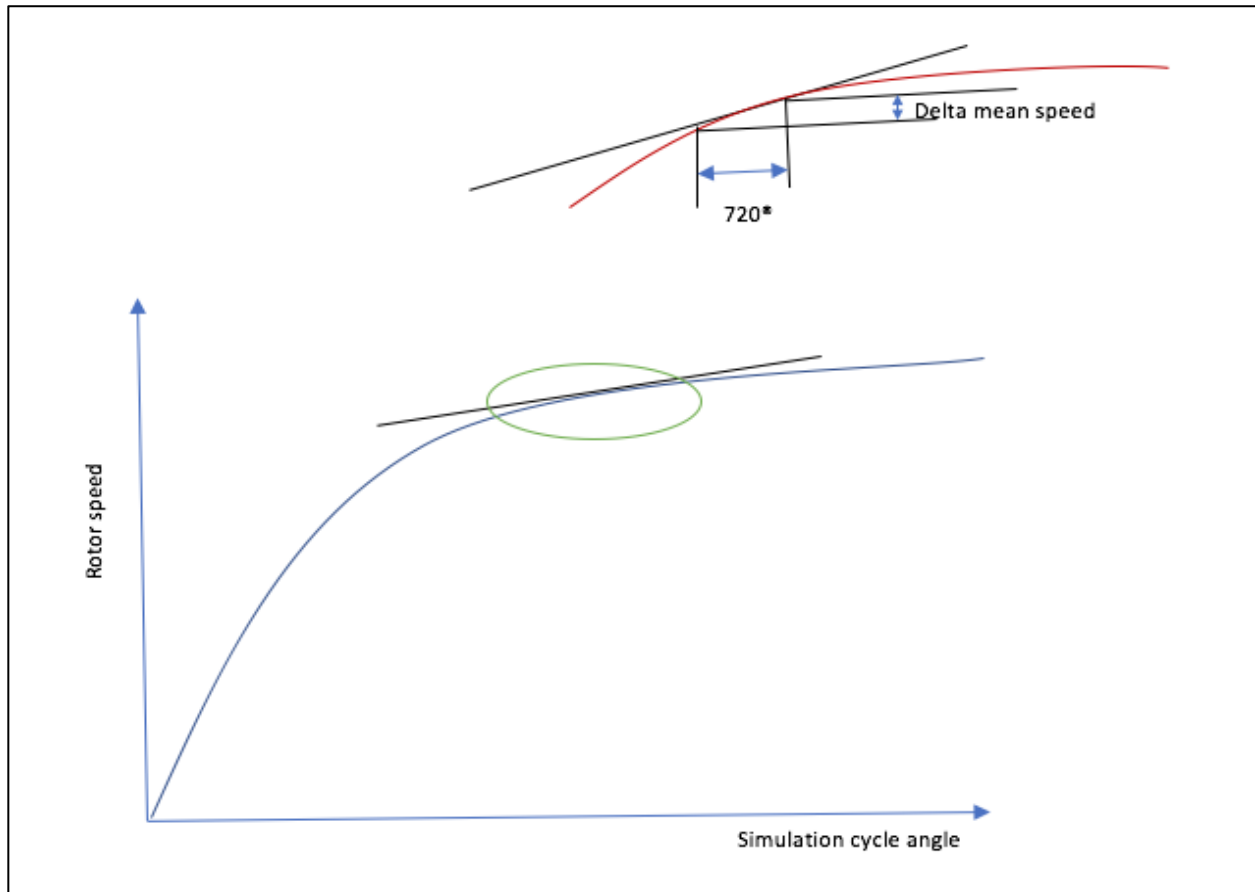


Figure 5:1 Slope tolerance of Turbo-speed for convergence.

The convergence achieved is considered as the slope of the velocity curve becomes less than the tolerance value imposed; in these conditions, it can be argued that in fact the curtain speed to asymptotically to a constant value.

5.1.2. Condition 2:

Second condition to reach convergence is put on the delivery boost pressure. Where difference in the target boost pressure and boost pressure in the current cycle is measured and if this difference is within the acceptable tolerance limit then we are met with this condition and if all other conditions are fulfilled then it's fine to stop the simulation of that rpm of engine.

$$\frac{P_{boost_{target}} - P_{boost_{nturbo}}}{P_{boost_{target}}} \leq Toll_{pboost} \quad (5.290)$$

Where:

- P_boost target is the boost pressure to be achieved.
- P_boost_nturbo is the boost pressure achieved in the current cycle.
- Toll_pboost is the acceptable tolerance limit set to stop the simulation.

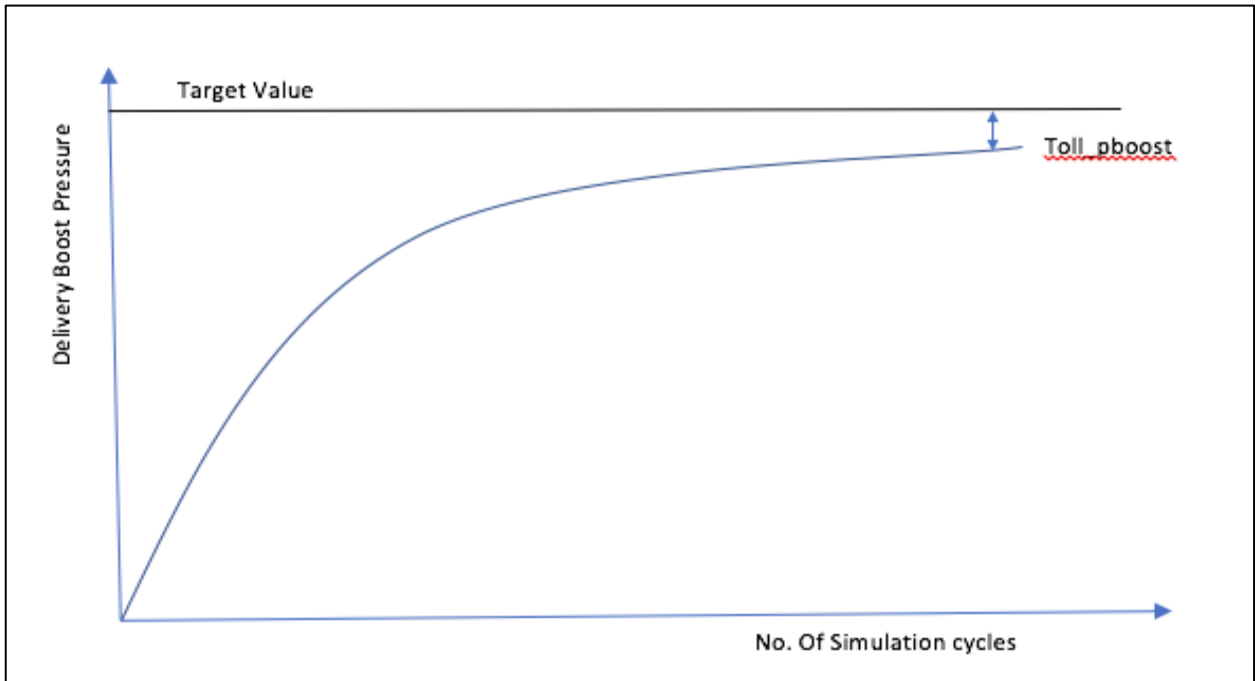


Figure 5:2 Convergence tolerance in Boost pressure.

5.1.3 Condition 3:

Third condition to reach convergence is put on the Turbocharger power balance. Same concept goes for power curve as it is explained in boost pressure curve in figure 2. Where difference in the compressor power and turbine power for the current running cycle is measured and if this difference is within the acceptable tolerance limit then we are met with this condition and if all other conditions are fulfilled then it's fine to stop the simulation of that rpm of engine.

$$convPower_{turbo} \leq Toll_power \quad (5.291)$$

Where:

- convpower_nturbo is the difference in the compressor power and turbine power for the current running cycle.
- Toll_power is acceptable tolerance for power balance between compressor and turbine.
- So, to see the effects of this algorithm, we run the simulation for two different engines “TD-4” and “F1C”.

5.2. Engine 1 “TD-4”

This is a 4-stroke diesel engine (inline-4) with fixed geometry turbocharger (FGT) and intercooler. Which produces maximum power of 72.35 KW @ 3550 rpm and maximum torque of 228 Nm @ 1750 rpm. Specification of this engine is shown in “table 5.1”.

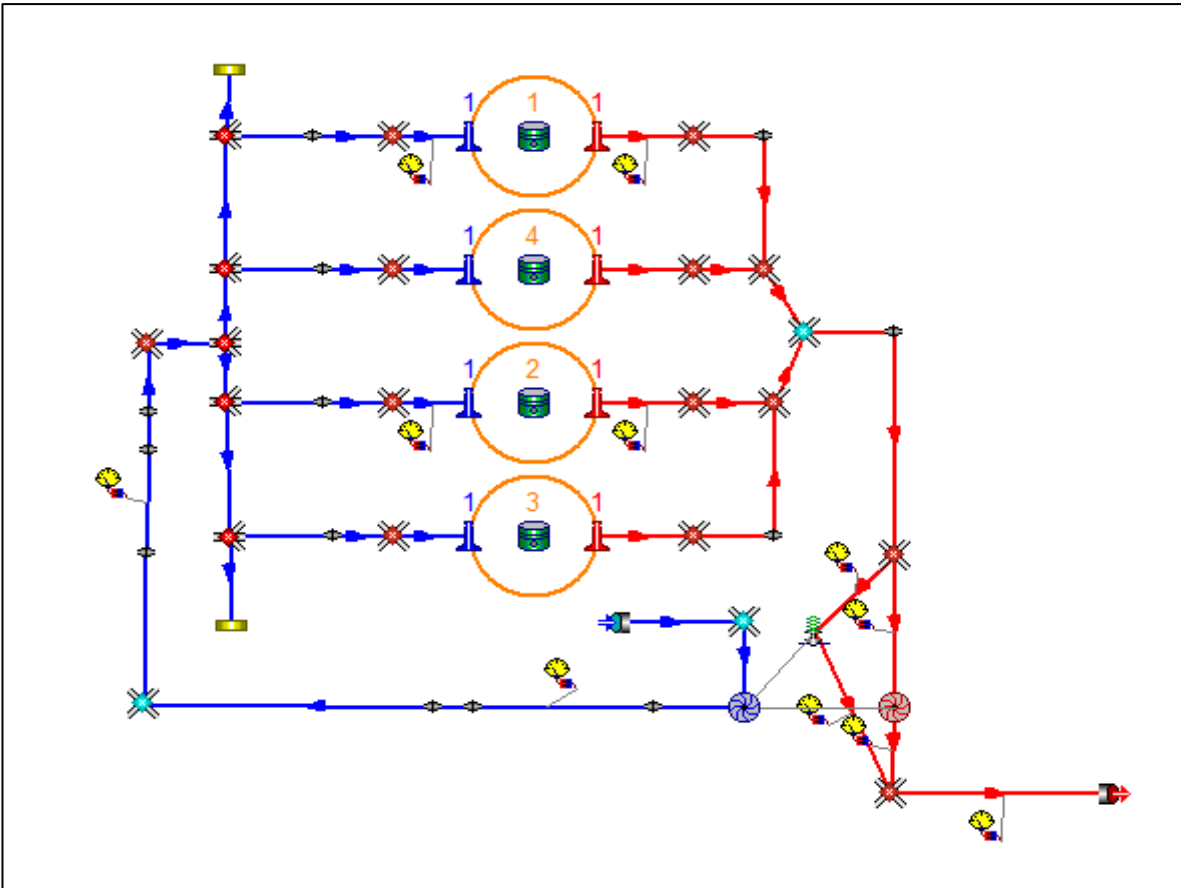


Figure 5:3 Schematic of “TD-4” engine in Gasdyn.

5.2.1. Specification:

Cycle and injection mode	4-stroke Diesel, direct injection
Number of cylinder	4 in line
Total displacement	2 771 dm ³
Bore	93 mm
Stroke	102 mm
Compression ratio	17.5:1
Firing order	1-3-4-2
Valves per cylinder	2 (1 intake – 1 exhaust)
Air metering	FGT Turbocharger with intercooler
Maximum brake torque	228 Nm @ 1750 rpm
Maximum brake power	72.5 kW @ 3550 rpm

Table 5-1 Specification of “TD-4” engine.

5.2.2. Results:

Now the simulation for “TD-4” engine is run to see the convergence with old algorithm for only 2 rpm i.e (1000, 2000 rpm). Results are plotted using matlab tool (TurboPost) in figures below.

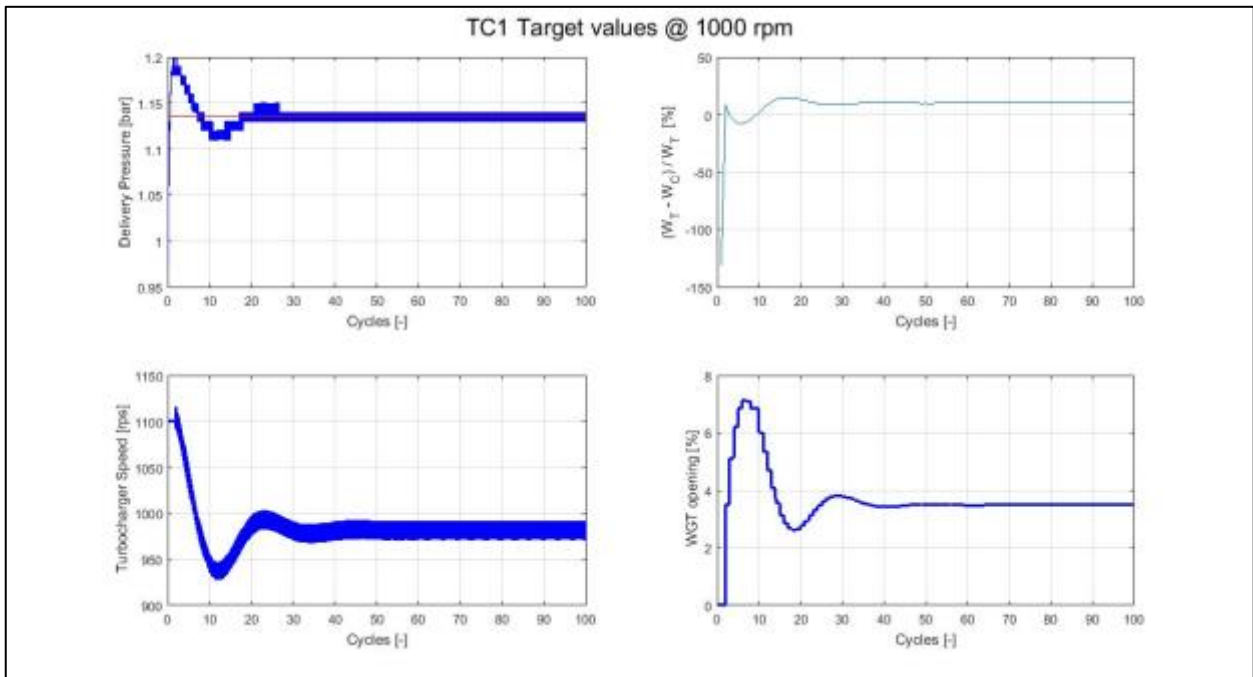


Figure 5:4 Convergence of “TD-4” engine at 1000 RPM with old algorithm.

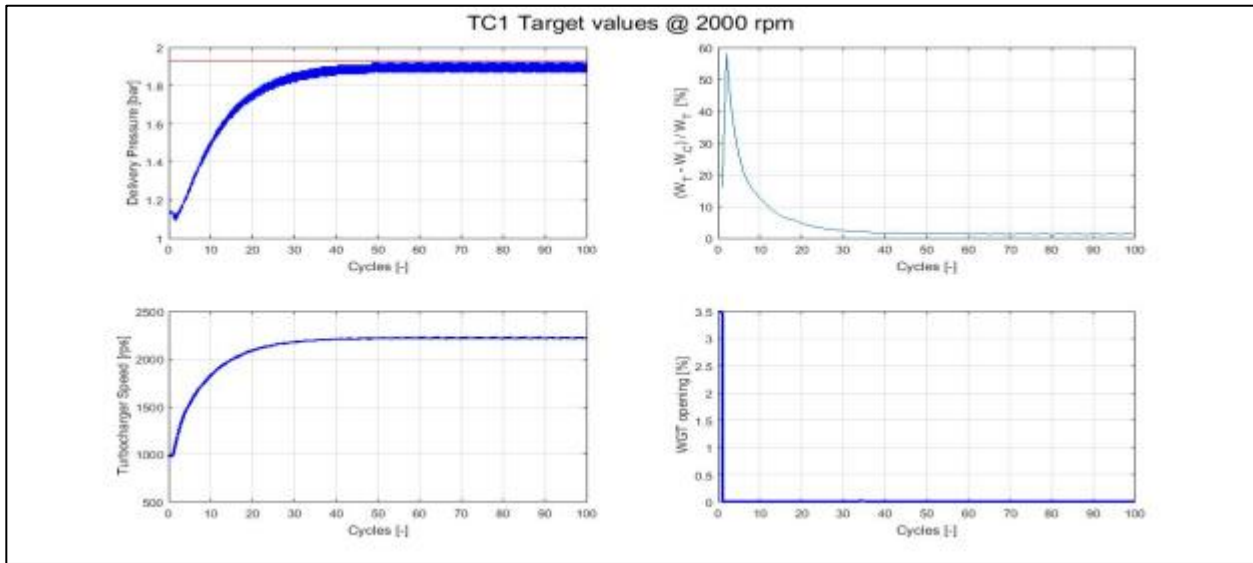


Figure 5.5 Convergence of “TD-4” engine at 2000 RPM with old algorithm.

As we can see from figure 5.4, simulation runs for 100 cycles without stopping. Whereas after 30 cycles there is no change in the results of simulation. We can notice here that boost pressure and turbocharger speed curves are oscillating with some small amplitude around target value of boost pressure. Similar observation can be taken from results of figure 5.5.

5.3. Engine 2 “F1C”.

This is a 4-stroke diesel engine (inline-4) with variable geometry turbocharger (VGT) and intercooler. Which produces maximum power of 125 KW @ 3500 rpm and maximum torque of 400 Nm @ 1250 rpm. Specification of this engine is shown in “table 5.2”.

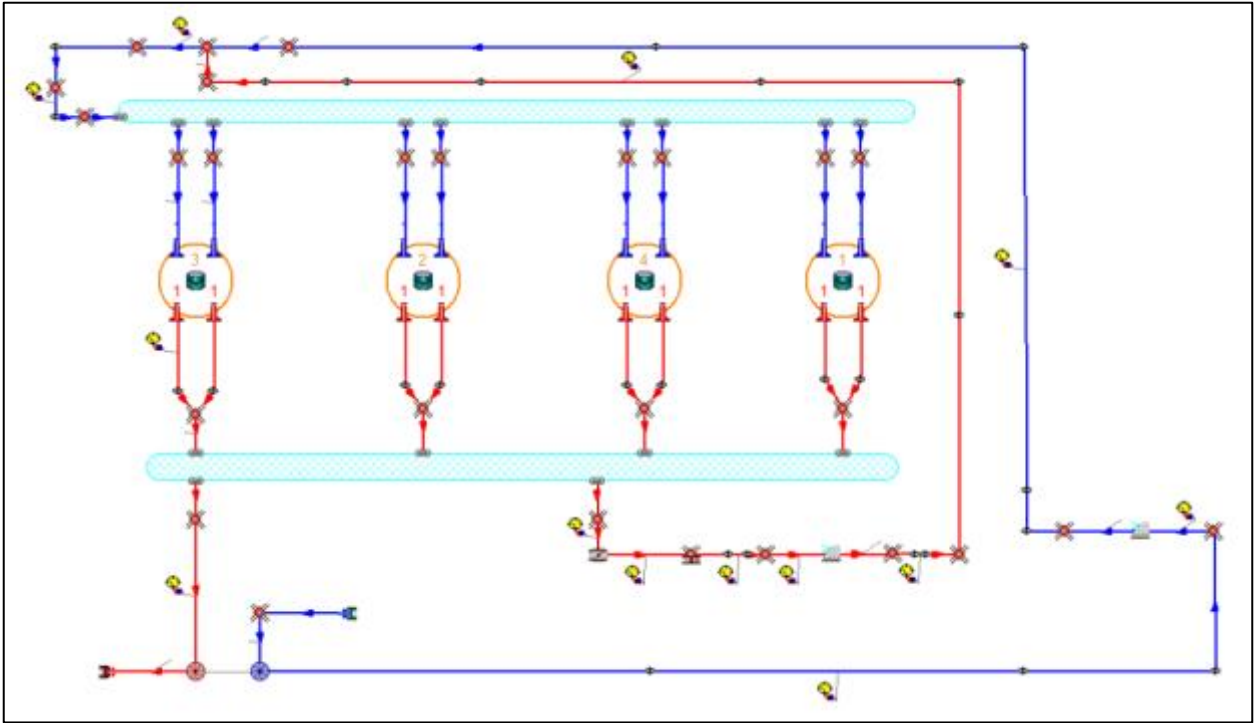


Figure 5:6 Schematic of “FIC” engine in Gasdyn.

5.3.1. Specification:

Cycle	4-stroke Diesel engine
Air metering	VGT Turbocharger with intercooler
Injection type	Direct, common rail system
Number of cylinder	4 in-line
Bore	95.8 mm
Stroke	104 mm
Total displacement	2.998 dm ³
Compression ratio	18.7:1
Firing order	1-3-4-2
Maximum brake power	125 kW@ 3500 rpm
Maximum brake torque	400 Nm @ 1250 rpm

Table 5-2 Specification of “FIC” engine.

5.3.2. Results:

Simulation for “FIC” engine is run to see the convergence with old algorithm for only 3 rpm (1000, 2000, 3500). Results are plotted using matlab tool (TurboPost) in figures below.

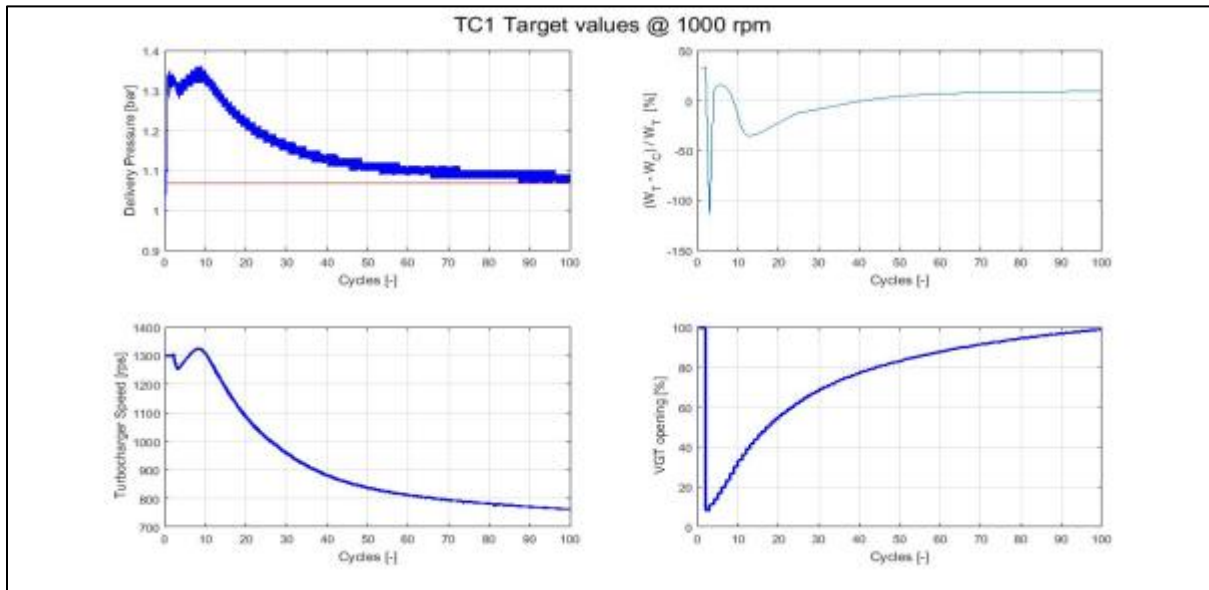


Figure 5:7 Convergence of “FIC” engine at 1000 RPM with old algorithm.

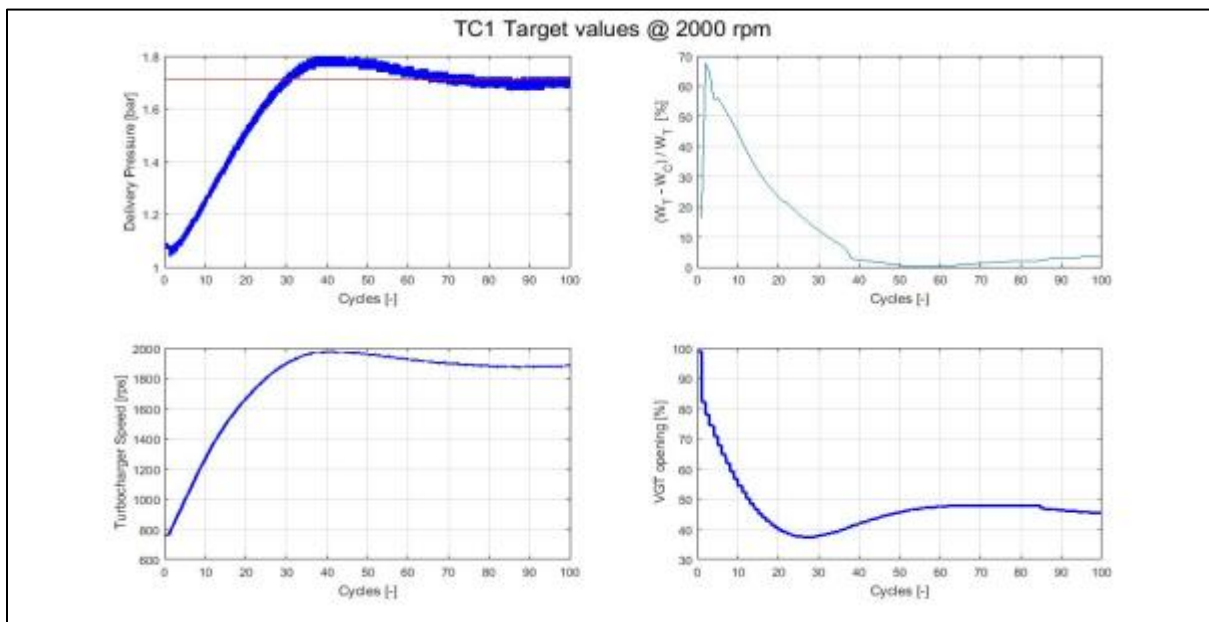


Figure 5:8 Convergence of “FIC” engine at 2000 RPM with old algorithm.

In figures 5.8, 5.9 and 5.10, we can notice that simulation runs for 100 cycles (max. cycles specified for simulation) without matching old convergence criteria. Although we can see from these figures that after 75-80 cycles there is not much change in boost pressure, turbocharger speed and power balance.

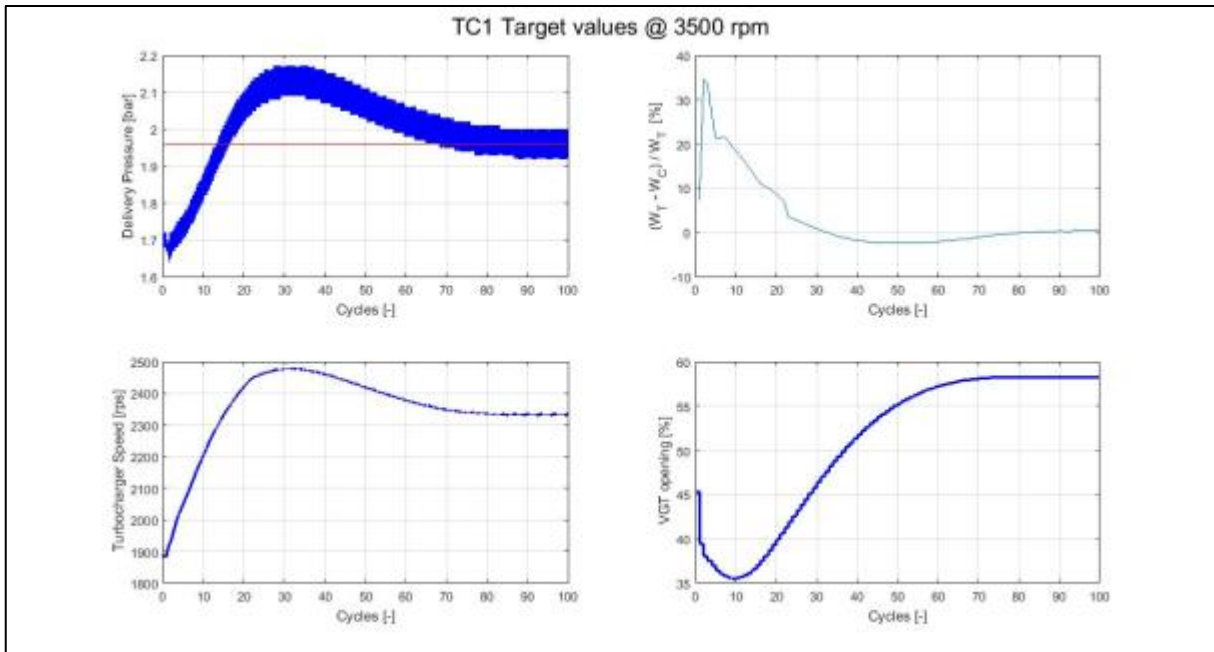


Figure 5:9 Convergence of “F1C” engine at 3500 RPM with old algorithm.

For old convergence algorithm to match, all the conditions mentioned in equations needs to be fulfilled only then the convergence criteria is met and simulation is stopped. But in practice, as we can see in results of “TD-4” and “F1C” engines case, it is very rare to meet all the conditions at the same time in the simulation.

With the application of previous algorithm, we have noticed that in many cases of turbocharger simulation, simulation runs until the last cycle and hence convergence criteria are not met fully. So, a new algorithm is made to reach the convergence accurately.

5.4. New Algorithm for Turbocharger convergence:

The problem with old criteria is that, if any one of the condition is not satisfied then simulation does not stop and instead, runs until the maximum no. of cycles specified before running the simulation (which in our case is 100 cycles). So, we developed some extra constrain and conditions to get the better convergence results, to save the computation time and other resources.

When the simulation for turbocharger is run with some predefined no. of simulation cycles for each engine regime and with tolerance limit, to stop the simulation, we put some conditions/constrains on various parameters to achieve the convergence and hence to stop the simulation for that regime. At first, we check the below mentioned conditions only after some

certain no. of cycles for example (after 5 cycles), so that we don't stop the simulation in early stage where for first few cycles we can easily be mistaken for the convergence tolerance criteria. For the same reason, all the below conditions are active after 5 cycles of the simulation.

5.4.1. Condition 1 (Derivative + Error):

In this case derivatives and errors are calculated for turbo speed, boost pressure and power balance. For each case of derivate and error to match with the tolerance limit a value of “1” is assigned and in total sum could go to 3. Various combinations are tried to see the effects on the convergence of turbocharger simulation like (1 constrain, 2 constrain and 3 constrains to be true). For example, if we put 3 constrain condition to be true, in this case, if all 3 conditions for derivative and error are not satisfied in the same cycles then simulation will run for the maximum no. of simulation cycle. But, to achieve a subtle convergence, we deployed other conditions to be activated after predefined no. of cycles like 40, 70 or 80 cycles. Other constrain are activated after some specified no. of cycles and if those constrains are fulfilled then convergence is achieved and simulation stops.

In this convergence condition, at first, derivate value is checked for the current running cycle and if derivate comes out to be close to zero or within acceptable tolerance limit assigned for convergence. Then the difference in target values and achieved values in the current cycle is measured (called Error) and if this error is less than the desired tolerance, convergence is achieved.

Derivative:

If

$$\text{Slope of Turbo speed curve} \leq \text{Conv}_{\text{derToll}_1} \quad \& \quad (5.292)$$

$$\text{Slope of } P_{\text{boost}} \text{ curve} \leq \text{Conv}_{\text{derToll}_2} \quad \& \quad (5.293)$$

$$\text{Slope of Conv}_{\text{power}} \text{ curve} \leq \text{Conv}_{\text{derToll}_3} \quad (5.294)$$

Then

Errors:

If

$$n_{\text{turbo}_{\text{new}}} - n_{\text{turbo}_{\text{old}}} \leq \text{Tech}_{\text{acc}} \quad \text{then} \quad \text{Conv}_{\text{Err}_1} = 1 \quad (5.295)$$

If

$$\text{Conv}_{\text{pboost}} \leq \text{Toll}_{\text{conv}_{\text{pboost}}} \quad \text{then} \quad \text{Conv}_{\text{Err}_2} = 1 \quad (5.296)$$

If

$$\text{Conv}_{\text{power}} \leq \text{Toll}_{\text{power}} \quad \text{then} \quad \text{Conv}_{\text{Err}_3} = 1 \quad (5.297)$$

If

$$Conv_{Err_1} + Conv_{Err_2} + Conv_{Err_3} \geq Tech_conv_constr \quad (5.298)$$

Then

$$matched(n_{turbo}) = 1 \quad (5.299)$$

Where:

- Conv_der_toll_1 is the acceptable tolerance for the slope on turbo speed curve.
- Conv_der_toll_2 is the acceptable tolerance for the slope on Boost pressure curve.
- Conv_der_toll_3 is the acceptable tolerance for the slope on power curve.
- Toll_conv_pboost is the acceptable tolerance for the Error (difference b/w target value and current value) on boost pressure curve.
- Toll_conv_power is the acceptable tolerance for the Error (difference b/w target value and current value) on power balance curve.
- Matched(n_turbo) = 1 means, convergence achieved and simulation stops.

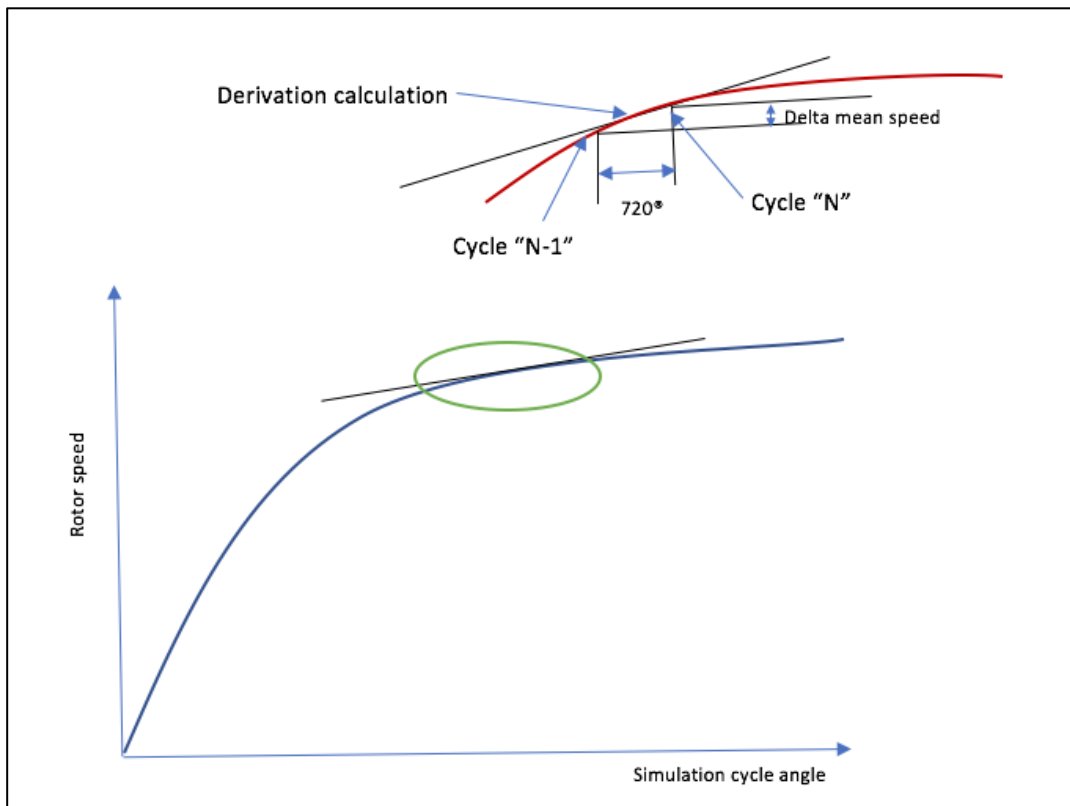


Figure 5:10 Slope tolerance of Turbo-speed for convergence.

As it's clear from the figure that as derivative or slope of the curve comes flat or close to zero and error are very small compare to the tolerance limit then we can say simulation is running very close to the final results. But we need to take care of oscillation part of the simulation,

which usually happens due to unsteady flow through turbocharger. So, to address that criteria, we introduced a condition as explained in section 5.4.2.

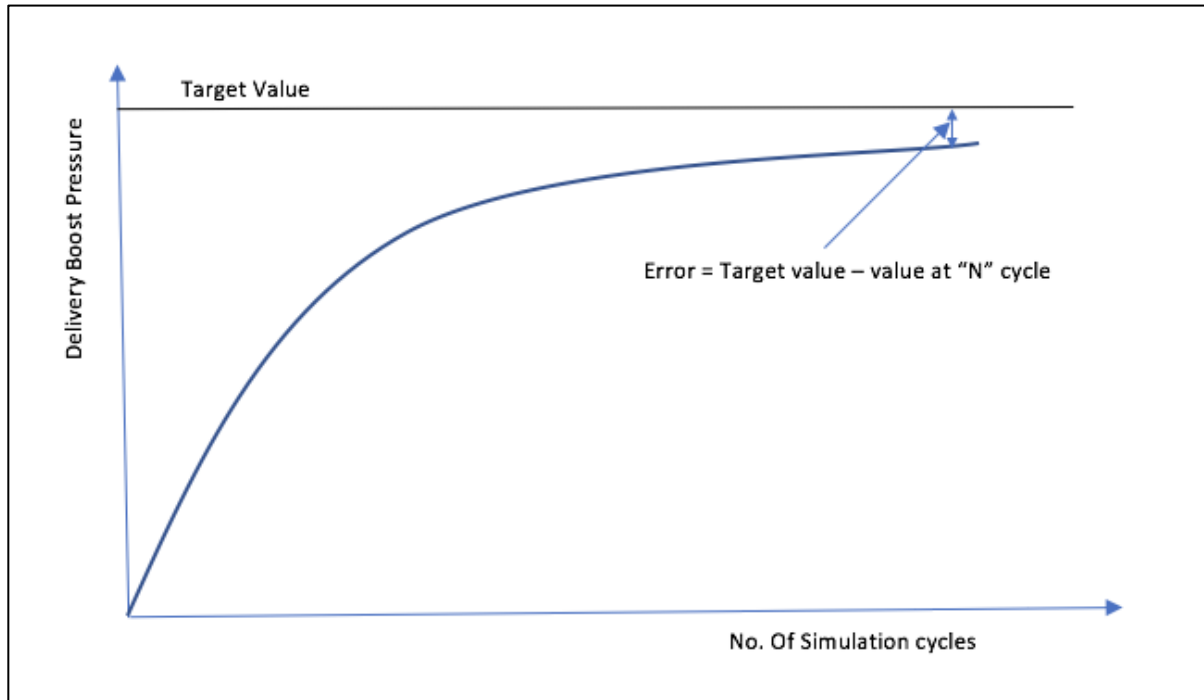


Figure 5:11 Error calculation of boost pressure for convergence.

The convergence achieved is considered as the slope of the turbocharger speed curve becomes less than the tolerance value imposed; in these conditions, it can be argued that in fact the current speed asymptotically approaches a constant value.

5.4.2. Condition 2 (Oscillation, check forced fluctuations in boost pressure and turbocharger power balance):

Second condition to reach convergence is forced on the delivery boost pressure and power balance of turbo. Where this condition is activated after “N” no of cycle, which could be 40, 70 or 80 cycles. This condition is basically to check if the oscillation of boost pressure and power balance is happening or not, if oscillation is occurring for some acceptable tolerance limit of amplitude compared with the target values, then we assume convergence is reached and simulation is forced to stop running for that regime.

If

$$ncycle \geq 50 \quad (5.300)$$

Then

$$Relative\ Error \left\{ \frac{P_{boost_mean}(n_{turbo}) - p_{boost_goal}(n_{turbo})}{p_{boost_goal}(n_{turbo})} \leq 0.1 \right. \quad \& \quad (5.301)$$

$$Conv_{power} < 0.10 \quad (5.302)$$

Then

$$matched(n_{turbo}) = 1 \quad (5.303)$$

where:

- Matched(n_turbo) = 1 means, convergence achieved and simulation stops.
- Conv_power is the percentage error in the power balance of turbo.
- Pboost_mean is the mean of the amplitude of pressure oscillations.
- Pboost_goal is the target boost pressure to be achieved.

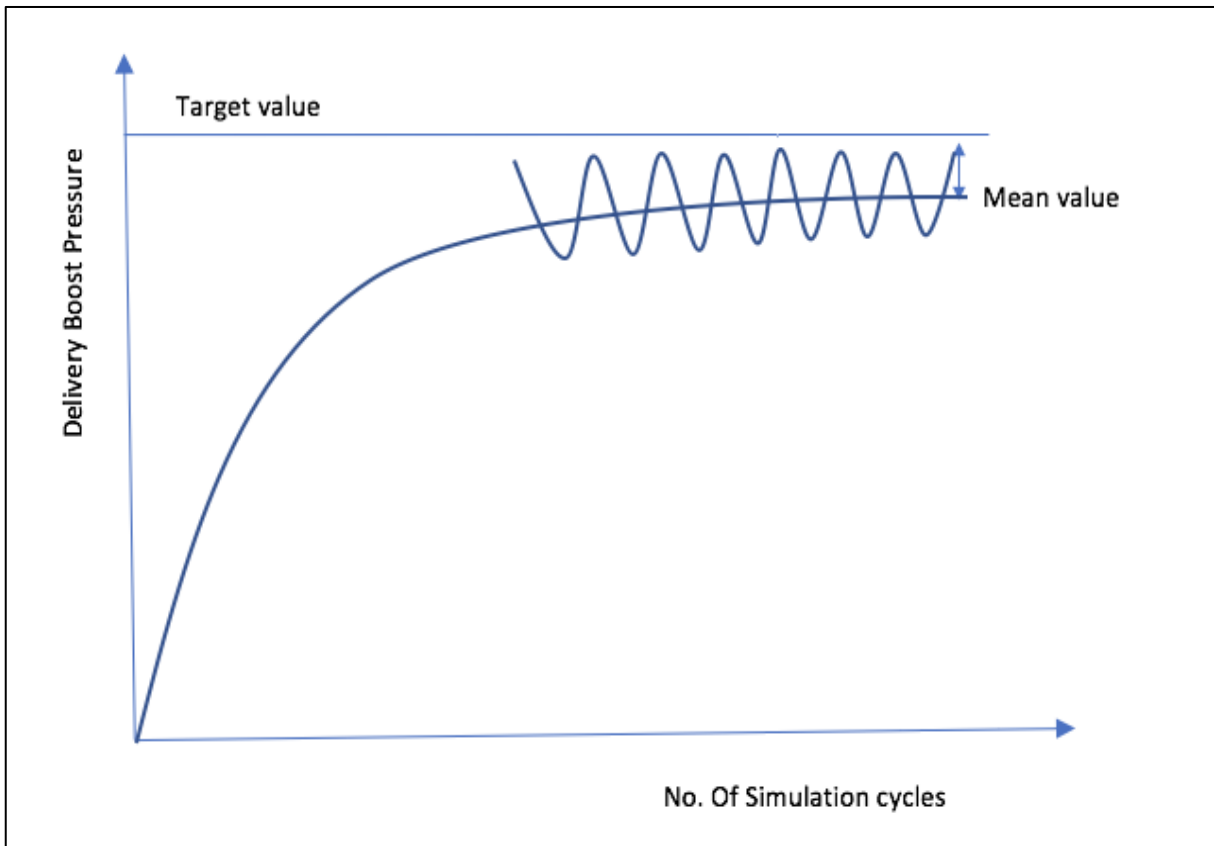


Figure 5:12 Oscillating curve of boost pressure close to it's target value.

5.4.3 Condition 3 (Steady turbocharger speed and turbocharger power balance):

Just like condition 2, condition 3 also is activated after “N” no of cycle, which could be 40, 50, 70 or 80 cycles. This condition basically checks 2 conditions i. e. stabilizing of derivative of

turbo-speed and Power converted curve for a given tolerance limit and if these 2 conditions are fulfilled after “N” cycle, then we get the convergence of turbocharger simulation and hence simulation stops for that regime. In terms of equations it can be seen as follow:

If

$$ncycle \geq 50 \quad (5.304)$$

Then

$$\frac{dN(nturbo)}{dt} - \frac{dN_{old}(nturbo)}{dt} \leq Tch_conv_der_Toll_1 \quad \& \quad (5.305)$$

$$Conv_power - Conv_power_old(nturbo) < 0.02 \quad (5.306)$$

Then

$$matched(n_{turbo}) = 1 \quad (5.307)$$

Where in equation 5.17, first part on the left side is the rate of change of turbocharger speed at cycle “N” and second part is rate of change of turbocharger speed at cycle “N-1”

So, to see the effects of this algorithm, we run the simulation for two different engines “TD-4” and “F1C” with the new convergence algorithm.

5.5. Convergence Results on TD-4:

5.5.1. One Constrain:

Now “TD-4” engine is run for 3 regime (1000, 2000 and 3500) with 1 constrain (means that the value of Tech_conv_constr is set to 1) and 70 cycles for condition 2 to be activated and 50 cycles for condition 3 to be activated.

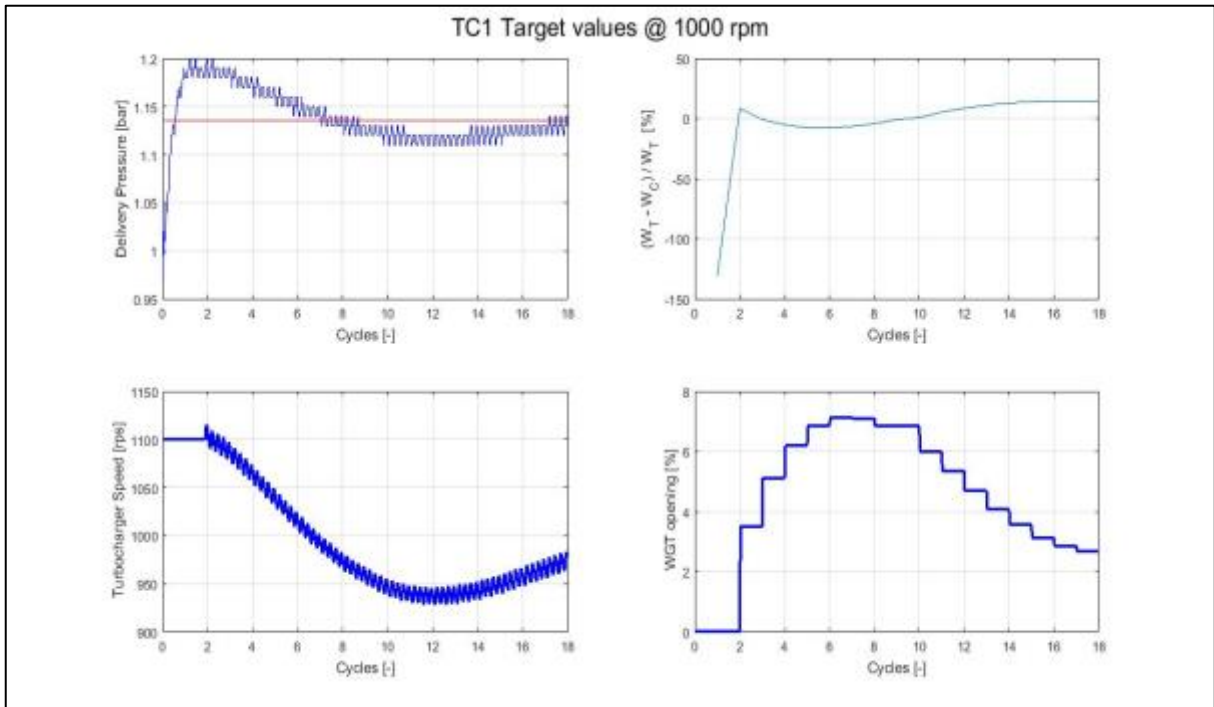


Figure 5:13 Convergence of "TD-4" engine at 1000 RPM with 1 constrain condition.

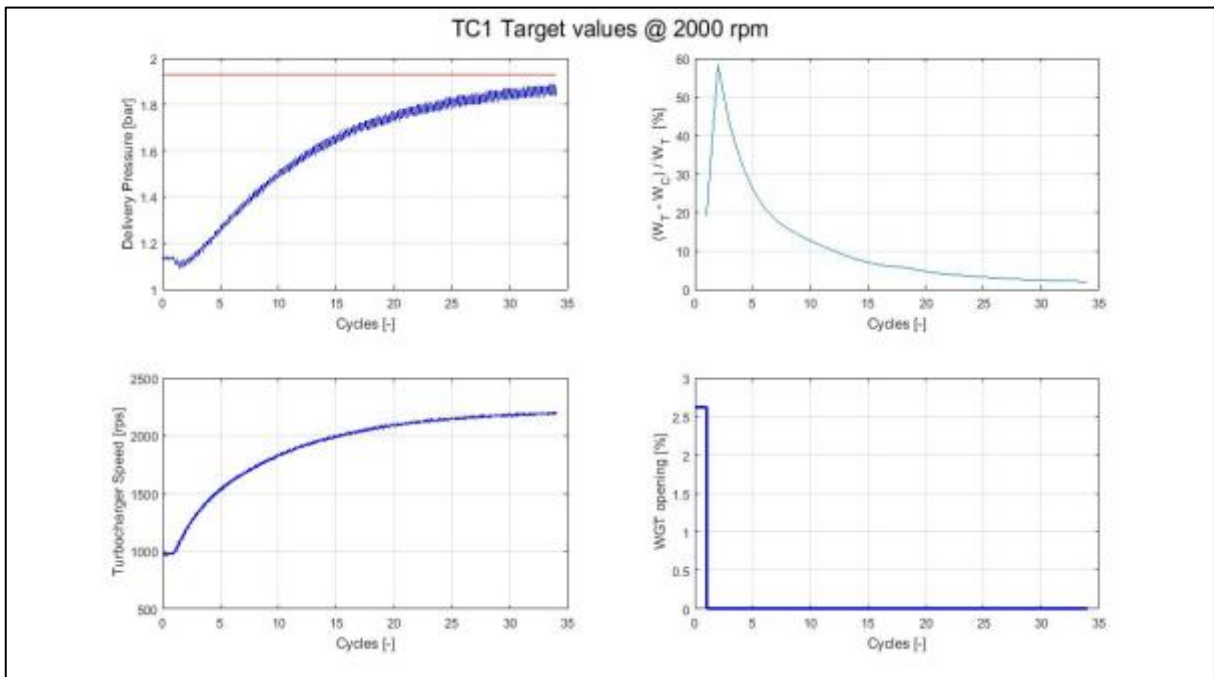


Figure 5:14 Convergence of "TD-4" engine at 2000 RPM with 1 constrain condition.

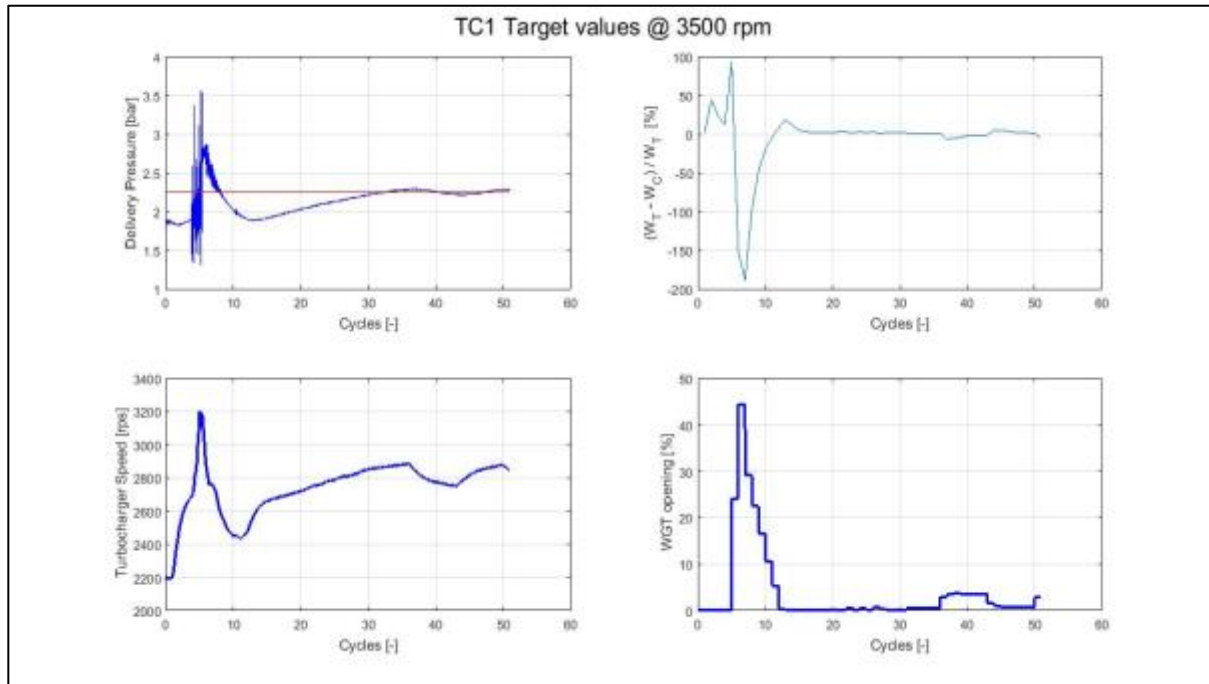


Figure 5.15 Convergence of “TD-4” engine at 3500 RPM with 1 constrain condition.

Here in figures 5.13, 5.15 and 5.15, we can see how new algorithm helps in reaching convergence in less no. of simulation cycles (18, 35 and 51 respectively) as compared to figures 5.4 and 5.5, where simulation run until 100 cycles. But for this simulation we put only one constrain, as anticipated, one constrain meets the criteria very early. So, we try different combination of no. of constrains and condition 2 and condition 3 activation cycles.

5.5.2. Two Constrain:

To see the effects on convergence, we run “TD-4” engine for 3 RPM (1000, 2000 and 3500) with 2 constrain (means that the value of Tech_conv_constr is set to “2”) and 70 cycles for condition 2 to be activated and 50 cycles for condition 3 to be activated. The results are plotted in figure 5.16, 5.17 and 5.18.

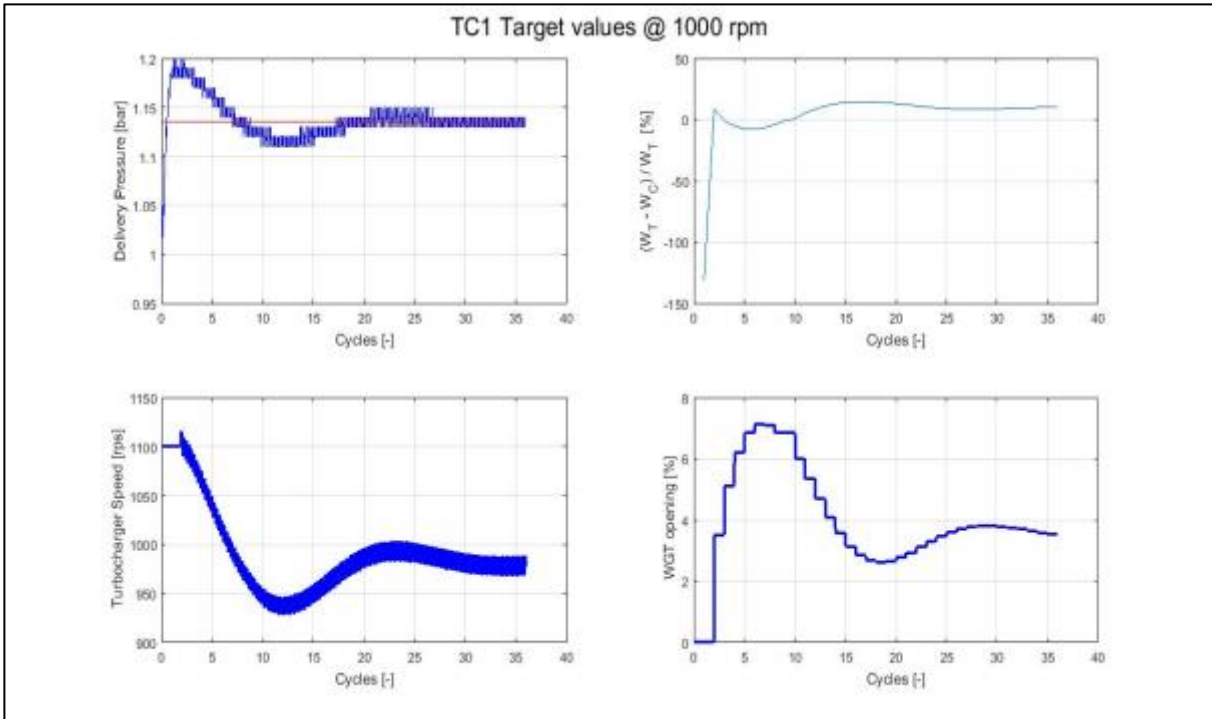


Figure 5:16 Convergence of "TD-4" engine at 1000 RPM with 2 constrain condition.

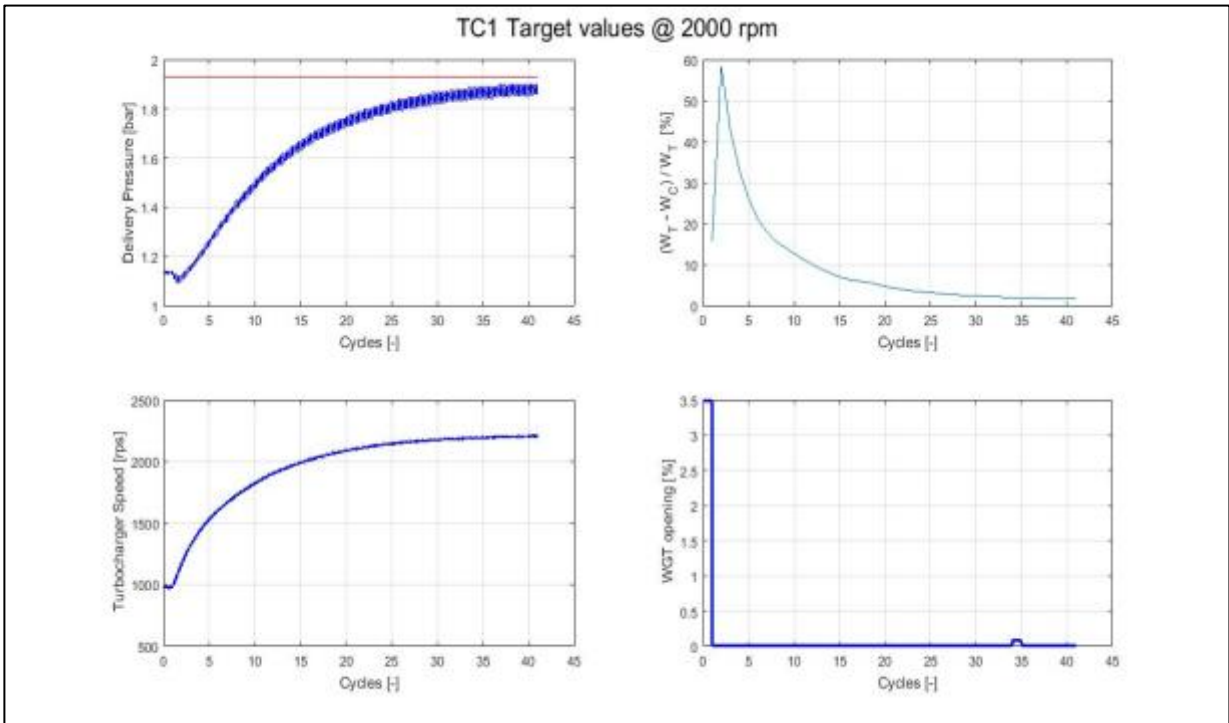


Figure 5:17 Convergence of "TD-4" engine at 2000 RPM with 2 constrain condition.

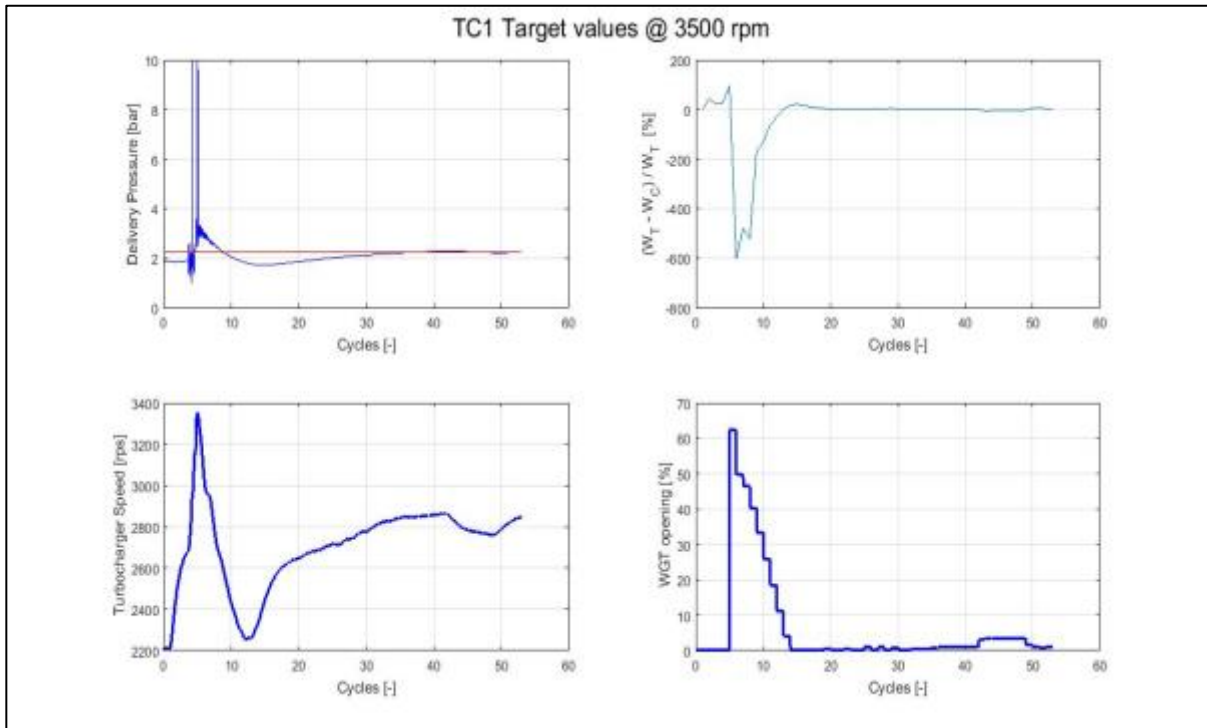


Figure 5:18 Convergence of “TD-4” engine at 3500 RPM with 2 constrain condition.

In figures 5.16, 5.17 and 5.18, we can see, how good the convergence is reached and algorithm stopped the simulation to run for further cycles. So, this new algorithm with 2 constrain seems to work well.

5.5.3. Three Constrain:

To see the effects on convergence, we run “TD-4” engine for 3 regime (1000 and 2000) with 3 constrain (means that the value of Tech_conv_constr is set to “3”) and 70 cycles for condition 2 to be activated and 50 cycles for condition 3 to be activated. The results are plotted in figure 5.19 and 5.20.

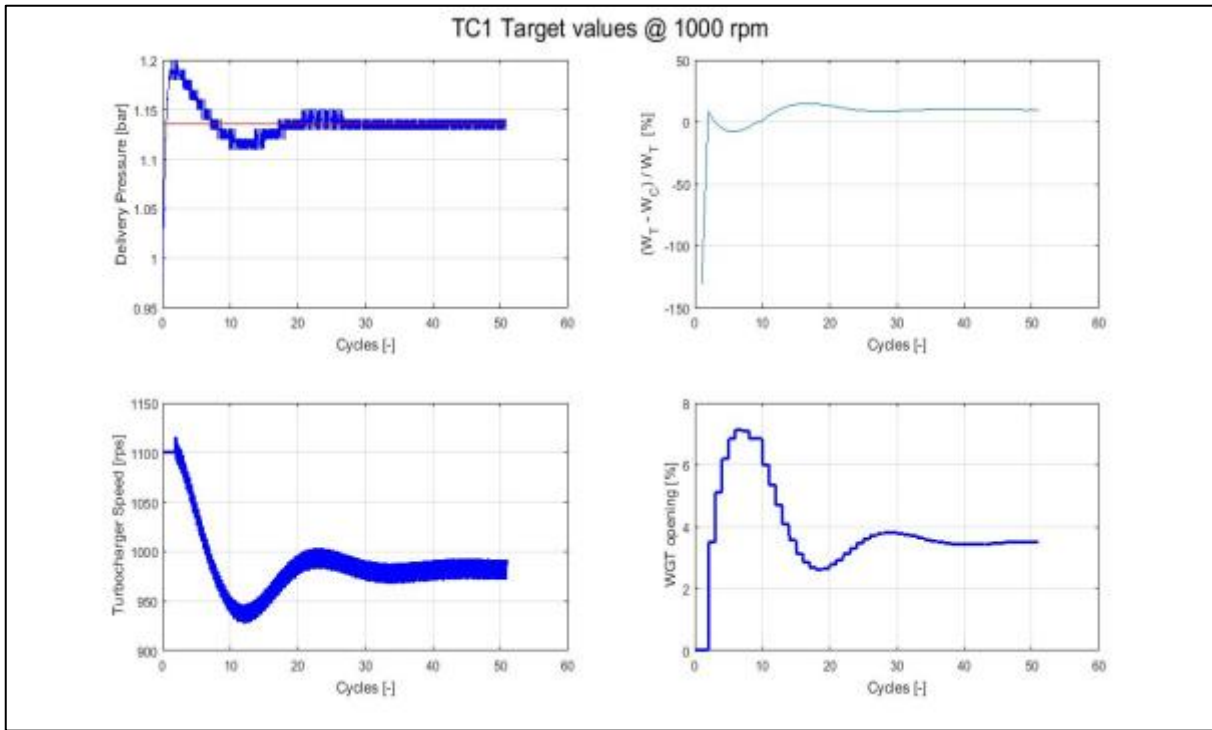


Figure 5:19 Convergence of “TD-4” engine at 1000 RPM with 3 constrain condition.

*** DEBUG TURBO CONV																
Regime	rpm	cycle	H_DER_M	dN_over_D_TCH_ACC	CONV_ERR	convPboost	tolConvPboo	CONV_ERR	convPower	tolPwr	CONV_ERR_Sum	CONVERTCH_CONV	matched	ntuTCH_Cond_2	TCH_Cond_3	TCH_Cond_4
1000	43	1	0.00037628	0.001	1	0.00024452	0.01	1	0.10129423	0.03	0	2	3	0	0	0
1000	44	1	0.00019512	0.001	1	0.00031639	0.01	1	0.100287	0.03	0	2	3	0	0	0
1000	45	1	0.00014747	0.001	1	0.00037544	0.01	1	0.0999084	0.03	0	2	3	0	0	0
1000	46	1	0.0000362	0.001	1	0.00039064	0.01	1	0.09932832	0.03	0	2	3	0	0	0
1000	47	1	0.00008688	0.001	1	0.00036537	0.01	1	0.0989999	0.03	0	2	3	0	0	0
1000	48	1	0.00011052	0.001	1	0.0003203	0.01	1	0.09860715	0.03	0	2	3	0	0	0
1000	49	1	0.00019236	0.001	1	0.00025489	0.01	1	0.09809414	0.03	0	2	3	0	0	0
1000	50	1	0.0001755	0.001	1	0.00018559	0.01	1	0.09839357	0.03	0	2	3	1	0	0
1000	51	1	0.00021328	0.001	1	0.00011149	0.01	1	0.09805919	0.03	0	2	3	1	0	1
2000	1	0	0.00053536	0.001	0	0.69861976	0.01	0	0.15417893	0.03	0	0	3	0	0	0
2000	2	0	0.09755714	0.001	0	0.02086926	0.01	0	0.58233086	0.03	0	0	3	0	0	0
2000	3	0	0.13553328	0.001	0	0.02080871	0.01	0	0.42717842	0.03	0	0	3	0	0	0

Table 5-3: Data from “Turbo_Conv_Debug” file at 1000 RPM with 3 constrain condition.

From the table 5.3, it’s clear how algorithm works good, as we can see in the round circle that even if 2 constrain out of 3 are fulfilled and after the activation of condition 2 and condition 3, we reach convergence in 51 cycles, as Tch_cond_4 value is “1” (condition 3).

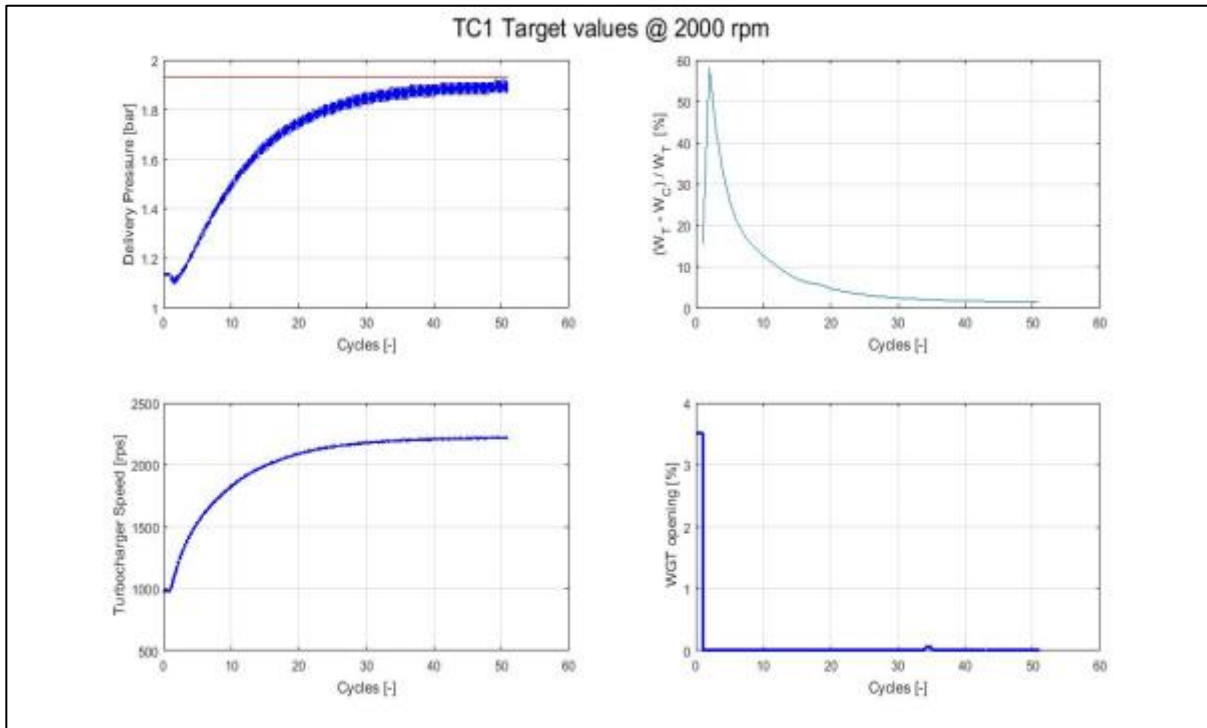


Figure 5:20 Convergence of “TD-4” engine at 2000 RPM with 3 constrain condition.

*** DEBUG TURBO CONV																
Regime(rpm/cycle)	DER_TCH_3	TCH_DER_M	dtW_over_D_TCH_ACC	CONV_ERR	convBoost	tolConvBox	CONV_ERR	convPower	tolPar	CONV_ERR	SumCONV	TCH_CONV	imatched/rst	TCH_Cond_2	TCH_Cond_3	TCH_Cond_4
2000	43	0.002	1	0.0005916	0.001	1	0.02383571	0.01	0.01521831	0.03	1	2	3	0	0	0
2000	44	0.002	1	0.0005539	0.001	1	0.02304464	0.01	0.01528678	0.03	1	2	3	0	0	0
2000	45	0.002	1	0.00048588	0.001	1	0.02212067	0.01	0.01453244	0.03	1	2	3	0	0	0
2000	46	0.002	1	0.00039601	0.001	1	0.02171456	0.01	0.0149331	0.03	1	2	3	0	0	0
2000	47	0.002	1	0.00043663	0.001	1	0.02114163	0.01	0.01448454	0.03	1	2	3	0	0	0
2000	48	0.002	1	0.00033112	0.001	1	0.02063188	0.01	0.01448351	0.03	1	2	3	0	0	0
2000	49	0.002	1	0.0003413	0.001	1	0.02015054	0.01	0.01360578	0.03	1	2	3	0	0	0
2000	50	0.002	1	0.00019503	0.001	1	0.01977746	0.01	0.01408334	0.03	1	2	3	1	0	0
2000	51	0.002	1	0.0003252	0.001	1	0.01941858	0.01	0.01397393	0.03	1	2	3	1	0	1
3500	1	0.002	0	0.00007205	0.001	0	0.18981513	0.01	0.01518215	0.03	0	0	3	0	0	0
3500	2	0.002	0	0.06423891	0.001	0	0.2054841	0.01	0.43992842	0.03	0	0	3	0	0	0
3500	3	0.002	0	0.08454369	0.001	0	0.20510489	0.01	0.21894812	0.03	0	0	3	0	0	0

Table 5-4: Data from “Turbo_Conv_Debug” file at 2000 RPM with 3 constrain condition

Similarly, from table 5.4, it’s clear how algorithm works good, as we can see in the round circle that even if 2 constrain out of 3 are fulfilled and after the activation of condition 2 and condition 3, we reach convergence in 51 cycles, as Tch_cond_4 value is “1” (condition 3).

So, from section 5.5, we can conclude that with 2 constrains and application of condition 2 and condition 3 gives us good results of convergence for turbocharger.

5.6. Convergence Results on F1C:

5.6.1. Two Constrain:

With the conclusion from section 5.5, we run the “F1C” engine for 3 regime 1000, 2000 and 3500 RPM with 2 constrain only (means that the value of Tch_conv_constr is set to 2) and 70 cycles for condition 2 to be activated and 50 cycles for condition 3 to be activated. Results are plotted in figures 5.21, 5.22 and 5.23.

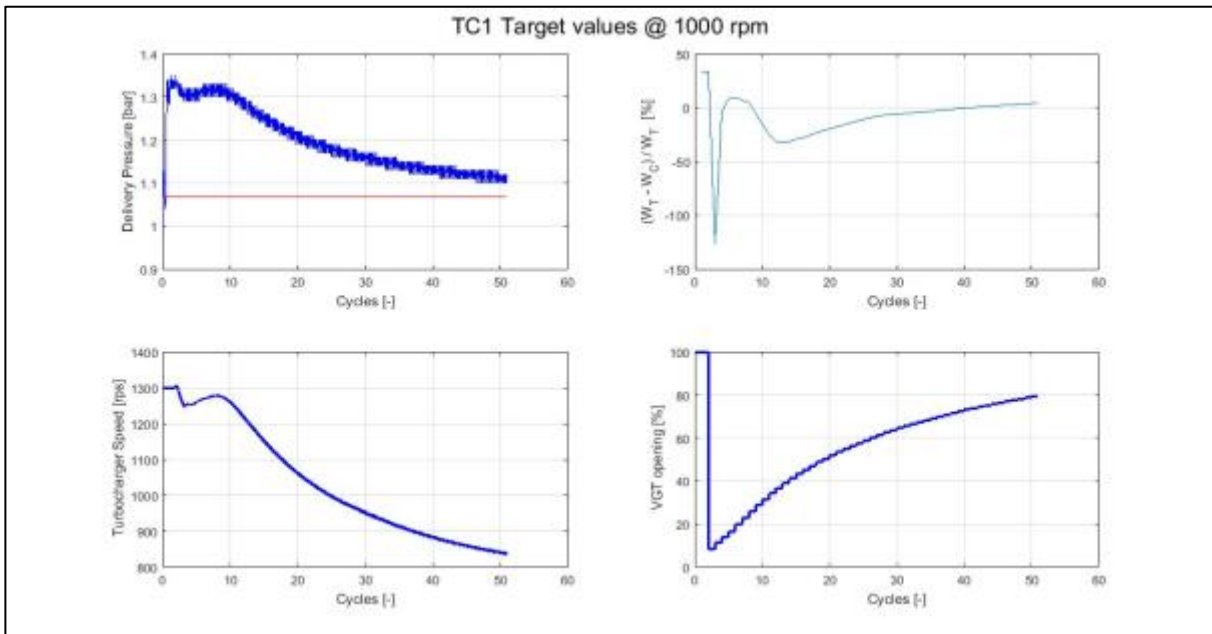


Figure 5.21 Convergence of “F1C” engine at 1000 RPM with 2 constrain condition.

*** DEBUG TURBO CONV																		
Regime[rpm]	cycle	TOL_3	TCH_DER_M	dM_over_D	TCH_ACC	CONV_ERR_1	convPboost	tolConvPbox	CONV_ERR_2	convPower	tolPwr	CONV_ERR_3	SumCONVER	TCH_CONV / matched	ntu	TCH_Cond_2	TCH_Cond_3	TCH_Cond_4
1000	46	0.002	0	0.00488923	0.001	0	0.04636613	0.01	0	0.02962234	0.09	0	0	2	0	0	0	0
1000	47	0.002	0	0.00469111	0.001	0	0.04500564	0.01	0	0.02750791	0.09	0	0	2	0	0	0	0
1000	48	0.002	0	0.00449091	0.001	0	0.04372828	0.01	0	0.03141878	0.09	0	0	2	0	0	0	0
1000	49	0.002	0	0.00428488	0.001	0	0.04250641	0.01	0	0.03526584	0.09	0	0	2	0	0	0	0
1000	50	0.002	0	0.00408827	0.001	0	0.04134407	0.01	0	0.03894489	0.09	0	0	2	1	0	0	1
1000	51	0.002	0	0.00389483	0.001	0	0.040245	0.01	0	0.04264971	0.09	0	0	2	1	0	0	1
2000	1	0.002	0	0.00363828	0.001	0	0.043159566	0.01	0	0.10838099	0.09	0	0	2	0	0	0	1
2000	2	0.002	0	0.02661949	0.001	0	0.00538765	0.01	0	0.64842971	0.09	0	0	2	0	0	0	1

Table 5-5: Data from “Turbo_Conv_Debug” file at 1000 RPM with 2 constrain condition.

Convergence Algorithm for Turbocharger:

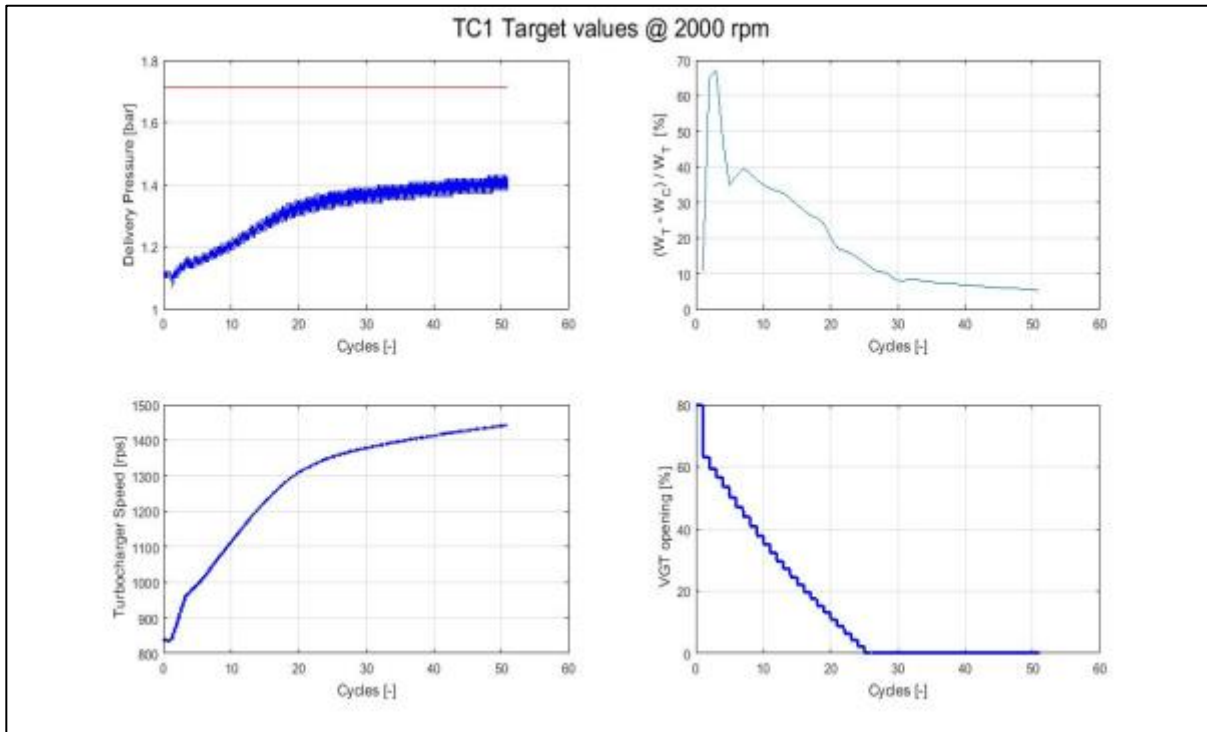


Figure 5:22 Convergence of “FIC” engine at 2000 RPM with 2 constrain condition.

*** DEBUG TURBO CONV																				
Regime(rpm/cycle)	_3	TCH_DER_M	dM_over_D	TCH_ACC	CONV_ERR_1	convBoost	tolComP	Conv_Pow	CONV_ERR_2	convPower	tolPwr	CONV_ERR_3	SumCONV	TCH_CONV	matched	Inta	TCH_Cond_2	TCH_Cond_3	TCH_Cond_4	
2000	46	0.002	1	0.00185235	0.001	0	0.22394224	0.01	0	0.05824626	0.03	0	0	0	2	0	0	0	0	1
2000	47	0.002	1	0.00182587	0.001	0	0.22250748	0.01	0	0.05823864	0.03	0	0	0	2	0	0	0	0	1
2000	48	0.002	1	0.00179418	0.001	0	0.22110083	0.01	0	0.05666812	0.03	0	0	0	2	0	0	0	0	1
2000	49	0.002	1	0.00172686	0.001	0	0.21975837	0.01	0	0.05473252	0.03	0	0	0	2	0	0	0	0	1
2000	50	0.002	1	0.00166253	0.001	0	0.21844025	0.01	0	0.0542413	0.03	0	0	0	2	1	0	0	0	1
2000	51	0.002	1	0.00163328	0.001	0	0.21715553	0.01	0	0.05281909	0.03	0	0	0	2	1	0	0	0	1
3500	1	0.002	0	0.00152428	0.001	0	0.39937315	0.01	0	0.10981718	0.03	0	0	0	2	0	0	0	0	1
3500	2	0.002	0	0.01735793	0.001	0	0.02852217	0.01	0	0.33967046	0.03	0	0	0	2	0	0	0	0	1
3500	3	0.002	0	0.00764349	0.001	0	0.04133493	0.01	0	0.46449	0.03	0	0	0	2	0	0	0	0	1

Table 5-6: Data from “Turbo_Conv_Debug” file at 2000 RPM with 2 constrain condition.

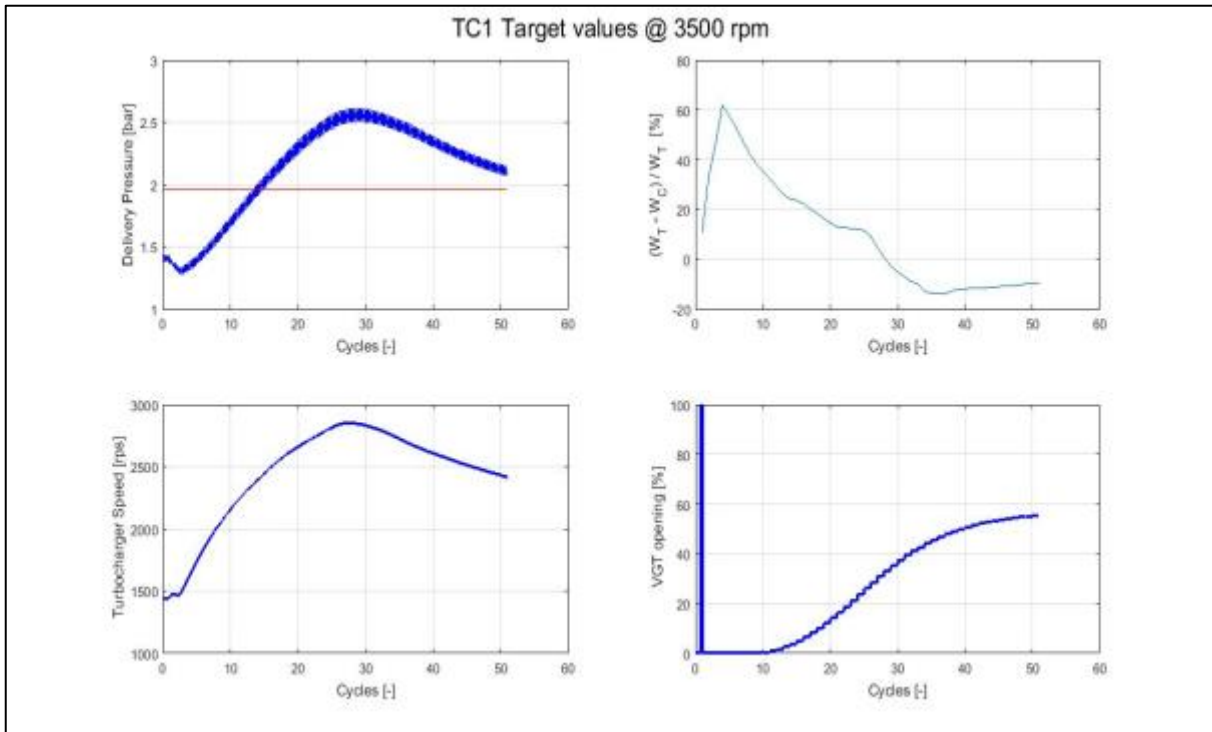


Figure 5:23 Convergence of “F1C” engine at 3500 RPM with 2 constrain condition.

*** DEBUG TURBO CONV																
Regime[rpm]	cycle	_3	TCH_DER_M	dN_over_D TCH_ACC	CONV_ERR_1	comBoost tol ComPbox CONV_ERR_2	comPower	tolPwr	CONV_ERR_3	SumCONV	TCH_CONV	matched ntu	TCH_Cond_2	TCH_Cond_3	TCH_Cond_4	
3500	46	02	0	0.0070357	0.001	0	0.11336801	0.01	0	0.10844776	0.03	0	2	0	0	1
3500	47	02	0	0.00686265	0.001	0	0.10497517	0.01	0	0.10671709	0.03	0	2	0	0	1
3500	48	02	0	0.0066903	0.001	0	0.09670246	0.01	0	0.10312022	0.03	0	2	0	0	1
3500	49	02	0	0.00650615	0.001	0	0.08875214	0.01	0	0.10074598	0.03	0	2	0	0	1
3500	50	02	0	0.00629454	0.001	0	0.08111589	0.01	0	0.0969008	0.03	0	2	1	0	1
3500	51	02	0	0.00607463	0.001	0	0.07382283	0.01	0	0.09371558	0.03	0	2	1	0	1

Table 5-7: Data from “Turbo_Conv_Debug” file at 3500 RPM with 2 constrain condition.

From section 5.4 and 5.5, it’s very clear that the new algorithm developed checks the conditions for convergence and force the simulation to stop to save time and resource.

As it can be seen in highlighted circles, even if no constrains in “Derivative and Error” are true, condition 2 and condition 3 gets active after 70 and 50 cycles respectively to check for convergence criteria and forces the simulation to stop, if these conditions are true.

So, With the introduction of new algorithm with 2 constrains and condition 2 and condition 3, as explained in section 5.4 the “Gasdyn” code gives reliable results for convergence in turbocharger cases.

5.7. PID control:

PID control flow chart of new algorithm for convergence criteria in turbocharger simulation is explained below in figure 5.10.

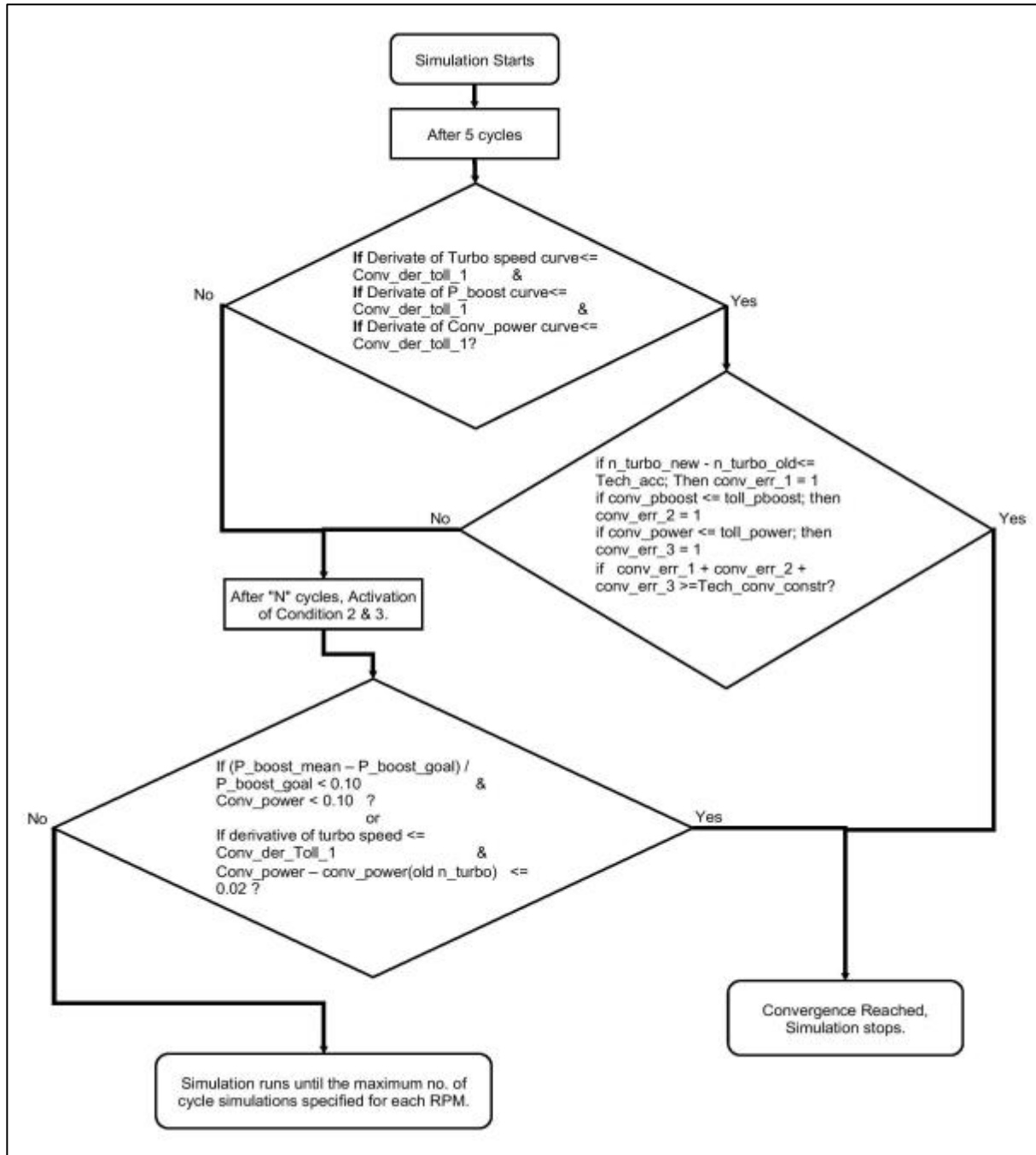


Figure 5:24: Flow chart of PID control for new convergence algorithm of turbocharger simulation in Gasdyn.

Convergence Algorithm for Turbocharger:

List of Figures:

FIGURE 1:1: ONE DIMENSIONAL SCHEME.	13
FIGURE 2:1: CLASSIFICATION OF SHOCK-CAPTURING NUMERICAL METHODS.	31
FIGURE 2:2 GRAPHICAL METHOD OF CHARACTERISTICS INTERPRETATION.	32
FIGURE 2:3 TRACKING OF CHARACTERISTIC LINES IN THE (x, t) DISCRETIZED.	35
FIGURE 2:4: POSITION DIAGRAM (A) AND STATE (B) FOR THE FAMILIES OF Λ AND B CURVES.....	37
FIGURE 2:5 :A-S DIAGRAM ON WHICH IT IS POSSIBLE TO RECOGNIZE THE REFERENCE VALUES OF: THE SPEED OF SOUND, PRESSURE AND ENTROPY.....	38
FIGURE 2:6 INFLUENCE OF THE FLOW CONDITIONS AT TIME $t+\Delta t$ IN A GIVEN SECTION OF THE DUCT.	42
FIGURE 2:7 GRID SPACE-TIME USED FOR THE CALCULATION OF THE RIEMANN VARIABLES WITH THE METHOD OF CHARACTERISTICS ..	44
FIGURE 2:8 TRACKING FEATURE LINES BACK IN TIME, STARTING FROM THE NODE S IN $Z+\Delta Z$ (POINT R') UP TO THE P POINTS TO THE TIME Z.	45
FIGURE 2:9 CALCULATION SCHEME OF TWO STEP METHOD LAX-WENDROFF.	53
FIGURE 2:10 REPRESENTATION OF THE MACCORMACK METHOD IN THE CASE OF FORWARD PREDICTOR-BACKWARD CORRECTOR.....	54
FIGURE 2:11: DAVIS SCHEME OF THE FLOW RESTRICTOR ELIGIBILITY REGION OF Φ	61
FIGURE 3:1 CHARACTERISTIC CURVE OF EXPANSION RATIO - FLOW PARAMETER OF A RADIAL TURBINE FOR VARIOUS SPEED PARAMETERS.	64
FIGURE 3:2 CHARACTERISTIC CURVE PERFORMANCE - THE SPEED RATIO OF A RADIAL TURBINE FOR VARIOUS SPEED PARAMETERS	65
FIGURE 3:3 SCHEMATIC VIEW OF A REPRESENTATIVE TURBINE.	65
FIGURE 3:4 CHARACTERISTIC CURVE OF EXPANSION RATIO - FLOW PARAMETER OF A RADIAL TURBINE	66
FIGURE 3:5 BOUNDARY CONDITION IN TERMS OF THE PRESSURES OF A RADIAL TURBINE	70
FIGURE 3:6: BOUNDARY STATE IN TERMS OF THE SCOPE OF A RADIAL TURBINE.....	71
FIGURE 3:7 PRESSURE PROFILE AND THE TEMPERATURE UPSTREAM OF THE TURBINE.....	72
FIGURE 3:8 RESULTS OF THE RATE PARAMETER AND THE EXPANSION RATIO WITH THE CRANK ANGLE	73
FIGURE 3:9 POWER PERFORMANCE AND EFFICIENCY WITH THE CRANK ANGLE.	75
FIGURE 3:10 CHARACTERISTIC CURVE OF THE TOTAL COMPRESSION RATIO - FLOW PARAMETER OF A CENTRIFUGAL COMPRESSOR.....	76
FIGURE 3:11 EFFICIENCY CHARACTERISTIC CURVE - FLOW PARAMETER OF A CENTRIFUGAL COMPRESSOR.	77
FIGURE 3:12 REPRESENTATIVE DIAGRAM OF A COMPRESSOR.	78
FIGURE 3:13 BOUNDARY CONDITIONS OF A CENTRIFUGAL COMPRESSOR	79
FIGURE 3:14 CHARACTERISTIC CURVE OF THE TOTAL COMPRESSION RATIO - FLOW PARAMETER OF A CENTRIFUGAL COMPRESSOR.....	80
FIGURE 3:15 CHARACTERISTIC CURVE OF THE TOTAL COMPRESSION RATIO - FLOW PARAMETER OF A CENTRIFUGAL COMPRESSOR.....	81
FIGURE 3:16 CHARACTERISTIC CURVES OF CENTRIFUGAL COMPRESSOR.....	82
FIGURE 4:1: EXPLODED IHI TURBO RHF3.	87
FIGURE 4:2 (A) BRUSCO SHRINKAGE RESULTING CONTRACTED VEIN; (B) ABRUPT ENLARGEMENT CHARACTERIZED BY A ZONE OF DEAD WATER IN THE FIRST SECTION OF THE DUCT OF LARGER CROSS-SECTION.	89
FIGURE 4:3 ORIFICE MODELLING IN GASDYN.....	90
FIGURE 4:4 Y JUNCTION MODELLING IN GASDYN.....	91
FIGURE 4:5 EXPERIMENTAL RESULTS OF TURBINE (EXPANSION RATIO v/s MASS FLOW PARAMETER).....	93
FIGURE 4:6 EXPERIMENTAL RESULTS OF TURBINE (EFFICIENCY v/s VELOCITY RATIO).	94
FIGURE 4:7 EXPERIMENTAL RESULTS OF COMPRESSOR (COMPRESSION RATIO v/s MASS FLOW PARAMETER).....	96
FIGURE 4:8 EXPERIMENTAL RESULTS OF COMPRESSOR (EFFICIENCY v/s MASS FLOW PARAMETER).	97

FIGURE 4:9 EXTRAPOLATED RESULT OF TURBINE’S EXPANSION RATIO V/S MASS FLOW PARAMETER CURVE.	98
FIGURE 4:10 EXTRAPOLATED RESULT OF TURBINE’S EFFICIENCY V/S VELOCITY RATIO CURVE.	98
FIGURE 4:11 EXTRAPOLATED RESULT OF COMPRESSOR’S COMPRESSION RATIO V/S MASS FLOW PARAMETER CURVE.	99
FIGURE 4:12 EXTRAPOLATED RESULT OF COMPRESSOR’S EFFICIENCY V/S MASS FLOW PARAMETER CURVE.	99
FIGURE 4:13 GASDYN SCHEMATIC OF STEADY-STATE FLOW THROUGH TURBO-CHARGER.	102
FIGURE 4:14: COMPARISON OF BOOST PRESSURE (EXPERIMENTAL V/S SIMULATION) AT THE DOWNSTREAM OF COMPRESSOR.	103
FIGURE 4:15: COMPARISON OF MASS FLOW THROUGH COMPRESSOR LINE (EXPERIMENTAL V/S SIMULATION).	104
FIGURE 4:16: COMPARISON OF PRESSURE UPSTREAM OF TURBINE (EXPERIMENTAL V/S SIMULATION).	104
FIGURE 4:17: COMPARISON OF FLOW TEMPERATURE AT THE INLET OF TURBINE (EXPERIMENTAL V/S SIMULATION).	105
FIGURE 4:18: COMPARISON OF TURBOCHARGER SPEED (EXPERIMENTAL V/S SIMULATION RPM).	105
FIGURE 4:19: PLOT OF BOOST PRESSURE, TURBOCHARGER SPEED AND POWER BALANCE OF 1ST SIMULATED POINT.	106
FIGURE 4:20: PLOT OF ITERATIVE STEP’S VALUE FOR 1ST SIMULATED POINT DURING SIMULATION CYCLES.	106
FIGURE 4:21: PLOT OF BOOST PRESSURE, TURBOCHARGER SPEED AND POWER BALANCE OF 2ND SIMULATED POINT.	107
FIGURE 4:22: PLOT OF ITERATIVE STEP’S VALUE FOR 2ND SIMULATED POINT DURING SIMULATION CYCLES.	107
FIGURE 4:23: PLOT OF BOOST PRESSURE, TURBOCHARGER SPEED AND POWER BALANCE OF 3RD SIMULATED POINT.	108
FIGURE 4:24: PLOT OF ITERATIVE STEP’S VALUE FOR 3RD SIMULATED POINT DURING SIMULATION CYCLES.	108
FIGURE 4:25: PLOT OF BOOST PRESSURE, TURBOCHARGER SPEED AND POWER BALANCE OF 4TH SIMULATED POINT.	109
FIGURE 4:26: PLOT OF ITERATIVE STEP’S VALUE FOR 4TH SIMULATED POINT DURING SIMULATION CYCLES.	109
FIGURE 5:1 SLOPE TOLERANCE OF TURBO-SPEED FOR CONVERGENCE.	112
FIGURE 5:2 CONVERGENCE TOLERANCE IN BOOST PRESSURE.	113
FIGURE 5:3 SCHEMATIC OF “TD-4” ENGINE IN GASDYN.	114
FIGURE 5:4 CONVERGENCE OF “TD-4” ENGINE AT 1000 RPM WITH OLD ALGORITHM.	115
FIGURE 5:5 CONVERGENCE OF “TD-4” ENGINE AT 2000 RPM WITH OLD ALGORITHM.	116
FIGURE 5:6 SCHEMATIC OF “F1C” ENGINE IN GASDYN.	117
FIGURE 5:7 CONVERGENCE OF “F1C” ENGINE AT 1000 RPM WITH OLD ALGORITHM.	118
FIGURE 5:8 CONVERGENCE OF “F1C” ENGINE AT 2000 RPM WITH OLD ALGORITHM.	118
FIGURE 5:9 CONVERGENCE OF “F1C” ENGINE AT 3500 RPM WITH OLD ALGORITHM.	119
FIGURE 5:10 SLOPE TOLERANCE OF TURBO-SPEED FOR CONVERGENCE.	121
FIGURE 5:11 ERROR CALCULATION OF BOOST PRESSURE FOR CONVERGENCE.	122
FIGURE 5:12 OSCILLATING CURVE OF BOOST PRESSURE CLOSE TO IT’S TARGET VALUE.	123
FIGURE 5:13 CONVERGENCE OF “TD-4” ENGINE AT 1000 RPM WITH 1 CONSTRAIN CONDITION.	125
FIGURE 5:14 CONVERGENCE OF “TD-4” ENGINE AT 2000 RPM WITH 1 CONSTRAIN CONDITION.	125
FIGURE 5:15 CONVERGENCE OF “TD-4” ENGINE AT 3500 RPM WITH 1 CONSTRAIN CONDITION.	126
FIGURE 5:16 CONVERGENCE OF “TD-4” ENGINE AT 1000 RPM WITH 2 CONSTRAIN CONDITION.	127
FIGURE 5:17 CONVERGENCE OF “TD-4” ENGINE AT 2000 RPM WITH 2 CONSTRAIN CONDITION.	127
FIGURE 5:18 CONVERGENCE OF “TD-4” ENGINE AT 3500 RPM WITH 2 CONSTRAIN CONDITION.	128
FIGURE 5:19 CONVERGENCE OF “TD-4” ENGINE AT 1000 RPM WITH 3 CONSTRAIN CONDITION.	129
FIGURE 5:20 CONVERGENCE OF “TD-4” ENGINE AT 2000 RPM WITH 3 CONSTRAIN CONDITION.	130
FIGURE 5:21 CONVERGENCE OF “F1C” ENGINE AT 1000 RPM WITH 2 CONSTRAIN CONDITION.	131
FIGURE 5:22 CONVERGENCE OF “F1C” ENGINE AT 2000 RPM WITH 2 CONSTRAIN CONDITION.	132
FIGURE 5:23 CONVERGENCE OF “F1C” ENGINE AT 3500 RPM WITH 2 CONSTRAIN CONDITION.	133
FIGURE 5:24: FLOW CHART OF PID CONTROL FOR NEW CONVERGENCE ALGORITHM OF TURBOCHARGER SIMULATION IN GASDYN.	134

List of Tables:

TABLE 5-1 SPECIFICATION OF "TD-4" ENGINE.....	115
TABLE 5-2 SPECIFICATION OF "F1C" ENGINE.	117
TABLE 5-3: DATA FROM "TURBO_CONV_DEBUG" FILE AT 1000 RPM WITH 3 CONSTRAIN CONDITION.	129
TABLE 5-4: DATA FROM "TURBO_CONV_DEBUG" FILE AT 2000 RPM WITH 3 CONSTRAIN CONDITION	130
TABLE 5-5: DATA FROM "TURBO_CONV_DEBUG" FILE AT 1000 RPM WITH 2 CONSTRAIN CONDITION.	131
TABLE 5-6: DATA FROM "TURBO_CONV_DEBUG" FILE AT 2000 RPM WITH 2 CONSTRAIN CONDITION.	132
TABLE 5-7: DATA FROM "TURBO_CONV_DEBUG" FILE AT 3500 RPM WITH 2 CONSTRAIN CONDITION.	133

Bibliography

- [1] R. Benson, *The Thermodynamics and Gas Dynamics of Internal- Combustion Engines*, Clarendon Press, 1982.
- [2] R. D.E. Winterbone, *Design Techniques for Engine Manifolds*, Professional Engineering Publishing, 1999.
- [3] R. D.E. Winterbone, *Theory of Engine Manifold Design*, Professional Engineering Publishing, 2000.
- [4] V. D. B. S. M. a. M. C. Fabio Bozza, "1D Simulation and Experimental Analysis of a Turbocharger Compressor for Automotive Engines under Unsteady Flow Conditions," in *SAE International*, 2011.
- [5] V. D. Bellis, "1D simulation and experimental analysis of a turbocharger turbine for automotive engines under steady and unsteady flow conditions," in *68th Conference of the Italian Thermal Machines Engineering Association, ATI2013*.
- [6] S. Marelli, "Steady and pulsating flow efficiency of a waste-gated turbocharger radial flow turbine for automotive application," *Energy*, 2010.
- [7] F. B. S. M. a. M. C. Vincenzo De Bellis, "Experimental Investigation and 1D Simulation of a Turbocharger Compressor Close to Surge Operation," in *SAE International*, 2015.
- [8] G. M. A. O. F. P. G. D'Errico, "Integrated 1D-3D Fluid Dynamic Simulation of a Turbocharged Diesel Engine with Complete Intake and Exhaust Systems," in *SAE International*, 2010.
- [9] S. Marelli, "Pulsating flow performance of a turbocharger compressor for automotive application," *International Journal of Heat and Fluid Flow*, 2013.
- [10] F. P. S. M. a. M. C. A. Onorati, "Unsteady Behavior in Turbocharger Turbines: Experimental Analysis and Numerical Simulation," in *ICE2007, SAE International Conference on Internal Combustion Engine*, Capri, 2007.
- [11] A. O. T. C. G. M. F. P. L. Cornolti, "1D simulation of a turbocharged Diesel engine with comparison of short and long EGR route solutions," *Applied Energy*, 2013.